PB99-128670

FIELD APPLICATION OF A THERMAL-SPRAYED TITANIUM ANODE FOR CATHODIC PROTECTION OF REINFORCING STEEL IN CONCRETE

FINAL REPORT

SPR 365

RESEARCH UNIT

Oregon Department of Transportation

REPRODUCED BY:
U.S. Department of Commerce
National Technical Information Service
Springfield, Virginia 22161
NTIS

FIELD APPLICATION OF A THERMAL-SPRAYED TITANIUM ANODE FOR CATHODIC PROTECTION OF REINFORCING STEEL IN CONCRETE

FINAL REPORT

SPR 365

by

Galen E. McGill, P.E.
Oregon Department of Transportation, Salem OR 97310

and

Stephen D. Cramer,
Bernard S. Covino, Jr., Sophie J. Bullard, Gordon R. Holcomb,
W. Keith Collins, R. Dale Govier, and Rick D. Wilson
Albany Research Center, U.S. Department of Energy, Albany, OR 97321

for

Oregon Department of Transportation, Research Unit
200 Hawthorne Ave. SE, Suite B-240, Salem, OR 97310

and

Federal Highway Administration
400 Seventh Street SW, Washington, DC 20590

January 1999

PROTECTED UNDER INTERNATIONAL COPYRIGHT
ALL RIGHTS RESERVED.
NATIONAL TECHNICAL INFORMATION SERVICE
U.S. DEPARTMENT OF COMMERCE

1. Report No. FWHA-OR-RD-99-13	2. Government Accession No.	3. Recipient's Catalog No.
4. Title and Subtitle Field Application Of A Thermal-Sprayed Titanium Anode For Cathodic Protection Of Reinforcing Steel In Concrete		5. Report Date January 1999 6. Performing Organization Code
7. Author(s) Galen E. McGill, P.E., Stephen D. Cramer, Bernard S. Covino, Jr., Sophie J. Bullard, Gordon R. Holcomb, W. Keith Collins, R. Dale Govier and Rick D. Wilson		8. Performing Organization Report No.
9. Performing Organization Name and Address Oregon Department of Transportation Policy & Research Section, Research Unit 200 Hawthorne Avenue SE, Suite B-240 Salem, Oregon 97301-5192		10. Work Unit No. (TRAIS) 11. Contract or Grant No. SPR 365
12. Sponsoring Agency Name and Address Oregon Department of Transportation Policy & Research Section, Research Unit 200 Hawthorne Avenue SE, Suite B-240 Salem, Oregon 97301-5192 and Federal Highway Administration 400 Seventh Street SW Washington, DC 20560		13. Type of Report and Period Covered Final Report 14. Sponsoring Agency Code
15. Supplementary Notes		

16. Abstract

This study provided the first field trial of a catalyzed, thermal-sprayed titanium anode for cathodic protection of steel reinforced concrete structures. Catalyzed titanium as an anode material offers the advantage of long life due to the inherent non-corrosive nature of the metal in atmospheric exposure. To continue to serve as an anode, the titanium will require a periodic and easily accomplished re-application of the catalyst rather than re-application of the metal. The purpose of this study was to evaluate the installation and operation of the catalyzed titanium anode and to evaluate the economics of the titanium anode system compared to thermal-sprayed zinc.

The initial phase of the study included modification of the spray equipment for spraying titanium wire and determination of the optimal spray parameters for applying the titanium anode to the bridge. Coating resistivity was found to be the best measure for evaluating the effectiveness of the coating. Decreasing spray distance, increasing current, and using nitrogen as the atomizing gas (propellant) all decrease coating resistivity. A multiple regression equation developed from the collected data showed that, for the data collected in this study, spray gun travel speed and atomizing gas pressure have an insignificant effect on coating resistivity

Coating analysis showed that the arc-sprayed titanium is a non-homogeneous coating due to reactions with atmospheric gases. The coating contains, on average, 88 weight percent titanium. The principal coating constituents are α-Ti containing interstitial nitrogen and interstitial oxygen, and γ-TiO with the possibility of some TiN. The coating consists of alternating layers of α-Ti rich and γ-TiO rich material. The use of nitrogen as the atomizing gas results in a coating with less cracking, more uniform chemistry, and therefore, lower coating resistivity than is produced using air atomization.

The field trial resulted in installation of 280 m^2 (3015 ft^2) of catalyzed, arc-sprayed titanium on the Depoe Bay Bridge. Several lessons were learned during the field trial. Although use of a grade 1, annealed titanium wire for spraying was found to reduce equipment wear, frequent equipment maintenance caused by rapid wear of the copper spray tips had a significant impact on operator productivity. The switchmode power supply furnished with the spray equipment was unable to provide the stable arc needed for smooth operation of the spray equipment. Current distribution plates embedded flush in a concrete patch material proved to be the best method for providing a low resistance connection between the anode and the power supply.

Although some difficulty was experienced during the field trial, the costs for performing this work exceeded the bid costs for installing arc-sprayed zinc on this same structure by just 18 percent. If the long-term performance of the catalyzed titanium anode system is proven, the arc-sprayed titanium system will provide a life cycle cost advantage over the arc-sprayed zinc system.

17. Key Words	18. Distribution Statement		
CATHODIC PROTECTION, THERMAL SPRAY, TITANIUM ANODE, REINFORCED CONCRETE, BRIDGES	No restrictions		
19. Security Classif. (of this report) Unclassified	20. Security Classif. (of this page) Unclassified	21. No. of Pages 123 + appendices	22. Price

Form DOT F 1700.7 (8-72) Reproduction of completed page authorized

SI* (MODERN METRIC) CONVERSION FACTORS

APPROXIMATE CONVERSIONS TO SI UNITS

Symbol	When You Know	Multiply By	To Find	Symbol
		LENGTH		
in	inches	25.4	millimeters	mm
ft	feet	0.305	meters	m
yd	yards	0.914	meters	m
mi	miles	1.61	kilometers	km
		AREA		
in^2	square inches	645.2	millimeters squared	mm^2
ft^2	square feet	0.093	meters squared	m^2
yd^2	square yards	0.836	meters squared	m^2
ac	acres	0.405	hectares	ha
mi^2	square miles	2.59	kilometers squared	km^2
		VOLUME		
fl oz	fluid ounces	29.57	milliliters	mL
gal	gallons	3.785	liters	L
ft^3	cubic feet	0.028	meters cubed	m^3
yd^3	cubic yards	0.765	meters cubed	m^3
	NOTE: Volumes greater than 1000 L shall be shown in m^3.			
		MASS		
oz	ounces	28.35	grams	g
lb	pounds	0.454	kilograms	kg
T	short tons (2000 lb)	0.907	megagrams	Mg
		TEMPERATURE (exact)		
°F	Fahrenheit temperature	5(F-32)/9	Celsius temperature	°C

APPROXIMATE CONVERSIONS FROM SI UNITS

Symbol	When You Know	Multiply By	To Find	Symbol
		LENGTH		
mm	millimeters	0.039	inches	in
m	meters	3.28	feet	ft
m	meters	1.09	yards	yd
km	kilometers	0.621	miles	mi
		AREA		
mm^2	millimeters squared	0.0016	square inches	in^2
m^2	meters squared	10.764	square feet	ft^2
ha	hectares	2.47	acres	ac
km^2	kilometers squared	0.386	square miles	mi^2
		VOLUME		
mL	milliliters	0.034	fluid ounces	fl oz
L	liters	0.264	gallons	gal
m^3	meters cubed	35.315	cubic feet	ft^3
m^3	meters cubed	1.308	cubic yards	yd^3
		MASS		
g	grams	0.035	ounces	oz
kg	kilograms	2.205	pounds	lb
Mg	megagrams	1.102	short tons (2000 lb)	T
		TEMPERATURE (exact)		
°C	Celsius temperature	1.8 + 32	Fahrenheit	°F

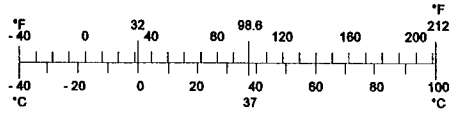

* SI is the symbol for the International System of Measurement

(4-7-94 jbp)

ACKNOWLEDGMENTS

The authors would like to thank Jack Bennett, formerly of Eltech Research Corporation, for his many contributions to this project. The authors also would like to thank Frank Rogers, of Thermion, Inc., for assistance with adaptation of the spray equipment. The authors also gratefully acknowledge Marty Laylor and the rest of the technical advisory committee for their direction and review of this work.

DISCLAIMER

This document is disseminated under the sponsorship of the Oregon Department of Transportation and the United States Department of Transportation in the interest of information exchange. The State of Oregon and the United States Government assume no liability of its contents or use thereof.

The contents of this report reflect the views of the authors who are solely responsible for the facts and accuracy of the material presented. The contents do not necessarily reflect the official views of the Oregon Department of Transportation or the United States Department of Transportation.

The State of Oregon and the United States Government do not endorse products of manufacturers. Trademarks or manufacturers' names appear herein only because they are considered essential to the object of this document.

This report does not constitute a standard, specification or regulation.

FIELD APPLICATION OF A THERMAL-SPRAYED TITANIUM ANODE FOR CATHODIC PROTECTION OF REINFORCING STEEL IN CONCRETE

TABLE OF CONTENTS

ABSTRACT i
SI (MODERN METRIC) CONVERSION FACTORS ii
ACKNOWLEDGMENTS iii
DISCLAIMER iii
1.0 INTRODUCTION 1
1.1 BACKGROUND 1
1.2 PROBLEM DEFINITION 1
1.3 THERMAL-SPRAYED TITANIUM ANODE 2
1.4 EXPERIMENT OBJECTIVES 3
1.5 WORK PLAN SYNOPSIS 3
2.0 PRELIMINARY INVESTIGATION AND EQUIPMENT DEVELOPMENT 5
2.1 ENVIRONMENTAL AND HEALTH CONCERNS 5
2.2 EQUIPMENT TESTING, DEVELOPMENT AND MODIFICATION 5
2.2.1 Titanium Resistance Probe 5
2.2.2 Arc-Shorting Control 7
2.2.3 Automated Short Circuit Detection 8
2.2.4 Spray Performance Test 9
3.0 SHOP TESTING 11
3.1 SPRAY PARAMETER OPTIMIZATION 11
3.1.1 Experiment Design 11
3.1.2 Deposit Efficiency Measurements 12
3.1.3 Parameter Study 14
3.2 BOND STRENGTH TESTING 18
3.3 APPLICATION OF TITANIUM SPRAY OVER SUBSTRATE CRACKS 20
3.4 OPERATIONAL CONCRETE SLABS 20
4.0 COATINGS CHARACTERIZATION 25
4.1 SELECTED PROPERTIES OF THE TI-O-N SYSTEM 25
4.2 THERMAL-SPRAYED TITANIUM COATINGS PREPARATION 30
4.3 CHARACTERIZATION TECHNIQUES 32
4.3.1 X-Ray Fluorescence (XRF) 32
4.3.2 X-Ray Diffraction (XRD) 32
4.3.3 Gas Analysis 33
4.3.4 Analytical Scanning Electron Microscopy (ASEM) 33
4.3.4.1 Manual Point Analysis 34

4.3.4.2 Automatic Point Analysis *35*
4.3.5 X-Ray Photoelectron Spectroscopy (XPS) 35
4.3.6 Coating Resistance 36
4.4 CHARACTERIZATION RESULTS 36
4.4.1 X-Ray Fluorescence 36
4.4.2 Gas Analyses 37
4.4.3 X-ray Diffraction 37
4.4.4 Analytical Scanning Electron Microscopy 38
4.4.5 X-ray Photoelectron Spectroscopy 52
4.4.6 Coating Microstructure 58
4.4.7 Coating Resistance 61
4.5 COATINGS SUMMARY 63
4.5.1 Coating Chemistry 63
4.5.2 Coating Mineralogy 64
4.5.3 Coating Microstructure 64
4.5.4 Coating Properties 64
5.0 ELECTROCHEMICALLY AGED ANODES 67
5.1 ANODE ELECTROCHEMICAL AGING 68
5.1.1 Anode Application to Concrete 68
5.1.1.1 Laboratory Aging Experiment *68*
5.1.1.2 Field Trial *70*
5.1.2 Electrochemical Aging Conditions 70
5.1.2.1 Laboratory Aging Experiment *70*
5.1.2.2 Field Trial *71*
5.2 CHARACTERIZATION TECHNIQUES 72
5.2.1 ICCP PERFORMANCE 73
5.2.2 Anode Properties 73
5.2.2.1 Anode Structure *73*
5.2.2.2 Anode Resistivity *73*
5.2.2.3 Anode Bond Strength *73*
5.2.2.4 Coating Durability *74*
5.2.3 ANODE-CONCRETE INTERFACIAL CHEMISTRY 74
5.2.3.1 X-ray Fluorescence *74*
5.2.3.2 X-ray Diffraction *74*
5.2.3.3 Analytical Scanning Electron Microscopy *74*
5.2.3.4 Micro-pH Measurements *75*
5.3 CHARACTERIZATION RESULTS 76
5.3.1 ICCP Performance 76
5.3.2 Anode Properties 78
5.3.2.1 Anode Structure *78*
5.3.2.2 Anode Resistivity *80*
5.3.2.3 Anode Bond Strength *82*
5.3.3 Anode-Concrete Interfacial Chemistry 82
5.3.3.1 X-ray Fluorescence *82*

5.3.3.2 X-ray Diffraction *83*
5.3.3.3 Analytical Scanning Electron Microscopy *84*
5.3.3.4 Micro-pH Measurements *94*
5.4 ANODE ELECTROCHEMICAL AGING SUMMARY 95
6.0 FIELD INSTALLATION 97
6.1 DESCRIPTION 97
6.2 SPECIFICATIONS 98
6.3 INSTALLATION 98
6.3.1 Current Contact Plates 98
6.3.2 Titanium Installation 101
6.3.2.1 Equipment *101*
6.3.2.2 Titanium Wire *101*
6.3.2.3 Application *101*
6.3.3 Catalyst 105
6.4 FINAL TESTING 106
6.4.1 Visual inspection 106
6.4.2 Anode Voltage Drop 109
6.4.3 Current-Potential Relationship 111
6.5 COST ANALYSIS 111
7.0 CONCLUSIONS AND RECOMMENDATIONS 113
7.1 CONCLUSIONS 113
7.1.1 Shop Testing 113
7.1.2 Characterization 114
7.1.3 Electrochemically Aged Anodes 114
7.1.4 Field Testing 115
7.2 RECOMMENDATIONS 116
7.2.1 Coatings Characterization 116
7.2.2 Electrochemically Aged Anodes 117
7.2.3 Overall Recommendations 117
8.0 REFERENCES 119

APPENDICES

APPENDIX A: SPECIFICATIONS FOR FIELD APPLICATION OF ARC-SPRAYED TITANIUM

APPENDIX B: CALCULATION OF AREA PER CURRENT DISTRIBUTION PLATE

LIST OF TABLES

Table 3.1: Spray Parameters 11
Table 3.2: Properties of Coatings on Glass Plates 15
Table 3.3: Multiple Regression Analysis Results 17
Table 3.4: Bond Strength Test Results from Concrete Plates 18
Table 3.5: Regression Results for Equation 3-2 (Plate 1 and Plate 45 data excluded) 19
Table 3.6: Concrete Mix Design 21
Table 3.7: Operational Concrete Slab Treatments 21

Table 4.1: Stable Low-Pressure Phases In The Ti-O System. 27
Table 4.2: Stable Low-Pressure Phases In The Ti-N System 28
Table 4.3: Physical Properties Of Titanium And Its Oxides And Nitrides. 29
Table 4.4: Transport Properties Of Titanium And Its Oxides And Nitrides. 29
Table 4.5: Samples Used For Characterization Of Arc-Sprayed Titanium Coatings. 32
Table 4.6: Manual Point Wave-Length Dispersive X-Ray Analyses Of Ti-N Standards. 35
Table 4.7: Automatic Point Wave-Length Dispersive X-Ray Analyses Of Ti-N Standard. 35
Table 4.8: Results of LEECO gas analyses on coating samples. 37
Table 4.9: Relative amounts of major phases in coatings, estimated from XRD results. 38
Table 4.10: Average coating composition, from ASEM composition depth profiles. 51
Table 4.11: Minimum and maximum element concentrations in coatings, from ASEM composition depth profiles 51
Table 4.12: XPS depth profile data for sample TiPN. 53
Table 4.13: Composition of phases in freezing structures, coating sample TiCA. 61
Table 4.14: Anode coating resistivity. 63

Table 5.1: Electrochemically-aged titanium anode samples. 72
Table 5.2: Thickness of aged anodes. 79
Table 5.3: Resistivity of aged anodes. 81
Table 5.4: Bond strength of anodes, laboratory aging experiment. 82
Table 5.5: Chemistry of anode-concrete interface in laboratory aging experiment. 83
Table 5.6: Crystallographic phases at anode-concrete interface in laboratory aging experiment. 84
Table 5.7: pH of anode-concrete interface and bulk concrete. 95

Table 6.1: Variation in Voltage and Potential with Changes in Applied Current 111
Table 6.2: Cost Summary 112

LIST OF FIGURES

Figure 2.1: Resistance probe design 6
Figure 2.2: Effect of sheet width on coating resistance measurement 7
Figure 2.3: Schematic for automated short circuit detection system 8

Figure 3.1: X-Y traversing system for spray parameter optimization work. 12
Figure 3.2: Typical titanium deposit efficiency per spray pass 13
Figure 3.3: Fit of regression equation to empirical data 16
Figure 3.4: Crack simulation 20
Figure 3.5: Voltage and current for five Ti-coated slabs in series 22
Figure 3.6: Individual slab voltages 23

Figure 4.1: Ti-O phase diagram *(Oxygen-Titanium, "Alloy Phase Diagrams", 1992)*. Lines 1 and 2 represent the average O content of some typical splats in the arc-sprayed Ti anode. 26
Figure 4.2: Ti-N phase diagram *(Nitrogen-Titanium, "Alloy Phase Diagrams", 1992)*. Line 1 represents the average N content of typical splats in the arc-sprayed Ti anode. 28
Figure 4.3: Schematic representation of the thermal-spray coatings process for titanium anodes. 31
Figure 4.4: SEM photomicrographs of TiPA cross-section: (a) SE image, 350X; (b) BE image, 350X; (c) BE image, 140X. Arrow shows path of ASEM traverse and the location of seven Ti gradient bands in the coating. 39
Figure 4.5: ASEM composition depth profile for TiPA cross-section shown in Figure 4.4. Glass-coating interface and outer surface of coating are shown with seven Ti gradient bands. 40
Figure 4.6: SEM photomicrographs of TiPA surface: (a) SE image, 65X; (b) SE image, 165X; (c) SE image, 330X; (d) BE image, 330X. Arrows: a) small, highly oxidized, finely cracked splat; b) small, highly oxidized droplet that froze before impacting the surface. 42
Figure 4.7: SEM photomicrographs of TiPN cross-section: (a) SE image, 350X; (b) BE image, 350X; (c) BE image, 140X. Arrow shows path of ASEM traverse and the location of six Ti gradient bands in the coating. 44
Figure 4.8: ASEM composition depth profile for TiPN cross-section shown in Figure 4.7. Glass-coating interface and outer surface of coating are shown with six Ti gradient bands. 45
Figure 4.9: SEM photomicrographs of TiPN surface: (a) SE image, 65X; (b) SE image, 1650X; (c) SE image, 330X. 46
Figure 4.10: SEM photomicrographs of TiCA cross-section: (a) SE image, 320X; (b) BE image, 320X; (c) BE image, 130X. Arrow shows path of ASEM traverse and the location of six Ti gradient bands in the coating. 47
Figure 4.11: ASEM composition depth profile for TiCA cross-section shown in Figure 4-10. Concrete-coating interface and outer surface of coating are shown with six Ti gradient bands. 48
Figure 4.12: SEM photomicrographs of TiCN cross-section: (a) SE image, 350X; (b) BE image, 350X; (c) BE image, 140X. Arrow shows path of ASEM traverse and the location of five Ti gradient bands in the coating. 49
Figure 4.13: ASEM composition depth profile for TiCN cross-section shown in Figure 4.12. Concrete-coating interface and outer surface of coating are shown with five Ti gradient bands. 50
Figure 4.14: Cracks in Ti gradient bands: (a) SE image, 900X; (b) BE image, 900X. Arrows: a) incipient crack along sharp gradient boundary; b) diffuse gradient boundary; c) crack along Ti(O,N)-rich boundary. 52
Figure 4.15: $Ti2p_{3/2}$ and $Ti2p_{1/2}$ peaks as a function of sputter etching for sample TiPN. 55
Figure 4.16: N1s peak as a function of sputter etching for sample TiPN. 55
Figure 4.17: O1s peak as a function of sputter etching for sample TiPN. 56
Figure 4.18: Composition depth profile for sample TiPN. 57
Figure 4.19: Composition depth profile for sample TiPA. 58
Figure 4.20: Freezing structures in TiCA formed using air atomization, BE images: (a) General view showing four analysis areas, 200X; (b) analysis area 1, 2400X; (c) analysis areas 3a and 3b, 3600X; (d) analysis areas 4a and 4b, 1800X. 60

Figure 4.21: Comparison of literature resistivity values with those computed from resistance measurements made with the ODOT resistance probe on metal foils. 62

Figure 5.1: Design of the laboratory concrete slabs. 69
Figure 5.2: Laboratory electrochemical aging of the five thermal-sprayed titanium anodes on concrete slabs. 71
Figure 5.3: Slab voltage as a function of electrochemical aging. 76
Figure 5.4: Voltage requirements of thermal-sprayed titanium anodes at current density of 2.1 mA/m^2 as a function of RH. 77
Figure 5.5: Secondary electron SEM photomicrographs of thermal-sprayed titanium anode surface before and after electrochemical aging: (a) unaged, uncatalyzed; (b) aged 1520 kC/m^2, uncatalyzed; (c) aged 1520 kC/m^2, catalyzed; (d) Depoe Bay Bridge field trial, aged 146 kC/m^2. 70X. 78
Figure 5.6: BE SEM photomicrograph of cross-sectioned, catalyzed anode (slab 6), aged 1520 kC/m^2. 13.5X. 85
Figure 5.7: BE SEM photomicrograph of cross-sectioned, catalyzed anode (slab 6), aged 1520 kC/m^2. Four areas are shown where the SEM photomicrographs in Figure 5.8 were taken. 17X. 86
Figure 5.8: Four SE SEM photomicrographs of slab 6 areas shown in Figure 5.7: (a) unaltered concrete; (b) dense concrete; (c) concrete-reaction zone interface; (d) reaction zone. 350X 87
Figure 5.9: BE SEM photomicrographs of anode cross-sections: (a) unaged, uncatalyzed; (b) uncatalyzed (slab 5), aged 1520 kC/m^2; (c) catalyzed (slab 6), aged 1520 kC/m^2; (d) Depoe Bay Bridge field trial, aged 146 kC/m^2. 20X. 88
Figure 5.10: Cross-sectioned, catalyzed anode (slab 6), aged 1520 kC/m^2: (a) BE SEM image; (b) Ti K_α x-ray map; (c) Ca K_α x-ray map; (d) Co K_α x-ray map. Arrow in (a) shows path of ASEM traverse for composition depth profile. 25 X. 90
Figure 5.11: Composition depth profile for catalyzed thermal-sprayed titanium anode (slab 6) after electrochemical aging; path of traverse is shown in Figure 5.10(a). 91
Figure 5.12: Cross-sectioned, catalyzed thermal-sprayed titanium anode from the Depoe Bay Bridge field trial after electrochemical aging 146 kC/m^2: (a) backscattered electron SEM image; (b) Ti K_α x-ray map; (c) Ca K_α x-ray map; (d) Co K_α x-ray map. Arrow in (a) shows path of ASEM traverse for composition depth profile. 150X. 92
Figure 5.13: Composition depth profile for catalyzed anode from Depoe Bay Bridge after electrochemical aging 146 kC/m^2; path of traverse is shown in Figure 5.12(a). 93

Figure 6.1: Depoe Bay Bridge 97
Figure 6.2: Surface Mounted Current Distribution Plate 99
Figure 6.3: Flush-mounted current distribution plates with temporary wiring installed. 100
Figure 6.4: Catalyst application 106
Figure 6.5: Typical disbonded area 107
Figure 6.6: Connections for anode voltage drop testing 110

Figure B.1: Variable definitions for circular sheet of titanium B-1
Figure B.2: Allowable titanium surface area vs. plate size B-2
Figure B.3: Allowable titanium area vs. plate size (metric) B-3

1.0 INTRODUCTION

1.1 BACKGROUND

Oregon is graced with a rugged and majestic coastline. The ruggedness of the coastline along US 101, combined with the remoteness of many of the coastal areas in the 1920s and 1930s, make the bridge engineering accomplishments of Conde B. McCullough impressive. McCullough was the internationally recognized designer of most of the major structures that link the Oregon Coast Highway. McCullough combined a keen sense of aesthetics with engineering innovation to create a magnificent sequence of structures spanning the rivers and estuaries of the coast. His arched-bridge theme extends the length of the Oregon Coast Highway and provides Oregon with a significant number of bridges listed on the National Historic Register.

McCullough probably did not envision the damage his bridges would suffer from the effects of corrosion in the coastal environment. Today, however, the effects of the coastal environment are apparent. Chloride-induced corrosion of reinforcing steel is the primary contributor to the deterioration of Oregon's coastal bridges.

1.2 PROBLEM DEFINITION

Techniques to arrest the corrosion of concrete-embedded reinforcing steel began development in the 1970s, through the work of Dick Stratfull of the California Department of Transportation (CalTrans) (*Stratfull, 1974*). The early development of cathodic protection systems focused on systems to protect decks from corrosion resulting from de-icing salt. None of these techniques, however, were applicable to the marine corrosion problem that occurs on the underdeck and substructure components of a bridge. Not only must it be possible to apply cathodic protection to the vertical and overhead surfaces of the substructure; it must also conform to the complex, decorative shapes typically found on historic structures.

An early solution to this problem was a high-carbon content conductive paint material. Because the installed coating is black, it requires an overcoat to maintain the appearance of the bridge. While this coating can be successfully installed, there is a high probability of electrical short circuits between the coating and the rebar, and the coating has poor conductivity. In addition, durability problems in freeze-thaw conditions and in areas of surface wetting, such as splash zones, have been documented (*Swiat and Rog, 1987*).

Building on work performed by CalTrans (*Carello, et al, 1989*), the Oregon Department of Transportation (ODOT) selected arc-sprayed zinc as the anode material for use in cathodic

protection systems for coastal bridges and have applied 33,630 square meters (362,000 square feet) of arc-sprayed zinc to coastal structures.

The arc-sprayed zinc coatings meet the desired properties for installation on a bridge substructure — high conductivity, preservation of architectural shapes and details, good bond strength and a color that matches concrete. Initially, zinc can even serve as a galvanic anode, but its function as an active metal is also its major disadvantage, as the coating is consumed and requires periodic replacement of the zinc. ODOT currently uses a life estimate of 12 to 15 years for a 0.508 mm (20 mil) zinc coating. CalTrans recently increased their system life estimate to 20 years for the first thermal-sprayed zinc system installed on the San Rafael Bridge in May 1983 (*McGovern, 1994*).

Although the system life estimates for zinc are not entirely certain at this time, it is certain that the zinc will eventually require replacement. Along with this replacement come the high costs associated with gaining access to the underside of the bridge, removing and reapplying the zinc, and containing the waste by-products of this process. The cost for obtaining access and containing wastes on recent ODOT cathodic protection contracts have been as high as 46% of the total contract cost, or $\$257.81/m^2$ ($\$23.96/ft^2$) of anode surface area (*Holcomb and Cryer, 1998*).

1.3 THERMAL-SPRAYED TITANIUM ANODE

The primary advantage to using titanium instead of zinc is titanium's excellent corrosion resistance. In seawater the corrosion rate is reported as 0.0008 mm/yr (*Uhlig and Revie, 1985*). Titanium is an active-passive metal. The pure metal will actively corrode with the electrode potential equal to -1.63 v (standard hydrogen electrode potential at 25 ° C) for $Ti^{2+} + 2e^- \rightarrow Ti$, compared to the less active potential for the zinc reaction, $Zn^{2+} + 2e^- \rightarrow Zn$, of -0.763 v (standard hydrogen electrode potential at 25 ° C) (*Uhlig and Revie, 1985*). Titanium, however, readily passivates, forming a thin, tightly adherent protective oxide film. Titanium then remains passive until a sufficiently high applied potential is reached. At this potential and above it the metal resumes active behavior and corrosion will occur.

While the oxide film is beneficial from the perspective of corrosion resistance of the metal, the resistance of the film interferes with titanium's ability to perform as an anode. If titanium is connected to an impressed current system as an anode, the resistive surface film will prevent significant current flow until the breakdown potential is exceeded. Above this potential, corrosion of the titanium will occur. However, a catalyst exists which allows the titanium/catalyst system to serve as an anode without application of a high potential and breakdown of the titanium oxide film (*Bennett, et al, 1995a and 1995b*).

In this titanium/catalyst system, the titanium serves as a conductive medium for distributing the cathodic protection current and as a support structure for the catalyst. The catalyst allows anodic reactions to take place at a lower energy level but is not consumed in the anodic reactions. With time, however, the catalyst may dissipate through migration, leaching or reaction with other

compounds, but since the titanium is not consumed in the anodic reactions, the catalyst can be reapplied at any time without requiring replacement of the titanium.

The most likely anodic reaction for the catalyzed titanium system has been reported to be: (*Bennett, et al, 1995a*).

$$4OH^- \rightarrow O_2 + 2H_2O + 4e^- \qquad \textbf{(1-1)}$$

This reaction will tend to decrease the pH at the anode/concrete interface.

1.4 EXPERIMENT OBJECTIVES

This project is based upon initial research performed by Eltech Research Corporation that resulted in the development of a process to catalyze thermal-sprayed titanium coatings. The laboratory testing performed by Eltech showed promising results for the catalyzed thermal-sprayed titanium. Although the results should be viewed with caution, accelerated life testing has indicated an anode lifetime for catalyzed titanium in excess of 40 years (*Bennett, et al, 1995a and 1995b*).

The Eltech research examined three different techniques for applying titanium to the concrete surface: wire flame spray, plasma spray using powdered metal and wire arc-spray. The wire arc-spray appeared to give the best combination of titanium deposit efficiency and application rate (*Bennett, et al, 1995a and 1995b*). Based on Eltech's results as well as ODOT's own experience with wire arc spray for zinc application, the focus of this field trial was on the arc spray process.

The objective of this study was to evaluate the installation and operation of an arc-sprayed, catalyzed, titanium anode on an actual reinforced concrete structure. Included in the study was a determination of the optimal installation parameters and an examination of the economics of the catalyzed titanium anode versus arc-sprayed zinc.

1.5 WORK PLAN SYNOPSIS

The initial phase of this study was a shop investigation of the spray parameters to achieve an optimum coating. Desired coating properties are: low coating resistance, low titanium usage, high production rate and high bond strength. Also included in this phase was an investigation of health and environmental concerns for the materials being used and the development and modification of equipment necessary for the installation and testing of the titanium.

The initial work was intended to provide the basis for writing specifications for installation of the catalyzed titanium anode to 280 m^2 (3015 ft^2) of the Depoe Bay Bridge. The Depoe Bay Bridge was selected for this work because of an ongoing contract for rehabilitation and cathodic protection of the bridge. This existing contract offered two advantages. With a contractor and work platform/enclosure already on site, the costs for this experimental work were greatly reduced. Since the rest of the substructure and underdeck areas of the bridge will be coated with zinc, this bridge provides an opportunity for a side-by-side comparison of arc-sprayed, catalyzed titanium and arc-sprayed zinc. In this phase of work, training, based on what was learned in the first phase, was provided to the contractor, and the installation was monitored to identify problems and evaluate the economics of installation.

This study's final phase was an 18-month evaluation of system operation. Information on system operation is included in this report.

2.0 PRELIMINARY INVESTIGATION AND EQUIPMENT DEVELOPMENT

2.1 ENVIRONMENTAL AND HEALTH CONCERNS

The first task accomplished in this project was verification that there are no health or environmental concerns with the titanium or the catalyst material. Titanium is fairly inert in the environment, and there are no known environmental impacts from titanium. The catalyst material is an irritant but it poses no known serious health effects. The dust or mist of the catalyst can cause respiratory tract irritation if inhaled, so a NIOSH-approved dust mask or breathing apparatus should be worn. Eye and skin protection should also be used during catalyst installation to prevent eye or skin irritation.

2.2 EQUIPMENT TESTING, DEVELOPMENT AND MODIFICATION

2.2.1 Titanium Resistance Probe

Since the titanium in this system serves to distribute current throughout the zone, the resistance of the titanium coating is more important than the thickness. Resistance and thickness are related by the following formula:

$$R = \frac{\rho \cdot L}{A} \qquad \textbf{(2-1)}$$

where: R = resistance (Ω),

ρ = resistivity (Ω-cm),

L = length of coating (cm), and

A = coating cross-sectional area (cm^2).

Since the cross-sectional area of the coating is equal to the width of the coating being measured (w) multiplied by the coating thickness (T), Equation 2.1 becomes:

$$R = \frac{\rho \cdot L}{w \cdot T} \qquad \textbf{(2-2)}$$

If the resistance-measuring probe is constructed so the width of coating being measured is equal to the length of the coating being measured, the equation reduces to:

$$R = \frac{\rho}{T} \qquad \textbf{(2-3)}$$

This measure, which is independent of length and width as long as width and length are equal, is commonly reported with the units of ohms per square. The significance of this measurement is that, on a coating that is reasonably uniform on a macroscopic scale, the resistance readings will be independent of the size of the square.

The probe constructed for this project consisted of spring-loaded contact pins installed in a 127 mm x 152 mm x 13 mm (5" x 6" x 0.5") sheet of fiberglass (see Figure 2.1 - Resistance probe design). The spring-loaded pins provided 6.35 mm (0.25") of movement and were used to obtain good contact with the rough concrete surface.

To eliminate contact resistance, a four-pin measurement technique was used to connect the probe to a Nilsson 400 AC resistance meter. The outer rows of pins are used to pass a constant current through the titanium coating. The inner pins are used to measure the voltage drop through the coating. To obtain uniform current flow through the length of coating being measured, the current distribution pins were spaced closely (9.5 mm; 0.375").

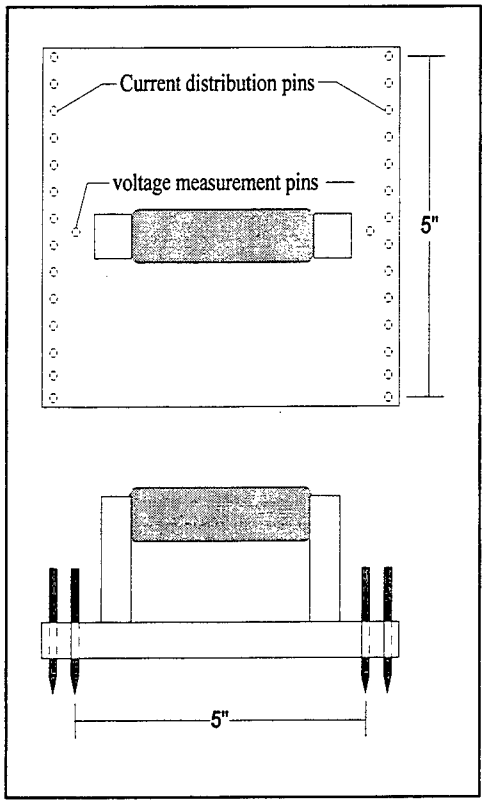

Figure 2.1: Resistance probe design

This probe provides accurate results when the sample being measured is of the same width as the probe. When a sheet of width greater than the probe is measured, errors are introduced as a result of additional current paths outside the outer edge of the probe. The effect of the additional parallel current paths is a reduction in the measured resistance of the sample.

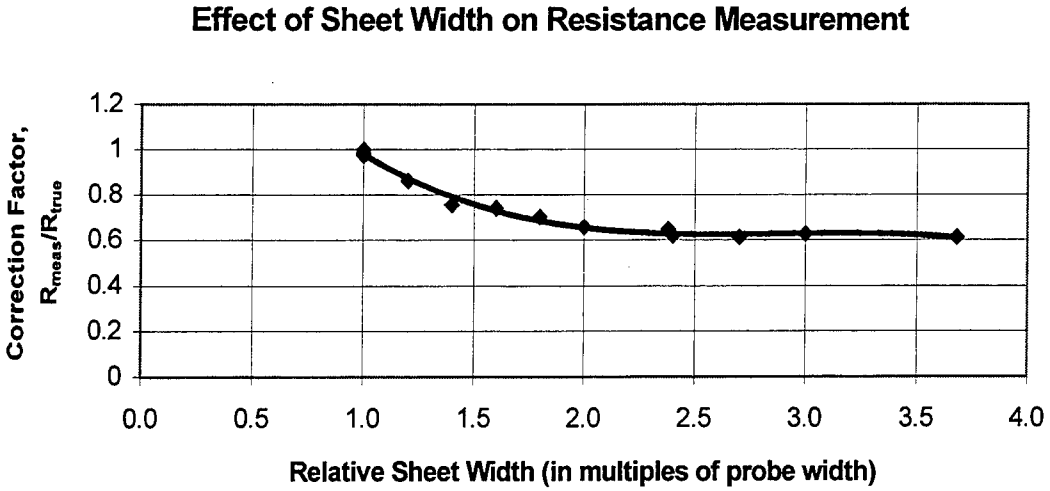

Figure 2.2: Effect of sheet width on coating resistance measurement

The impact of sheet width was investigated empirically using aluminum foil. Although arc-sprayed titanium was not used for this empirical study, the results should be similar, regardless of the material used, and provided the sheet is thin. Figure 2.2 illustrates that for sheet width greater than two times the probe width, the measured resistance will be about 60% of the true resistance. Eltech performed a similar study using sheets of conductive gel, and their results indicated that as sheet width increased the measured resistance decreased to about 50% of the true resistance. Based on these results, the specifications for the field trial require a measured coating resistance of 0.25 ohms/square (50% of the design value of 0.5 ohms/square).

2.2.2 Arc-Shorting Control

The spray equipment used for the shop spraying and for the field application was the Thermion Bridgemaster arc-spray system. A significant feature of this equipment is its patented arc-shorting control system, which monitors the voltage across the arc gap and stops the wire feed when this voltage becomes too low. A decreasing voltage is an indication that the arc gap is closing; stopping the wire feed allows the arc gap to be re-established before the wires become shorted. When the voltage increases, the wire feed restarts. This process occurs very quickly and is transparent to the equipment user except for the fact there is little or no problem with shorted feed wires.

A similar arc-shorting control technique was desired for spraying the titanium. The arc-shorting control system included in this model of the Thermion arc-spray equipment was designed for the much lower arc voltages associated with spraying zinc. The titanium is sprayed at an arc voltage

of 36 to 41 volts compared to 24 to 26 volts for zinc. For this project, Thermion's arc-shorting control system was modified to provide arc-shorting control at the higher titanium arc voltage.

2.2.3 Automated Short Circuit Detection

Short circuits can occur when undetected surface metal, such as a tie wire, provides contact between the rebar and the arc-sprayed anode. When they occur in highly conductive anodes such as zinc, short circuits provide a local, low-resistance path between the anode and the rebar, rendering the system ineffective at distributing the protection current throughout the zone. Since the arc-sprayed titanium anode is much less conductive than the zinc, such short circuits are of less consequence. If the short circuit occurs away from the current distribution plate, resistance in the coating can mask the effect of the short circuit. Although the effect of the short circuit on the system would tend to be more localized, the short circuit would still decrease the effectiveness of the system.

When applying arc-sprayed zinc anodes, an automated short circuit detection system monitors the differential metal corrosion cell voltage occurring between the zinc and steel in contact with the electrolyte within the concrete pores. When this voltage drops too low, indicating a short circuit, the detection system stops the spray equipment to warn the operator of the short circuit condition. A similar system was desired for application of arc-sprayed titanium anodes. However, since passivated titanium is a much less active metal than zinc, the steel-titanium corrosion cell voltage cannot be reliably used for detecting short circuits.

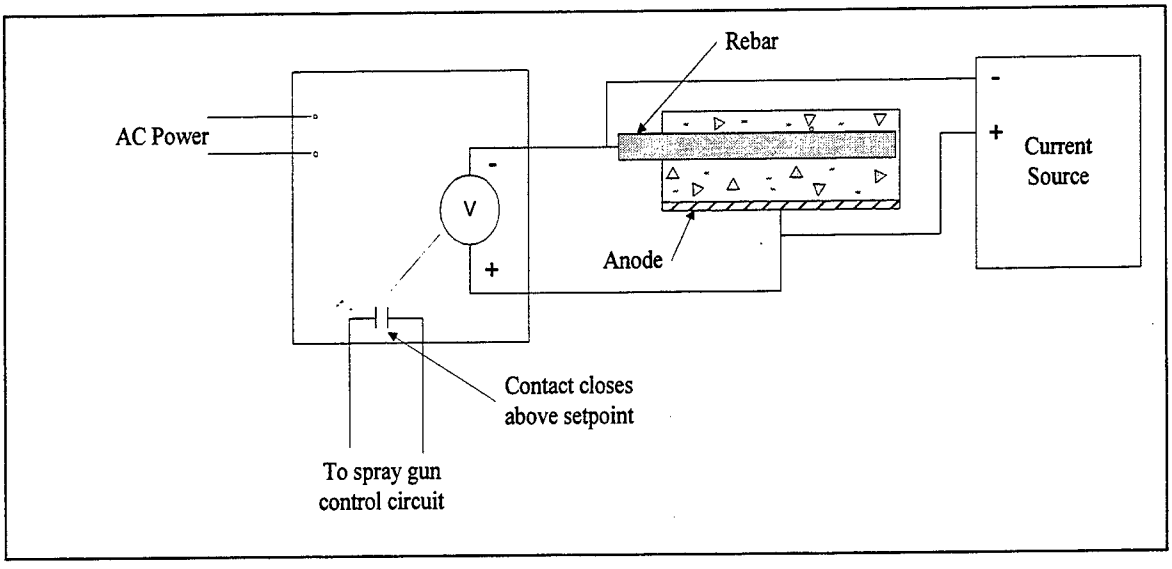

Figure 2.3: Schematic for automated short circuit detection system

A system was assembled using the same system used for spraying zinc, with the addition of a constant current supply to achieve a reliable voltage difference between the rebar and the titanium. A constant current supply was selected because this type of supply is tolerant to short-circuiting. The short detection system consists of an alarm voltmeter with a programmable setpoint and a relay. The meter used for this purpose was model number Q2005AVR2-SPC, manufactured by Newport Electronics. The setpoint for the meter was 0.150 volts, so a voltage difference of 0.15 volts or less between the titanium and the rebar would stop the spray equipment.

The system functioned with one short circuit detected during spraying. There were, however, several features of the system which caused less than optimal performance. Because a constant current source was used, the voltage decreased as the area sprayed increased. Increasing area decreases the equivalent resistance of the circuit because additional parallel resistive paths are added to the circuit. The relationship between equivalent resistance and parallel resistive paths is:

$$R_{Eq} = \frac{1}{\left(\frac{1}{R_1} + \frac{1}{R_2} + \cdots + \frac{1}{R_N}\right)} \qquad \textbf{(2-4)}$$

This fact required periodic adjustments to the amount of current delivered to compensate for the change in surface area. At the same time, polarization of the system caused the voltage of the system to increase. Also, because of the resistance in the titanium coating, current delivery to the titanium must occur near the area being sprayed to minimize voltage drop in the coating. If this is not done, voltage drop in the coating could mask a short circuit. To eliminate this possible problem, temporary connections to the sprayed titanium were made by taping the current source lead to the titanium with duct tape near the area being sprayed.

These three problems made the voltage measurement displayed on the short circuit detection system difficult to interpret. Before large-scale field application, further work is needed on this system to create a more infallible system.

2.2.4 Spray Performance Test

Initial testing was performed to determine the range of possible operating parameters for arc-spraying titanium with the Thermion Bridgemaster system and to determine the effect of the high arc temperature on the equipment. The first step in this process was to determine whether 3.2 mm (1/8-inch) diameter titanium wire could be effectively sprayed. If not, the plan was to proceed using 2.4 mm (3/32-inch) titanium wire that had been successfully sprayed previously. The larger diameter wire was tried because a higher application rate is possible with larger diameter wire. Two 4.55 kg (10 lb) spools of annealed, grade 2 titanium were purchased for this test.

The test spraying of 3.2 mm (1/8-inch) diameter wire was successful, and there were no heat-related problems in an approximately 10-minute spray test. During this test, smooth arc operation was achieved between 250 and 350 amps, resulting in arc voltages between 36 and 41 volts. Air pressure was varied from 586 to 724 kPa (85 to 105 psi).

3.0 SHOP TESTING

3.1 SPRAY PARAMETER OPTIMIZATION

3.1.1 Experiment Design

This portion of the experiment was intended to determine the spray parameters which result in the optimum deposit efficiency and minimum coating resistance. The spray parameters investigated are shown in Table 3.1 below:

Table 3.1: Spray Parameters

Variable	Test Settings	
Current	250, 290, 350 A	
Propellant Pressure	586, 655, 724 kPa	85, 95, 105 psi
Spray Distance	102, 178, 254 mm	4, 7, 10 inches
Propellant Gas	Compressed Air, Nitrogen	
Gun Speed	0.3, 0.46, 0.6 m/s	12, 18, 24 in/s

To obtain constant spray distance and gun speed, samples were sprayed using a custom-designed and fabricated X-Y traversing system. The system used two stepper motors, one each for the X and Y directions, and a programmable indexer to control the spray pattern, gun acceleration and gun speed. Spray distance was set using height adjustments in the support frame legs.

The samples sprayed during this phase were 127 mm x 152 mm x 13 mm (5" x 6" x 1/2") concrete blocks. Since the size of the concrete block was small, the weight of the uncoated samples was in the range of 500 - 600 grams. This allowed the weight gain of the samples, which is required to determine deposit efficiency, to be measured directly on a 2 kg balance. Samples were weighed prior to spraying and immediately after each pass. A minimum of four spray passes was applied to each sample, and additional passes were added as required to achieve a coating resistance of less than 0.5 ohms/square.

An encoder on the wire feed roll shaft was used to measure the length of wire fed through the spray machine. The amount of time the spray head was over the sample was calculated from the gun speed and spray pattern. Since the total spray time was measured, the amount of titanium used over the sample was also calculated. Using the weight gain of the sample and the weight of titanium used, the deposit efficiency of each pass was calculated.

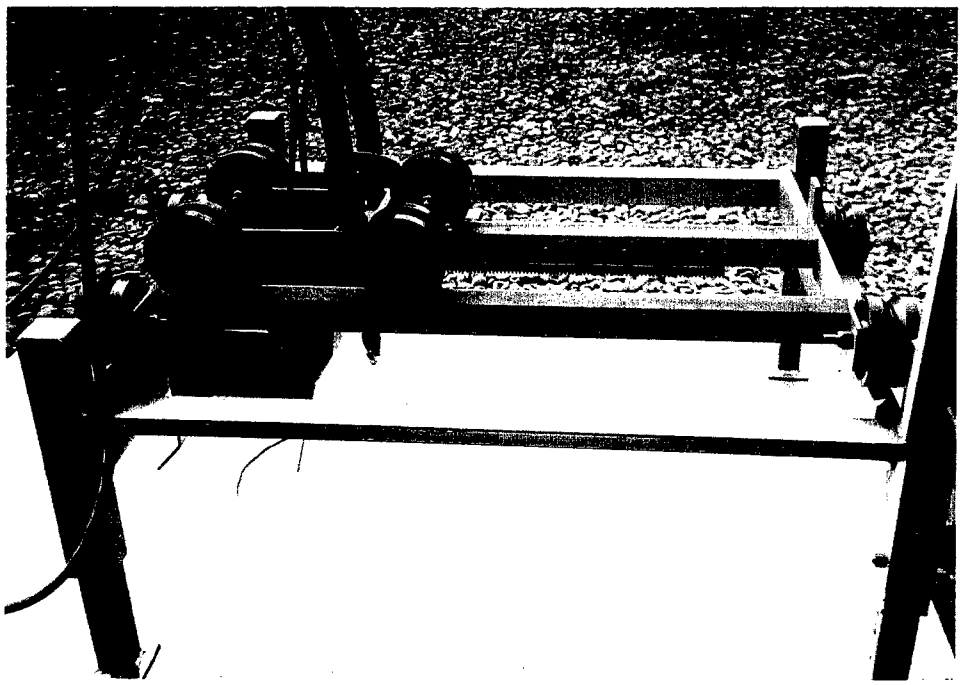

Figure 3.1: X-Y traversing system for spray parameter optimization work.

3.1.2 Deposit Efficiency Measurements

Previous studies have used steel plates for spray parameter studies (*Berndt, et al, 1995*). Measurement of deposit efficiency on concrete samples showed the initial deposit efficiency of arc-sprayed titanium on concrete was much different than the deposit efficiency of sprayed titanium on steel. Deposit efficiency measurements on steel tend to show relatively uniform deposit efficiencies per pass, while measurements on concrete show deposit efficiencies increase significantly over the first three to four passes.

There are two mechanisms to explain the low initial deposit efficiency observed on concrete samples -- water evaporation and particle stream abrasion. Although the concrete samples appeared dry from two months of storage in an office environment, the heat from the spray process may have evaporated some remaining water from the sample. The effect would be to decrease the weight of the sample which would decrease the measured weight gain of the sample and cause an apparent decrease in deposit efficiency.

This effect was observed while preheating a concrete sample prior to spraying it for bond strength testing. The sample was weighed, heated, sprayed and weighed once again. The sample was observed to lose 3.3 g. This is an extreme example, however, since this sample received extended heat input with a torch. The heat input to a sample during spraying is of shorter duration, so the weight loss from water evaporation in the sample is likely to depress the deposit efficiency measurement by only a small amount.

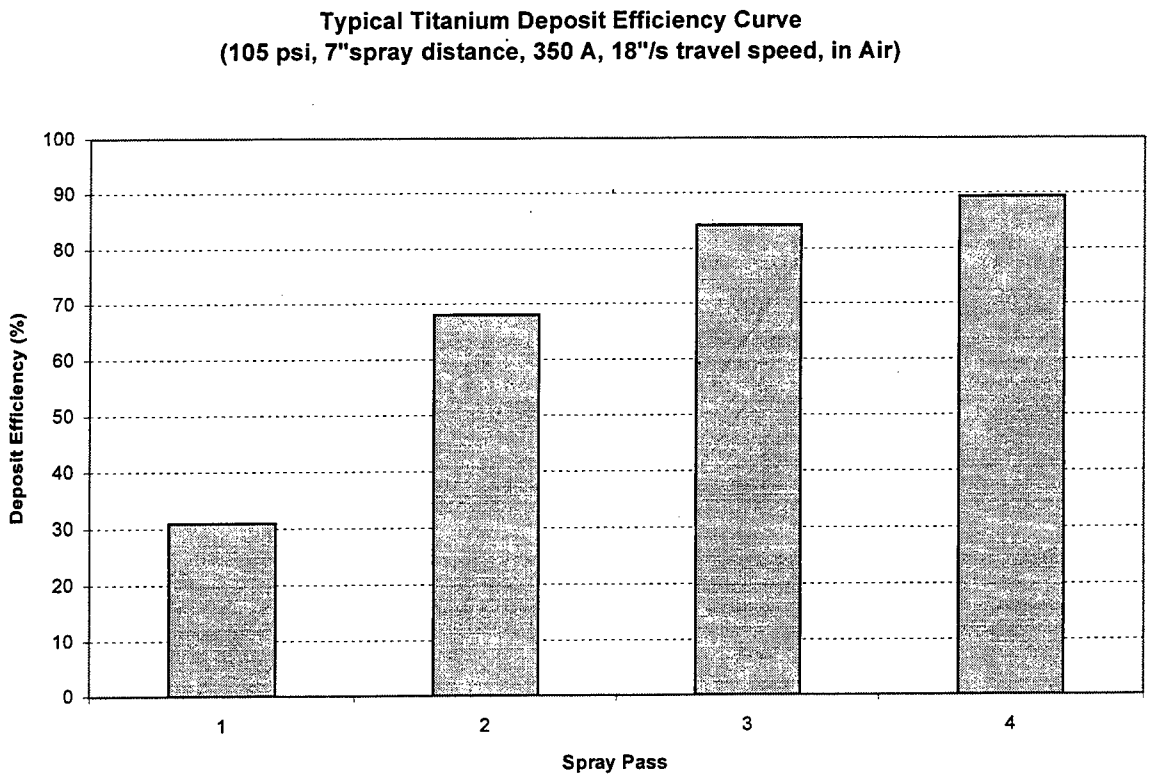

Figure 3.2: Typical titanium deposit efficiency per spray pass

The effect of water evaporation on the deposit efficiency measurement could be determined by oven drying a sample prior to spraying to remove the moisture content. The drying should take place at a low temperature to avoid damaging the concrete. This test was not performed during this study.

A possibly more significant contributor to the low deposit efficiency of the initial pass is the abrading effect of the particle stream from the spray gun. Although not as severe as abrasive blasting, the molten metal droplets impinging on the concrete surface perform a similar function. Visual observations after the first spray pass showed areas where small aggregate was removed from the substrate. As the particles abrade the substrate, not only is there an apparent decrease in deposit efficiency due to a decrease in the weight of the sample, but there is also a real loss in deposit efficiency as the particles that rebound from and break away from the substrate decrease the amount of titanium remaining on the surface.

An additional difficulty with deposit efficiency measurements is that titanium, at high temperatures, readily absorbs and reacts with nitrogen and oxygen, so the sample weight gain measurements include weight gain from these elements. What this means is the calculated deposit efficiency is higher than the true deposit efficiency due to the weight gain from these elements which are present interstitially and as titanium compounds. The coating analysis work

described in Chapter 4 revealed that titanium accounts for an average of 87 weight percent using air atomization and 88 weight percent using nitrogen atomization. Thus, all reported deposit efficiency results based on weight gain are high by 12 – 13 percent.

3.1.3 Parameter Study

The initial plan for this phase of the project was to collect deposit efficiency measurements for various spray parameters. The collected data would then be analyzed using multiple regression techniques to yield a mathematical relationship to account for interactive effects between variables to determine the optimum spray parameters in terms of titanium usage. It was thought that the spray parameters, which yielded the highest deposit efficiency, would be the parameters which should be used for field spraying, since these parameters minimized the use of titanium wire. During this data collection phase, coating resistance data was also collected, in recognition of the possibility that deposit efficiency would not provide a complete picture.

The attempt to construct a multiple regression equation for the relationship between deposit efficiency and the spray parameters was unsuccessful. The best fits to the data yielded R^2 values around 40%, leaving 60% of the variability in the data unexplained. An attempt to develop a relationship between coating resistance and the spray parameters provided only a slight improvement in the regression results, generating an R^2 value of about 50%. This was not very surprising since reasonably good correlation was expected between coating resistance and deposit efficiency. However, when a simple regression equation was constructed for the relationship between coating resistance and deposit efficiency, the R^2 value was less than 20%, indicating very little relationship between these two dependent variables.

During the shop-spraying portion of this study, two samples were sprayed on glass plates to allow an investigation of the coating thickness at the specified coating resistance. Each sample was sprayed at different spray parameters, so an investigation of the effect of changing parameters on coating properties was possible. The glass plate provided a uniform substrate that allowed determination of an average coating thickness. The coating was uniform, varying by about ± 0.013 mm (0.0005") across the sample. Thickness measurements were made by measuring the thickness of the glass plate with a micrometer at specific points on the plate, both prior to spraying and again after spraying. The calculated results are shown in Table 3.2.

Both samples were sprayed at a gun travel speed of 0.457 m/s (18 in/s). From these results, it is apparent that changes in spray parameters can have a large impact on the structure of the coating. These two sets of parameters led to large differences in the coating density, which resulted in a 2:1 difference in coating resistivity. The electrical characteristics of the coating determine how well the coating will perform its intended purpose of distributing current throughout the zone. These results indicate, for arc-sprayed titanium anodes, deposit efficiency should not be the primary dependent variable for optimization of spray parameters.

Table 3.2: Properties of Coatings on Glass Plates

Parameters	Avg. Thickness	Wt. Gain	Coating Resistance	Coating Density	Coating Resistivity
Air, 724 kPa, 300A, 178 mm (Air, 105 psi, 300A, 7")	0.19 mm (0.007")	7.17 g (0.25 oz)	0.375 ohms	1.95×10^{-3} g/mm^3	6.99×10^{-3} ohm-cm
N, 793 kPa, 275 A, 152 mm (N, 115 psi, 275 A, 6")	0.13 mm (0.005")	6.53 g (0.23 oz)	0.27 ohms	2.6×10^{-3} g/mm^3	3.43×10^{-3} ohm-cm

Another multiple regression relationship was attempted using the sample resistance multiplied by the sample weight gain as the dependent variable. This product accounts for the interaction between these two variables and provides a measure of effectiveness of the deposited titanium for conducting current. To gain a better understanding of this product (r x w), it is useful to study Equation 2-3. Although the relationship between thickness and weight gain is imperfect, due to variation in coating density and difficulty in measuring weight gain as discussed in Section 3.1.2, weight gain is expected to have a fairly high correlation with coating thickness. This means that the product of coating resistance (in ohms/square) and weight gain yields a quantity which is highly correlated to coating resistivity.

The log of the product was taken to account for non-linearity in the relationship between the dependent variable and the independent variables. The resulting equation provided a good fit to the data with a degree of freedom adjusted R^2 value of 80.9%. The best fit relationship is as follows:

$$\ln(r \times w) = 0.633 - 6.75 \times 10^{-6}(c \times d^2) + 3.33 \times 10^{-3} d^2 - 0.366p \qquad \textbf{(3-1)}$$

where: r = coating resistance in ohms/square,

w = sample weight gain in grams,

d = spray distance in cm,

c = current in amps, and

p = propellant (0 = air, 1 = nitrogen)

For the data collected during this study, the pressure of the propellant and the gun travel speed did not prove to be significant variables, so they were removed from the resulting equation. These variables, however, have been reported as significant in other work (*Berndt, et al, 1995*).

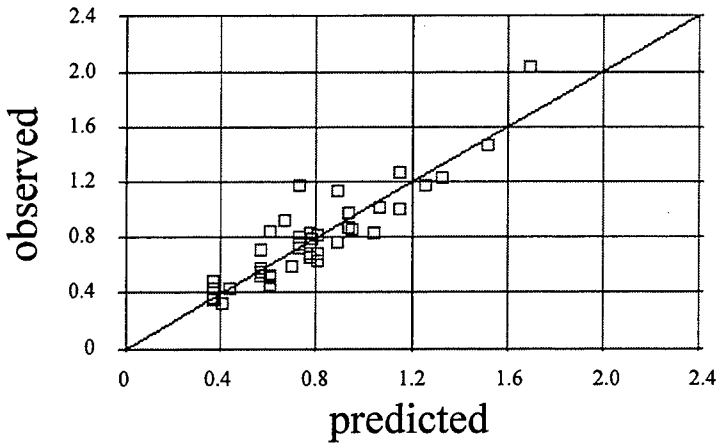

Figure 3.3: Fit of regression equation to empirical data

The most effective coating for distributing current is the coating with the lowest resistivity, approximated by the product of r and w in the regression analysis. The results of the regression analysis demonstrate the spray parameters which reduce the coating resistivity: nitrogen propellant, low spray distance and high current. Figure 3.3 and Table 3.3 present the results of the multiple regression analysis.

Although the regression results indicate that low spray distance, nitrogen propellant and high current provide a more effective coating, the shop spraying experience indicated that, at 102 mm (4"), 350 A, and a gun speed of 0.3 m/s (12 in/s), the coating tended to burn and blister. Additionally, operating the gun at 350 A produced sufficient heat to melt a hole in the arc shield on the gun. Manual application of arc-sprayed titanium, therefore, was specified to take place at around a 150 mm (6") spray distance and 300 A.

It is important to note that spray distance appears in the regression equation as a squared term, so the effect of a change in spray distance is amplified. At the specified spray parameters (300 A, air), the equation predicts that changing from a 100 mm (4 ") spray distance to 150 mm (6 ") requires a 17% increase in sample weight gain to achieve the required coating resistance of 0.5 ohms/square. The second term also indicates an interactive effect between current and the square of spray distance. For a given spray distance, higher current tends to produce a more effective coating, but the effect of higher current is greater for larger spray distances.

Table 3.3: Multiple Regression Analysis Results

Dependent variable: ln(Sample Resistance in ohms/square * Sample Wt gain in grams)

Parameter[1]	Estimate	Standard Error	T Statistic	P-Value
Intercept	0.633	0.045	13.9	0.00
Current * $(Distance)^2$	-6.75×10^{-6}	1.65×10^{-6}	-4.1	0.00
$(Distance)^2$	0.0033	0.00052	6.4	0.00
Propellant	-0.366	0.046	-8.0	0.00

[1] Current in amps; Distance in cm; Propellant: 0 = air, 1 = N_2

Analysis of Variance

Source	Sum of Squares	Df	Mean Square	F-Ratio	P-Value
Model	3.77	3	1.26	58.9	0.00
Residual	0.81	38	0.021		
Total (corr.)	4.58	41			

R-squared = 82.3 %
R-squared (adjusted for d.f.) = 80.9 %
Standard error of est. = 0.15
Mean absolute error = 0.104

Equation 3-1 provides a mathematical expression that can be used for predicting coating performance for a given set of spray parameters. Its most appropriate use, however, is to provide an understanding of the effect of changes in the independent variables on the dependent variable. Care must be taken when using Equation 3.1 for prediction outside the range of the data (in Table 3.1) used to construct the equation.

Equation 3-1 indicates that the use of nitrogen as a propellant is beneficial. Compressed air, however, was specified for use on the Depoe Bay Bridge because it is remote from nitrogen supply points. The spray equipment uses a large volume of propellant during spraying, so the extra costs to get nitrogen on site more than offset the savings in titanium usage from improved deposition efficiency.

Note that a titanium consumption rate, calculated from Equation 3-1 for a set of spray parameters, is a minimum consumption rate. The actual titanium usage is expected to be significantly higher due to titanium wire waste, inability to spray the coating to exactly the maximum permitted coating resistance, and variability in spray parameters during manual spraying.

3.2 BOND STRENGTH TESTING

Bond strength testing was performed by first affixing a 50 mm aluminum disk to the Ti coating surface with epoxy and then measuring the force required to pull the coating from the concrete plate substrate with a Proceq Dyna Z-5 adhesion tester. Since the titanium coating is thin, a potential problem was penetration of the epoxy through the coating to the concrete plate substrate. To minimize this problem, a viscous, quick setting epoxy was used. The epoxy used for this bond strength measurement was Duro Master Mend® TM-81 epoxy. To provide a reference point for the bond strength measurements, a bond test was taken on a bare concrete sample with the strength of 1710 kPa (248 psi). Measurement of the concrete area on the removed aluminum disks indicated bond failure occurred approximately 30-40% within the concrete and 60-70% at the interface or within the titanium.

Eight 127 mm x 152 mm (5" x 6") concrete plates were prepared for testing the bond strength of the sprayed titanium coating. All concrete plates, except Plate 1, were sprayed using nitrogen as the propellant. The nitrogen samples were sprayed with the same spray parameters [759 kPa (110 psi), 178 mm (7") spray distance and 290 amps]. The plate sprayed using air was sprayed at 724 kPa (105 psi), 100 mm (4") spray distance and 250 amps. The bond test results are shown in Table 3.4.

Table 3.4: Bond Strength Test Results from Concrete Plates

Plate	Bond Strength		Resistance $\left(\frac{ohms}{square}\right)$	Treatment
	kPa	psi		
1	1028	149	0.23	Sprayed using air
41	1269	184	0.365	Surface temp. = 17.2°C (63°F), N_2
2	924	134	0.34	Surface temp. = 18.9°C (66°F) , N_2
43	1414	205	0.37	Surface temp. = 13.3°C (56°F) , N_2
44	945	137	0.305	Surface temp. = 104.4°C (220°F) , N_2
45	1214	176	0.28	Sample submerged in water for 15 minutes immediately prior to spraying, N_2.
46	1221	177	0.37	Surface temp. = 1.1°C (34°F), N_2
47	1428	207	0.385	Surface temp. = 8.3°C (47°F), condensation present on surface prior to spraying, N_2.

Although these results cannot be considered an extensive study of the bond strength of titanium to concrete, multiple regression analysis applied to the test data for coatings sprayed using nitrogen propellant (Plates 1 & 45 excluded) resulted in Equation 3-2 (See Table 3.5.).

$$B = -3720 + 13400r + 5.6t \qquad (3\text{-}2)$$

where: B = coating bond strength in kPa,

r = coating resistance in ohms/square, and

t = substrate temperature in °C.

Table 3.5: Regression Results for Equation 3-2 (Plate 1 and Plate 45 data excluded)

Regression Statistics	
Multiple R	0.97
R^2	0.94
Adjusted R^2	0.90
Standard Error	69.55
Observations	6

ANOVA

	df	*SS*	*MS*	*F*	*Significance F*
Regression	2	229673	114837	23.74	0.014
Residual	3	14510	4837		
Total	5	244183			

Parameter	*Coefficients*	*Std. Error*	*t Stat*	*P-value*	*Lower 95%*	*Upper 95%*
Intercept	-3720	938.30	-3.96	0.029	-6706.02	-733.81
Coating Resistance	13400	2504.85	5.35	0.013	5428.36	21371.47
Surface Temperature	5.6	1.89	2.96	0.059	-0.41	11.59

The fit was good with an adjusted R^2 of 90%. The large coefficient for coating resistance in Equation 3-2 shows that the effect of coating resistance factors on coating bond strength is much more significant than that of substrate temperature. Since coating resistance is inversely proportional to coating thickness, Equation 3-2 demonstrates that increasing coating thickness decreases bond strength.

Although the fit of the equation to the observed values is good, Equation 3-2 should be used with care outside the resistance range of the data points (0.305 to 0.385 ohms/square). Equation 3-2 predicts a bond strength of zero at a coating resistance of 0.27 ohms/square, which contradicts observed bonding at lower coating resistance during the spray parameter optimization portion of this study. The equation's predictive capability is limited, and it should be used simply as an indicator of the effect these variables have on coating bond strength.

The titanium spray appeared to be much more tolerant of surface moisture than zinc. Reasonable bond strength was achieved even on the sample submerged in water prior to spraying. However, the presence of a high amount of moisture in the concrete appears to affect deposit efficiency, since more spray passes were required to achieve the desired coating resistance.

3.3 APPLICATION OF TITANIUM SPRAY OVER SUBSTRATE CRACKS

The ability of arc-sprayed titanium to span cracks in the concrete substrate was investigated by preparing concrete samples with simulated cracks. The samples were prepared using the 127 mm x 152 mm (5" x 6") concrete samples prepared for the spray parameter optimization study (Section 3.1). A sample was sawed in half and glued to an unsawed sample. Shims were placed between the two halves of the cut sample to achieve the desired crack width. (See Figure 3.4.)

The largest crack which the coating successfully bridged measured 0.127 mm (0.005") in width. This crack required eight spray passes to span the crack and achieve the desired coating resistance. The spray settings used for this test would typically achieve the desired resistance on an uncracked sample in four spray passes. Wider cracks require more spray passes creating a thicker coating. As the coating becomes thicker, it can begin to experience bonding problems.

An arc-sprayed titanium coating is not tolerant of cracks in the substrate. Only very narrow cracks can be spanned by the titanium without excess thickness build-up. During the field spraying, this limitation did not appear to create problems. Most cracks on the structure, although wide on the surface, become very narrow with depth. The coating seems to be able to adequately span such cracks by penetrating into the crack and bridging the crack where it becomes narrow. Where wide cracks did exist, there were typically sufficient alternate paths for current flow around the crack to provide current distribution to all areas of the anode. Had any problem cracks been discovered during the field application, titanium strips would have been installed to conduct current across the crack.

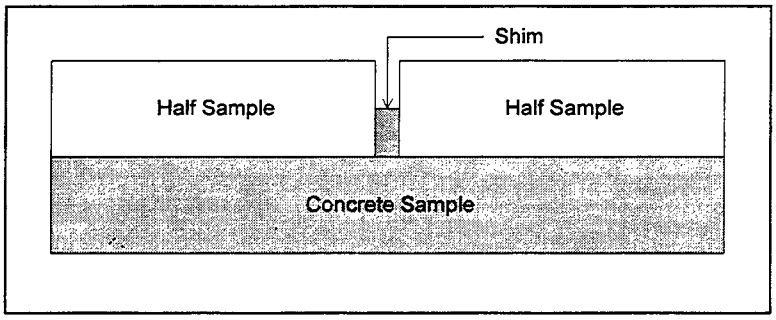

Figure 3.4: Crack simulation

3.4 OPERATIONAL CONCRETE SLABS

Five operational concrete slabs were prepared for accelerated testing. The dimensions for the concrete slabs cast for this experiment were 230 mm x 330 mm x 44 mm (9" x 13" x 1.75"). The slabs were cast with No. 16 expanded metal mesh covering the full dimensions of the bottom of

the form. A thin layer of the concrete mixture was spread in the bottom of the form prior to placing the mesh to ensure no voids behind the mesh. The resulting concrete cover over the mesh was 32 mm (1.25"). Steel wire was welded to the mesh and extended above the top surface of the form to provide a means to make electrical connections to the mesh.

The concrete mix design is shown in Table 3.6. The water : cement ratio was 0.48, which is similar to, but probably slightly less than typical for ODOT's older coastal structures. A smaller aggregate size was used in the slabs to obtain uniform current distribution, something not possible when large aggregate is present. To simulate marine-exposed concrete and to increase the conductivity of the slabs, 99.9% pure, reagent–grade sodium chloride was added to the concrete mix at the rate of 3 kg/m^3 (5 lb/y^3) of concrete.

Table 3.6: Concrete Mix Design

Cement	259 kg	570 lbs
Coarse aggregate[a]	704.5 kg[b]	1550 lbs[b]
Sand	738 kg[b]	1624 lbs[b]
Water	125 kg	275 lbs

[a]4.75 mm to 6.35 mm (0.19" to 0.25")
[b]Saturated surface dry basis

The samples received the titanium spray and catalysis treatments shown in Table 3.7. The catalyst was brush applied to the titanium coating on the slab surface approximately two months after the slabs were sprayed. The catalyst was applied to each slab (except Sample #5) with a power supply connected to provide 29 mA of cathodic protection current per square meter of anode surface area. Sample #5 was not catalyzed and serves as a control sample. Catalyst was brush applied to Sample #50 with the sample inverted to simulate an overhead surface. The purpose of simulating the overhead surface was to verify that the catalyst could effectively adhere to the titanium/concrete interface without assistance from gravity. The operating data to date (see Figure 3.5) indicate that overhead surfaces can be effectively catalyzed.

Table 3.7: Operational Concrete Slab Treatments

Slab	Propellant	Pressure	Current	Distance	Notes
5	Air	105	300	152 mm	Uncatalyzed sample, R = 0.2 Ω/square
6	Air	105	300	152 mm	Catalyzed R = 0.2 Ω/square
48	N_2	115	275	152 mm	Catalyzed R = 0.16 Ω/square
49	N_2	115	275	152 mm	Catalyzed R = 0.155 Ω/square
50	N_2	115	275	152 mm	Catalyzed simulated overhead surface R = 0.155 Ω/square

A hole was drilled in the concrete slab in the center of the sprayed titanium surface to make the electrical connection to the coating. Silicone was inserted into the hole prior to installing a plastic expansion anchor. A steel washer and ring connector was placed over a steel screw, and the screw was inserted into the anchor. Corrosion problems were expected from using steel parts for this anode connection, but properly sized titanium components could not be located.

The five slabs were connected in series to a power supply operating in constant current mode. Current was applied to the slabs for one month before they were transferred to a humidity-controlled room at the Albany Research Center, U.S. Department of Energy, Albany, Oregon. The slabs received cathodic protection current at an accelerated level of approximately 29 mA/m^2 (2.5 mA/ft^2) until the conclusion of the study.

The power supply output current and the output voltage (five slabs in series) for the first 300 days of operation is shown in Figure 3.5. The smoothing of the output current at day 227 corresponds to replacement of the constant current power supply.

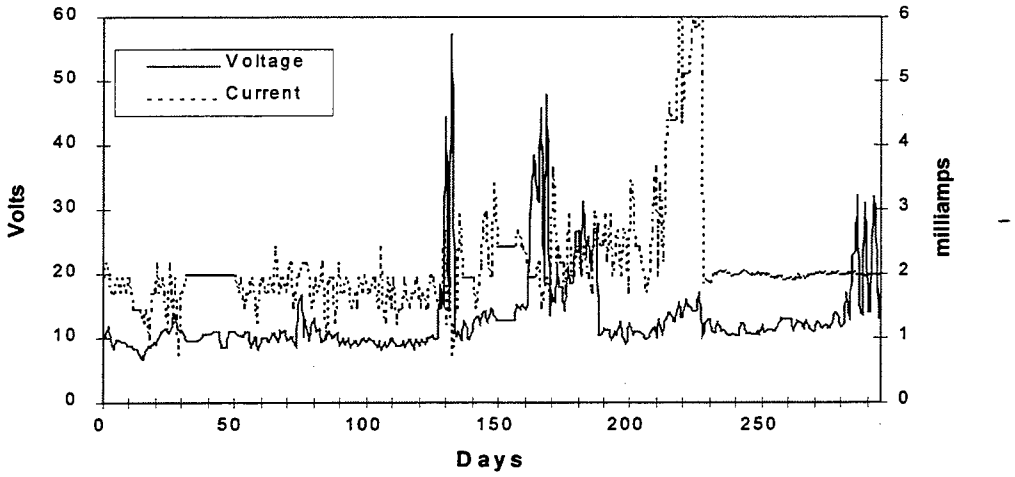

Figure 3.5: Voltage and current for five Ti-coated slabs in series

The expected corrosion was experienced and can be seen in Figure 3.5 as a rapid increase in system voltage beginning on day 131. That corrosion problem was corrected by replacing all slab connections, but a general rise in voltage level and some additional voltage peaks indicate that additional corrosion problems occurred. Slab connections were replaced once again on day 289.

As shown in Figure 3.6, the individual slab voltages for the catalyzed samples remained fairly stable. Individual slab voltages were measured independently of the steel electrical connections to the slabs. Although the voltage of the uncatalyzed slab did not increase as expected, its voltage exhibited large fluctuations with humidity variations. The peaks beyond day 300 are

related to variations in the room humidity from 30 to 100 pct relative humidity (RH). Although the voltage of the catalyzed samples also fluctuated with humidity, the uncatalyzed sample was much more sensitive to humidity changes.

The voltage of the uncatalyzed sample was expected to climb because the passivating oxide layer that forms on bare titanium is expected to resist current flow until the anodic breakdown potential of titanium is exceeded. Above this potential, titanium is no longer passive and corrosion will occur. The anodic breakdown potential varies with the purity of the titanium, the composition of the electrolyte and the temperature. As a reference point, the anodic breakdown potential of grade 2 titanium in a solution of 1 N NaCl at 25°C is 11.0 volts versus a Ag/AgCl reference electrode (*Boyer, et al, 1994*).

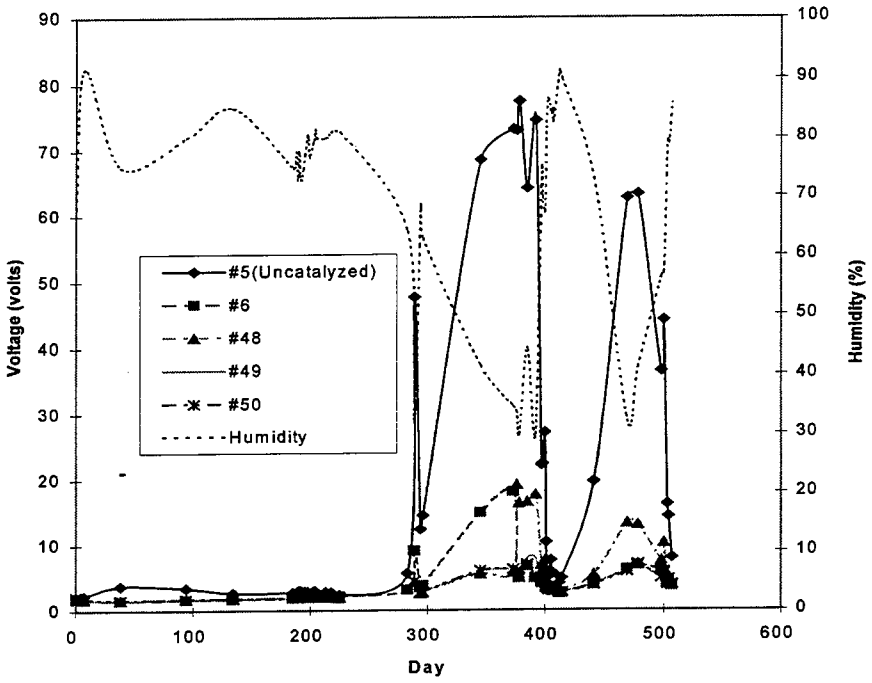

Figure 3.6: Individual slab voltages

Previous work performed by Eltech Research Corporation showed a substantial voltage increase for an uncatalyzed slab beginning at approximately 130 days (*Berndt, et al, 1995*). The current density for the Eltech study was 21.5 mA/m^2 (2 mA/ft^2). The uncatalyzed sample in the present study (Slab 5) showed large voltage increases during low humidity. The slab voltage returned to a voltage level similar to the catalyzed samples when the humidity increased.

4.0 COATINGS CHARACTERIZATION

Thermal spray coatings of titanium metal are increasingly being used in industrial applications, particularly to produce corrosion and wear resistant surfaces for the chemical process industries. These coatings are typically applied in an inert atmosphere or a vacuum using shrouds or chambers to prevent or minimize reactions with the atmosphere *(Krepski, 1993a)*. Coatings of titanium applied in air or nitrogen, as done in the present project *(McGill, et al., 1996; Bennett, et al., 1995)*, to form a nonconsumable anode for impressed current cathodic protection systems on reinforced concrete structures are a novel use of thermal spray technology. Titanium oxidation, which occurs in such applications, may affect the performance and service life of the anode. One method investigated here to reduce titanium oxidation was atomization of the molten titanium with a gas different from compressed air. Another method that could prove useful, though not investigated, would incorporate metals with higher valence ions such as niobium, tungsten or tantalum at low concentrations in the titanium. "Doping" in this way can reduce the titanium oxidation kinetics as a consequence of the semiconducting properties of the titanium oxidation products *(Hauffe, 1965; Kubaschewski and Hopkins, 1962a)*.

An understanding of the properties of thermal-sprayed titanium coatings requires an understanding of the significant alloy-atmosphere reactions and their effect on the chemistry, electrochemistry and mechanical properties of the anode coatings. Macroscopic and microscopic chemical analyses provide the basis for such an understanding. They show the degree to which reactions with the atmosphere have occurred and the spatial distribution of the reaction products within the coating. In doing so, they link the chemistry of the coating with the properties of the anode.

Thermal-sprayed titanium anodes are nominally a thin layer of coalesced titanium metal droplets or "splats." The surface of these splats may have oxidized as they impinged on the object being coated. At the beginning of this study, there was an appreciation that a number of reaction products could result from this oxidation. It was understood these reaction products could have significant effects on the properties of the resulting anode. These properties could include: anode structure, bond strength to substrate, mechanical durability, internal stresses, volume resistivity, contact resistance, and the thermodynamics and kinetics of electrochemical reactions supported by the anode and useful in impressed current cathodic protection (ICCP) systems for reinforced concrete bridges.

4.1 SELECTED PROPERTIES OF THE TI-O-N SYSTEM

Tabulated property data useful for interpreting and understanding the nature and performance of thermal-sprayed titanium anodes are presented below. The significant titanium-environment interactions for thermal-sprayed titanium anodes involves oxygen and nitrogen. The ternary Ti-

O-N system has not been well studied. Much more is known of the binary Ti-O and Ti-N systems. For this reason, the combined effects of oxygen and nitrogen on the anode will necessarily have to be inferred from the properties of binary systems.

In this regard, phase diagrams describe the temperature-composition-structure relationships for alloy systems under thermal and chemical equilibrium. Thermal-spray coatings would appear to be highly nonequilibrium systems, perhaps even with properties typical of rapid solidification (*Krepski, 1993b*). However, even for systems characterized by high cooling rates, equilibrium phase diagrams can provide useful guidance on composition and structure at the solidification front (*Collins, 1986*). Shown below are binary phase diagrams for Ti-O, Figure 4-1, and Ti-N, Figure 4-2. Tables 4.1 and 4.2 give specific composition and structure data associated with these phase diagrams.

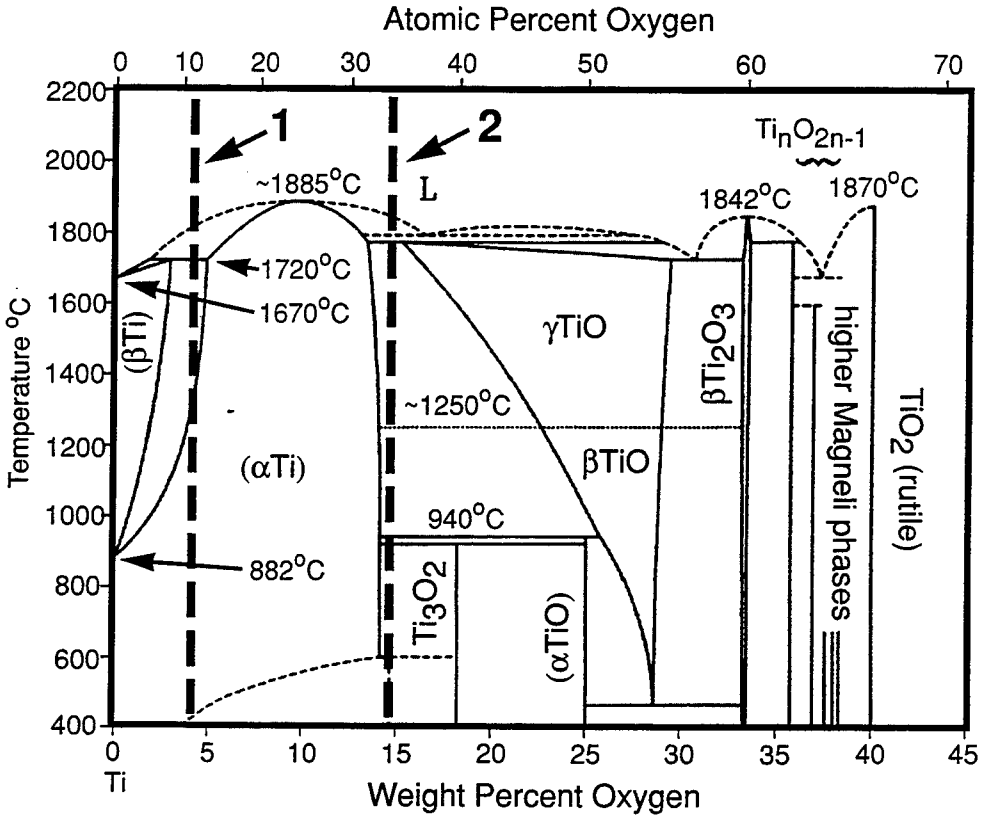

Figure 4.1: Ti-O phase diagram *(Oxygen-Titanium, "Alloy Phase Diagrams", 1992)*. Lines 1 and 2 represent the average O content of some typical splats in the arc-sprayed Ti anode.

Table 4.1: Stable Low-Pressure Phases In The Ti-O System.[a]

Phase	Composition, wt pct O	Space group
β-Ti	0 - 3	Im3m
α-Ti	0 - 13.5	$P6_3/mmc$
Ti_3O	~8 - ~13	P3lc
Ti_2O	~10 - 14	P3ml
γ -TiO	15.2 - 29.4	Fm3m
Ti_3O_2	~18	P6/mmm
β -TiO	~24 - 29.4	---
α-TiO	~25.0	A2/m or B*/*
β -$Ti_{1-x}O$	~29.5	I222
α -$Ti_{1-x}O$	~29.5	I4/m
β -Ti_2O_3	33.2 - 33.6	R3c
α -Ti_2O_3	33.2 - 33.6	R3c
β -Ti_3O_5	35.8	---
α -Ti_3O_5	35.8	C2/m
α'-Ti_3O_5	35.8	Cc
γ-Ti_4O_7	36.9	P1
β-Ti_4O_7	36.9	P1
α-Ti_4O_7	36.9	P1
γ-Ti_5O_9	37.6	P1
β-Ti_6O_{11}	38.0	A1
Ti_7O_{13}	38.3	P1
Ti_8O_{15}	38.5	A1
Ti_9O_{17}	38.7	P1
TiO_2, rutile	40.1	$P4_2/mnm$

[a] *Oxygen-Titanium, "Alloy Phase Diagrams", 1992.*

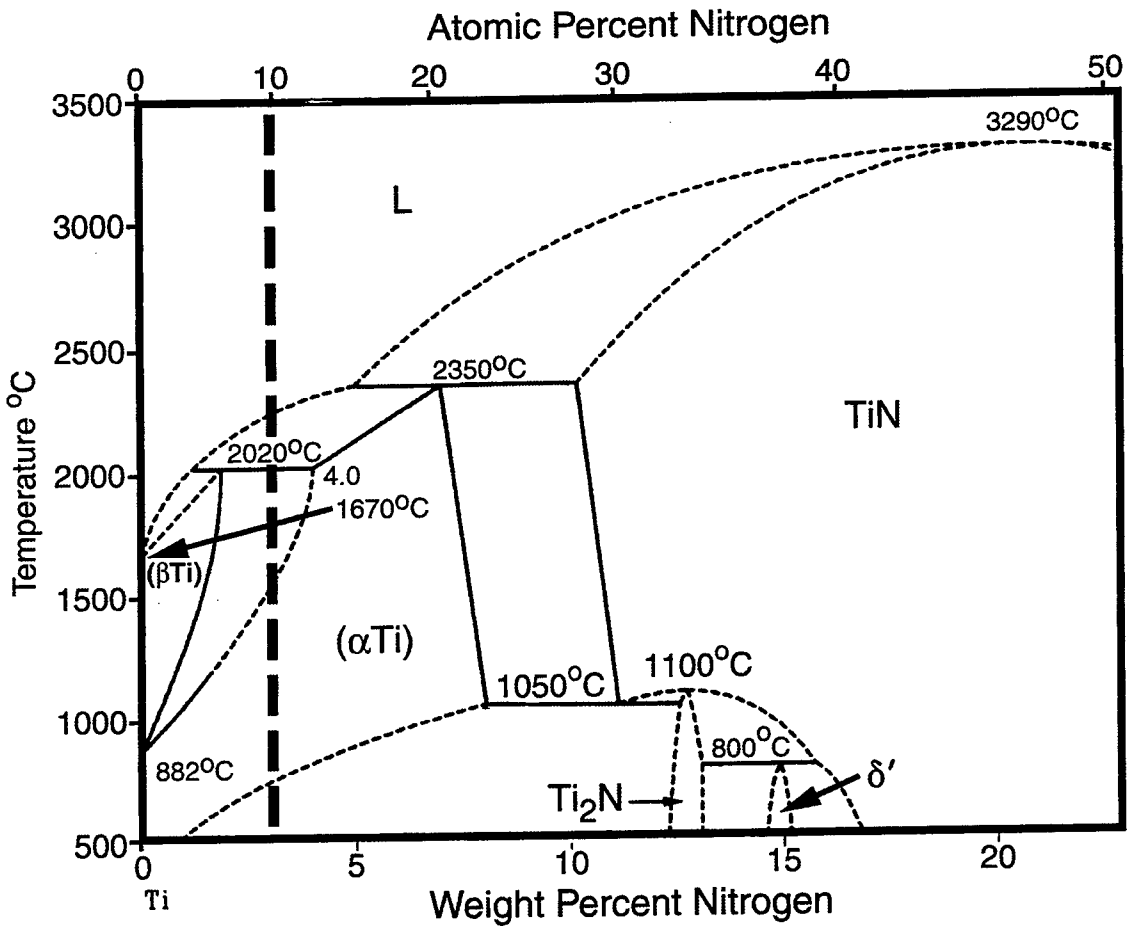

Figure 4.2: Ti-N phase diagram *(Nitrogen-Titanium, "Alloy Phase Diagrams", 1992)*. Line 1 represents the average N content of typical splats in the arc-sprayed Ti anode.

Table 4.2: Stable Low-Pressure Phases In The Ti-N System.[a]

Phase	Composition, wt pct N	Space group
α-Ti	0 – 8	$P6_3/mmc$
β-Ti	0 - 1.9	Im3m
Ti_2N	~13	$P4_2/mnm$
TiN	10 - >22.6	Fm3m
δ'	~15	$I4_1/amd$
ω	~0	---

[a] *Nitrogen-Titanium, "Alloy Phase Diagrams", 1992.*

The physical properties of compounds that could form during thermal spraying of titanium using either air or nitrogen as the atomizing gas are given in Table 4.3. In Table 4.3, volume ratio is the ratio of the compound molecular volume to the atomic volume of the metallic titanium in the compound.

Table 4.3: Physical Properties Of Titanium And Its Oxides And Nitrides.

Compound/Element	Molecular Weight	Melting Point, °C	Density, g/cm³	Volume ratio
Ti	47.9	1660	4.50	1.00
TiO	63.9	1750	4.93 [a]	1.20 [b]
TiO_2	79.9	1840	4.25 [a]	1.73 [b]
TiN	61.9	2930, N_2 liberated	5.44 [c]	1.09 [b]

[a] *"Engineering Property Data on Selected Ceramics-Single Oxides," 1981*
[b] *Kubaschewski and Hopkins, 1962a*
[c] *"Engineering Property Data on Selected Ceramics-Nitrides," 1976*

The transport properties of potential anode constituents are given in Table 4.4. Electrical resistivity is particularly important, because resistance measurements are used by the thermal spray applicators to gage when the titanium coating is sufficiently conductive. Coefficient of linear thermal expansion and thermal conductivity can aid in understanding the highly dynamic mass and heat transfer processes occurring when the molten titanium droplets are in flight and after they "splat" on the structure surface to be incorporated into the developing anode coating. Conduction classification suggests possible ways, such as alloying the Ti with other elements *(Hauffe, 1965; Kubaschewski and Hopkins, 1962a and 1962b)*, to alter splat oxidation processes and to change the coating electrical resistivity.

Table 4.4: Transport Properties Of Titanium And Its Oxides And Nitrides.

Compound/Element	Conduction Classification	Resistivity, μohm-cm	Coefficient Linear Thermal Expansion, μinch/inch-°C	Thermal Conductivity, cal/s-cm-°C
Ti	metallic	50 [b] 42 [c]	8.5 [d]	0.0495 [e]
TiO	metallic [a]	350 [b]	---	---
TiO_2	n-type [a]	>3 x 10^7 [f]	9.4 [g]	0.0156 [h]
TiN	n-type [a]	15.5 [i] 21.7 [j]	8.0 [g]	0.0579 [k]

[a] *Kubaschewski and Hopkins, 1962a*
[b] *Gruber and Krautz, 1986.*
[c] *Weast, 1980a.*
[d] *Weast, 1980b.*
[e] *Weast, 1980c.*
[f] *Campbell and Sherwood, 1967.*
[g] *Lackey, et al., 1987.*
[h] *Weast, 1980d.*
[i] *Munster and Sagel, 1956.*
[j] *Blocher, 1967*
[k] *"Engineering Property Data on Selected Ceramics-Single Oxides", 1981.*

4.2 THERMAL-SPRAYED TITANIUM COATINGS PREPARATION

Coatings were prepared for chemical analyses on glass and concrete substrates using the twin-wire arc-spray process and either air or nitrogen as the atomizing gas. Substrate surface preparation prior to coating was conducted as follows: (1) concrete -- sandblasted to provide suitable anchor tooth and air blasted to remove dust; (2) glass -- degreased with ethyl alcohol and dried. A Thermion Bridgemaster twin-wire arc-spray unit with a PowCon 630 SMP inverter power supply was operated at or near optimum conditions for thermal spray titanium applications. Using air as the atomizing gas, titanium was thermal-sprayed at 37 volts (dc) and 300 amps, a gas pressure of 0.62 – 0.76 MPa (90-110 psi), and a spray distance of 15 - 23 cm (6-9 inches). Using nitrogen as the atomizing gas, titanium was sprayed at 36-40 volts (dc) and 275 amps, a gas pressure of 0.72 – 0.79 MPa (105-115 psi), and a spray distance of 15 – 23 cm (6-9 inches).

Feedstock for the coatings was Grade 1 titanium wire, 3.2 mm (1/8-inch) diameter, specification AWS A5.16-90 ERTI 1, containing (in wt pct) 0.004 N, 0.01 C, 0.0009 H, 0.10 Fe 0.054 O, bal Ti. The wire was annealed in air at 700° C (1300° F) for 1 hour and air-cooled, then pickled in HNO_3-HF to remove oxides from the surface. Mechanical properties of the wire were: tensile strength, 376 MPa (54,500 psi); yield strength (0.2%), 257 MPa (37,200 psi); elongation, 36.6 pct; and reduction of area, 72.2 pct (*Gernitsky, 1995*). Hardness values were measured in the laboratory using a Knoop diamond microindenter and a 1000g load. The hardness of the cold drawn Ti wire averaged KHN_{1000} 173 (HRB 83) and the annealed wire averaged KHN_{1000} 122 (HRB 61). The measured hardness of the annealed wire was close to that reported in the literature for annealed Grade 1 Ti, HRB 64.7 to 87.1 (*Donachie, 1988a*).

Figure 4.3 shows schematically the process by which molten titanium droplets, "splats," form the anode coating. Molten droplets leave the electric arc and are entrained in the atomizing gas. In flight, droplets react with atmospheric gases and an oxidized skin forms on their surface. They impinge or "splat" on the substrate surface at high velocity, rupturing the oxide skin and spreading laterally over the surface. Because of the difference in density between the oxidized skin of the droplet and the unreacted metal core, the unreacted core will spread over the surface of solidified splats and/or substrate, and fragments of the oxidized skin will be entrained on the splat surface. In the process, smaller droplets may rebound out of the still molten splat, contributing to the overspray or returning to the coating as small solid particles. Not all droplets are fully molten when they hit the substrate surface and these globules, if they adhere to the surface, roughen the coating and can be the source of coating defects. Voids may form or be trapped along the interface between successive splats, when the splats do not completely weld to each other.

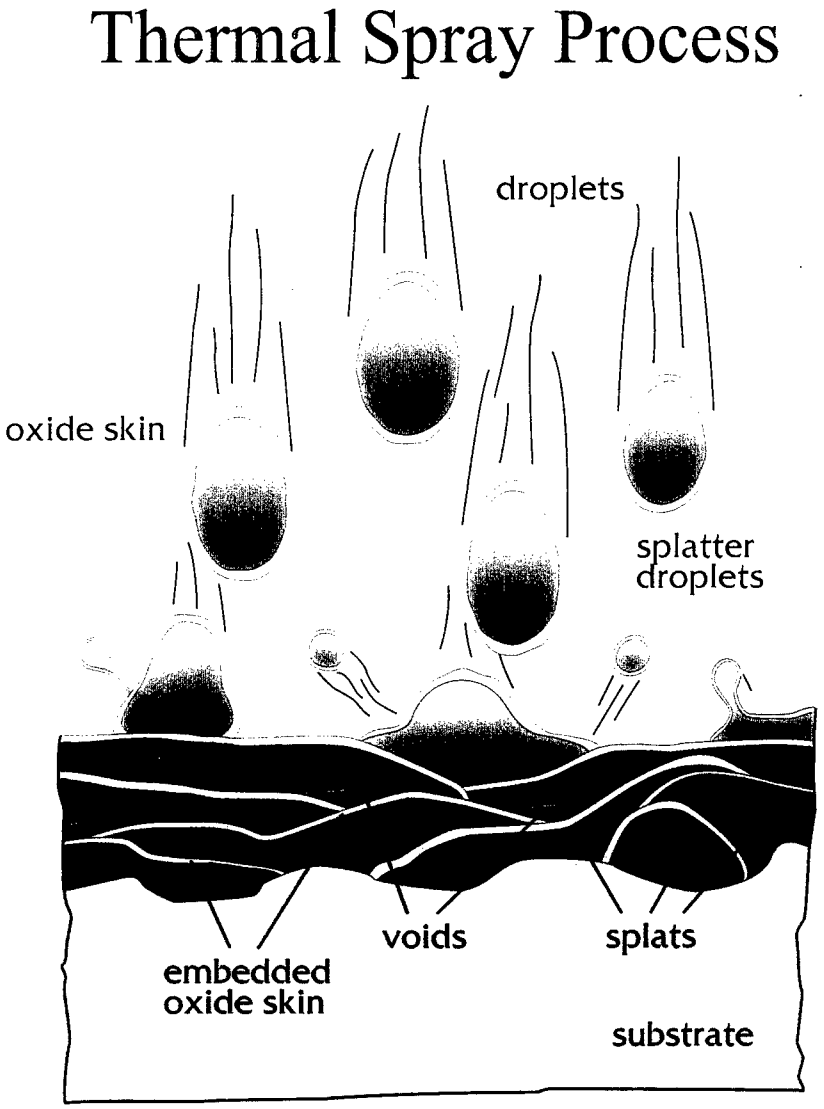

Figure 4.3: Schematic representation of the thermal-spray coatings process for titanium anodes.

Coatings prepared in this way from titanium were used for coatings characterization and are described in Table 4.5. The coatings were 50-150 μm (2 - 6 mils) in thickness and were formed by multiple passes of the spray head. Some were sprayed using air from a compressor as the atomizing gas; others were sprayed using bottled nitrogen (99.9% pure) as the atomizing gas. All samples were sprayed without any special shrouding to exclude ambient air from convective mixing with the beam of molten metal spray. The first four samples (TiCA, TiCN, TiPA, and TiPN) were sprayed in a laboratory environment using a robotic-mounted spray gun , Figure 3.1, to control the spray pattern and achieve a uniform coating thickness. The fifth sample, TiQA, was applied with a hand-held gun in the field to a quartz glass cylinder using air as the atomizing

gas and a Miller Model FC-6 constant potential DC welding power supply substituted for the PowCon 630 SMP.

Table 4.5: Samples Used For Characterization Of Arc-Sprayed Titanium Coatings.

Sample Identification	Substrate	Atomizing Gas
TiCA (See Table 3.4)	concrete plate	Air
TiCN (See Table 3.4)	concrete plate	Nitrogen
TiPA (See Table 3.2)	Pyrex glass plate	Air
TiPN (See Table 3.2)	Pyrex glass plate	Nitrogen
TiQA	quartz glass cylinder	Air

4.3 CHARACTERIZATION TECHNIQUES

Specific information sought from the chemical analyses were: (1) an identification of the phases present and their relative abundance in the coating; (2) the amount of interstitial oxygen and nitrogen associated with metallic titanium phases; and (3) the structure of the anode coating. It was also important to determine if there were benefits from using nitrogen as the atomizing gas compared to air. Because of the complex nature of the coatings, no single analytical technique directly gives this information. Coatings thermal-sprayed on glass and on concrete were examined by several techniques, to provide a more detailed understanding of the surface and bulk chemistry of the coatings. These techniques included X-ray fluorescence (XRF) and X-ray diffraction (XRD), gas analysis, electron microprobe (EMP), scanning electron microscopy (SEM), analytical scanning electron microscopy (ASEM), X-ray photoelectron spectroscopy (XPS) and coating resistance.

4.3.1 X-Ray Fluorescence (XRF)

Coating samples were analyzed by energy-dispersive X-ray fluorescence spectrometry to determine if contaminants (other than oxygen and nitrogen) were picked up by the titanium during the arc-spray process. A Philips PV9500 spectrometer system equipped with a Rh X-ray tube and Si-Li semiconductor detector was used. The samples analyzed were TiPA, TiPN and TiCA. They were degreased and dried before analysis. Coating flakes were stripped from TiPA and TiPN with a razor blade. The flakes were finely ground in an agate mortar and mounted on cellophane tape for analysis. Coatings were also analyzed *in situ* on small samples cut from TiPA, TiPN and TiCA.

4.3.2 X-Ray Diffraction (XRD)

Coating samples were analyzed by X-ray diffraction to identify crystalline phases and to determine if gases were dissolved interstitially in metallic Ti. Phase and lattice parameter analysis was performed using a Philips APD 3720 diffractometer system. The instrument was

equipped with an automated goniometer, Cu X-ray tube, variable divergence slit, focusing graphite monochromator and scintillation counter. The samples analyzed were TiPA, TiPN, TiQA and TiCA. Coating flakes were stripped from TiPA, TiPN and TiQA with a razor blade and finely ground in an α-alumina mortar for analysis. In addition, coatings were analyzed *in situ* using small samples cut from TiPA, TiPN and TiCA.

The presence of interstitial and altered crystallographic structure was determined by precise measurements of anode lattice parameters using the NIST 640 silicon powder "d" spacing standard. The measurement error for lattice parameter analyses was ± 0.001 A for the powder samples. The error for the *in situ* samples is larger because of sample roughness and the presence of fragments of low absorption coefficient glass substrate. Sample TiQA, which contained some glass fragments from mechanically stripping the coating from the substrate, was mixed with NBS "d" value standard and re-measured. The results, after correcting the data, showed measurement error increased to ± 0.002 A due to the glass substrate; the error for *in situ* samples was 2 to 3 times larger than for the powder samples. Since the error in lattice parameter measurement is about the same for both the "a" and "c" axes, the c/a ratio should not be significantly affected by these errors.

4.3.3 Gas Analysis

Coating samples were analyzed for total concentration of oxygen and nitrogen using a LEECO 436 oxygen-nitrogen gas analyzer. The samples analyzed were TiPA and TiPN. Coating flakes were stripped from the substrates with a razor blade. Coatings on Pyrex glass sprayed using air atomization were more adherent than those using nitrogen atomization.

Samples of the coating flakes were weighed and then sealed in a tin capsule for analysis. The coatings samples gave normal shaped gas evolution curves with a single peak for oxygen and some tailing of the oxygen peak. The gas analysis results represent the total oxygen and nitrogen present in the coating as Ti compounds plus that contained interstitially within metallic Ti.

An NBS glass standard was run to determine if adhering glass fragments affected the oxygen analyses. The NBS glass curve was very different from the coatings curve with three distinct gas evolution peaks. A small peak was present in the range where oxygen was evolved from the coatings samples. The two larger peaks appeared later in the determination. The absence of these larger peaks in the determination of oxygen in the coating samples suggests the glass fragments did not contribute oxygen to the coating samples analyses.

4.3.4 Analytical Scanning Electron Microscopy (ASEM)

Coatings were analyzed with an analytical scanning electron microscope and an electron microprobe (EMP) to determine the local composition and physical structure of the coatings. The results should establish the relationship between local chemistry, structure and properties of the coatings. Samples examined were TiPA, TiPN, TiCA and TiCN. All were analyzed *in situ*

by cutting samples from the sprayed substrate. Cross-sectioned samples were mounted on-edge in epoxy and polished to a 1 μm diamond surface finish. Coatings were also examined normal to the plane of the coating. Carbon coating was not required prior to analysis because of good coating conductivity. However, coatings formed using air atomization were less conductive than those using N atomization.

Images of the coatings were obtained with a LEO Stereoscan S440 scanning electron microscope using secondary and backscattered electrons. Secondary electron images yield primarily topographical detail. Backscattered electron images are sensitive to average atomic number of the analysis volume and accentuate composition differences. Since voids and cracks are one extreme in the spectrum of atomic number (i.e., ~ 0), the backscattered electron images show these features in stark detail.

XRF microanalyses were performed using the LEO Stereoscan S440 and an Oxford 3PC wavelength dispersive spectrometer with 4 crystals and an Oxford eXLII energy dispersive spectrometer with atmospheric thin window for detection of low atomic number elements. XRF microanalyses were also performed with a CAMECA SX-50 electron microprobe equipped with four wave-length dispersive spectrometers. The beam voltage was 10 kV. All analytical results were ZAF (atomic number, absorption and fluorescence) corrected and based on calibration standards. Interferences between x-ray lines and high absorption by matrix constituents presented special problems for the titanium alloys considered in this work.

Because the Ti_{LL} line overlaps the $N_{K\alpha}$ line, resulting in a peak combining the contributions from both lines, it was necessary to reduce the analytical results from the ASEM in the following way. Titanium values were obtained using the $Ti_{L\alpha}$ line. Nitrogen values were obtained by the technique used for Manual Point Analysis or that for Automatic Point Analysis. Comparisons of the results obtained by these techniques with those from standards are given in the following two subsections (4.3.4.1 and 4.3.4.2).

4.3.4.1 Manual Point Analysis

For manual point analyses (5 μm diameter analysis area), the nitrogen signal was extracted from the combined peak by subtracting the contribution from the Ti_{LL} line. This was done in the following way. The peaks of interest were ZAF corrected using the Quadrilateral ZAF procedure to give estimates of Ti, N and O in the sample. These results were then manually corrected by extracting the Ti_{LL} line from the combined peak. Ti_{LL} peak height was estimated from its known relationship to the $Ti_{L\alpha}$ peak. The Ti_{LL} peak height was then subtracted from the height of the combined peak to yield a computed $N_{K\alpha}$ peak height. Table 4.6 gives results for wave-length dispersive analyses of a series of Ti-N standards. It demonstrates the effectiveness of the procedure for computing the $N_{K\alpha}$ peak in a sample with a Ti matrix, and there is good agreement between the composition of the standards and that computed using the manual peak extraction procedure.

Table 4.6: Manual Point Wave-Length Dispersive X-Ray Analyses Of Ti-N Standards.

Ti-N Standard, weight pct N (atomic pct N)	Measured Nitrogen Content, weight pct N	
	Quadrilateral ZAF	Quadrilateral ZAF With Manual Correction
0.99 (3.3)	15.4	0.0
5.6 (16.9)	21.3	6.3
9.4 (26.2)	24.4	8.7
19.6 (45.5)	32.1	19.2

4.3.4.2 Automatic Point Analysis

For automatic point analyses along a predetermined line (5 μm wide analysis line), e.g., element depth profile, the nitrogen signal was extracted using the Oxford ZAF-4/FLS software. In this procedure, the assumption is made that the Ti_{LL} peak does not contribute significantly to the combined peak and that, in fact, the combined peak is due solely to the $N_{K\alpha}$ peak. Peak seeking was used to carefully construct a window for removing the x-ray background. Table 4.7 gives the results for automatic wave-length dispersive analyses of a series of Ti-N standards. The table shows that the analytical results agree moderately well with the standards at high nitrogen concentrations. It also shows, as one might expect as the Ti_{LL} contribution becomes more significant with decreasing nitrogen content, that this agreement deteriorates rapidly at lower nitrogen concentrations. These results do suggest that the element depth profiles provide reasonable values for the upper bounds of the nitrogen concentration in the titanium coatings. They also suggest that the depth profiles can effectively delineate the variation in composition of the coating cross-section.

Table 4.7: Automatic Point Wave-Length Dispersive X-Ray Analyses Of Ti-N Standard.

Ti-N standard, weight pct N (atomic pct N)	Measured nitrogen content using Oxford ZAF-4/FLS procedure, weight pct N
5.6 (16.9)	12.3
9.4 (26.2)	14.5
19.6 (45.5)	22.0

4.3.5 X-Ray Photoelectron Spectroscopy (XPS)

Coatings were analyzed by X-ray photoelectron spectroscopy to determine the composition of the outer surface of the coating and the chemical state of the reactants. Samples examined were TiPA and TiPN. Samples were analyzed *in situ* by cutting samples from the sprayed substrate. In addition, coating flakes were scraped from TiPA with a razor blade. The Ti-glass interface was also examined using these flakes.

Analyses were performed on a Surface Science Laboratory SSX-100 ESCA spectrometer, using a 600 μm analysis spot size. Argon ion sputter etching, at a rate of 0.7 A/s based on SiO_2, was used to incrementally remove material from the sample surface to produce a profile of coating composition as a function of coating depth (i.e., depth-profile). Two survey scans were performed on each sample, one before etching and one after etching for 180 s, to determine the elements present and the binding energies to use for depth profiling. Areas selected for the depth profiles were different from those used for the survey scans. Using the adventitious C peak as a guide, there was no evidence of charging of the sample surfaces during analysis.

4.3.6 Coating Resistance

Applicators of thermal-sprayed titanium anodes use anode resistance to judge when the coating is sufficiently conductive to meet design specifications. For service as an electrical conductor, designers of impressed current CP systems need a conductor with low , uniform resistance and a resistance that does not change significantly with electrochemical age.

Anode resistance was measured with a spring-loaded, multi-pin probe developed by ODOT. The probe was used to measure anode resistance during coating application and during electrochemical aging (see Section 2.2.1). The four-point measurement technique was used to eliminate contact resistance. Coating resistance, R, was measured with a Nilsson 400 ac-resistance meter. The probe dimensions were width of probe (w) and distance between the two rows of pins (i.e., coating length, L). The probe was designed so that $w = 1$. Average coating thickness, T, was measured from anode cross-section SEM photomicrographs. Coating apparent resistivity, ρ_a, was then computed from Equation 2-3 as:

$$\rho_a = R \cdot T \cdot w / C \cdot L = R \cdot T / C \qquad \textbf{(4-1)}$$

4.4 CHARACTERIZATION RESULTS

4.4.1 X-Ray Fluorescence

Samples were examined by optical microscopy before XRF analysis. Many flakes from TiPA and TiPN had a thin layer of glass firmly attached to the substrate side of the coating. The outer surface, in contact with the atmosphere, appeared oxidized and had mixed blue and gold hues. When *in situ* samples on glass, TiPN and TiPA, were backlit by strong illumination, light was visible through the coating at many discontinuities, voids and cracks. X-ray fluorescence spectra from flakes of TiPA and TiPN showed strong peaks for Ti and Si, with lesser amounts of K and Fe present. Si and K are constituents of Pyrex glass and likely present due to the glass fragments attached to the flakes. Spectra collected from *in situ* coatings on glass had smaller Si and Fe peaks. Estimates of the Fe concentration in the *in situ* coatings, using fundamental parameters, indicated less than 0.1 wt pct Fe. This is similar to the concentration of Fe present in the Grade 1 Ti, feed wire.

4.4.2 Gas Analyses

The results of the LEECO gas analyses are shown in Table 4.8. Carbon levels were typically around 1 atomic percent (at pct). Oxygen concentrations were of the same magnitude but always greater than nitrogen concentrations. Nitrogen concentrations were slightly higher using N atomization than air atomization. Based on these measurements, the oxygen concentration did not appear to change with the atomization gas. Assuming titanium is present in the coating as metallic Ti, TiO and TiN (or Ti(O,N)), the atomic ratio (O+N)/Ti suggests lower bounds for the fraction of titanium present as metallic Ti, ranging from 10 to 18 pct of the total titanium. The amount of metallic Ti would be substantially higher if some of the O and N were present interstitially in the metallic Ti matrix.

Table 4.8: Results of LEECO gas analyses on coating samples.

Sample ID	Concentration, at pct				(O + N)/Ti
	C	O	N	Ti	atom ratio
TiPA	1.4	29.4	15.0	54.2	0.82
TiPN	1.2	29.6	17.3	51.9	0.90

4.4.3 X-ray Diffraction

The major phases identified in all of the samples, both flake and *in situ*, were α-Ti having a close-packed hexagonal (hcp) structure, and a phase similar to TiN and/or TiO having a face-centered cubic (fcc) structure. No TiO_2 or the body-centered cubic (bcc) β-Ti were detected in the anode. The pattern for flakes from TiPA and TiPN also included a peak associated with Ti_5Si_3. This peak was not present in the results for the *in situ* samples. It suggests a reaction between the molten Ti droplets initially contacting the substrate and the glass. It is likely Ti_5Si_3 is the phase responsible for a good bond between the Pyrex glass substrate and the coating. The fcc phase appeared to have a slightly contracted lattice structure (relative to the lattice dimensions for the TiN standard), which is not unusual considering the nonequilibrium nature of the thermal spray coating.

The XRD measurements showed the α-Ti lattice was expanded, suggesting substantial O and N were dissolved interstitially in the hcp phase. In pure α-Ti free of interstitial elements, the lattice parameters are "a"-axis 2.950 A, " c"-axis 4.682 A, and the c/a ratio is 1.587 (*Bars, et al., 1983*). In the thermal-sprayed anode, the measured values were 2.973 A, 4.788 A and 1.610. They show the lattice is greatly expanded along the "c"-axis and suggest that the α-Ti lattice is saturated with O and/or N. Saturation values in α-Ti for N and O are 22 (*Bars, et al., 1983; Etchessahar, et al., 1987*) and 34 (*Bumps, et al., 1953*) at pct, respectively. It is probable the α-Ti lattice contains both interstitial O and N.

The measured "a"-axis for the fcc phase was 4.215 A. γ-TiO is the only titanium oxide with a fcc structure. The "a"-axis for γ-TiO is 4.180 A at 46 at pct O and decreases with increasing O content (*Bumps, et al., 1953*). The "a"-axis for the fcc TiN is 4.207 A at 28.5 at pct N and

increases with increasing N content (*Etchessahar, et al., 1987*). The likely structure for the fcc phase probably includes both O and N (e.g., Ti(O,N)) and represents a minimum in lattice energy generated by the inclusion of the larger N ion (1.71 A radius) in the same structure as the smaller O ion (1.32 A radius) (*Weast, 1980e*). A minimum lattice energy would correspond to a measured "a"-axis value intermediate between the values for the TiN and γ-TiO structures. The inclusion of two different sized ions in the fcc Ti(O,N) lattice should distort the lattice compared to both TiN or γ-TiO. The Ti(O,N) structure is expected to be brittle.

The relative amount of each major phase was estimated from the diffraction data and is given in Table 4.9. There was substantially less α-Ti and more Ti(O,N) present in the *in situ* samples than in the flake samples. This apparently is because the *in situ* results represent the outer surface of the coating, which is more strongly influenced by reactions between the coating and the atmosphere, whereas the flake results represent the average composition of the coating.

There was no difference in lattice expansion for coatings on Pyrex and on quartz. The c/a ratios for all of the samples suggest the α-Ti matrix contains a substantial amount of interstitial N and/or O. For the flake samples, there was less α-Ti and more Ti(O,N) in coatings formed using N atomization than air atomization, whereas there was no difference for the *in situ* samples.

Table 4.9: Relative amounts of major phases in coatings, estimated from XRD results.

Sample ID	c/a ratio for α-Ti lattice	α-Ti vol fraction	Ti(O,N) vol fraction
TiPA, *in situ*	1.609	0.28	0.72
TiPN, *in situ*	1.612	0.28	0.72
TiPA, flake	1.612	0.44	0.56
TiPN, flake	1.614	0.35	0.65
TiQA, flake	1.610	0.43	0.57

4.4.4 Analytical Scanning Electron Microscopy

A cross-section of TiPA, typical of coatings applied on glass using air atomization, is shown in Figure 4.4. Figure 4.4(a) is a secondary electron (SE) image and Figure 4.4(b) a backscattered electron (BE) image of the same area. The BE image shows banding in the coating related to composition differences which is not evident in the SE image. The banding is produced by composition gradients in the coating. The bright portion of each band contains higher concentrations of metallic Ti and the dark portion higher concentrations of Ti(O,N). Thus, the anode structure consists of a series of gradient bands (representing individual splats) with a bright layer richer in α-Ti and a dark layer richer in Ti(O,N). These alternating α-Ti-rich and Ti(O,N)-rich layers give the anode a highly layered appearance.

ASEM depth profiles, Figure 4.5, also indicate the presence of gradient bands by the "saw-tooth" pattern of the Ti curve. Seven gradient bands are suggested by the depth profile data and can be matched visually with seven distinct gradient bands in Figure 4.4(b). The depth profile data

show the bright layer of each band contains 70-80 at pct Ti while the dark layer contains 60-65 at pct Ti. The balance is N and O in amounts varying between 10 and 20 at pct each.

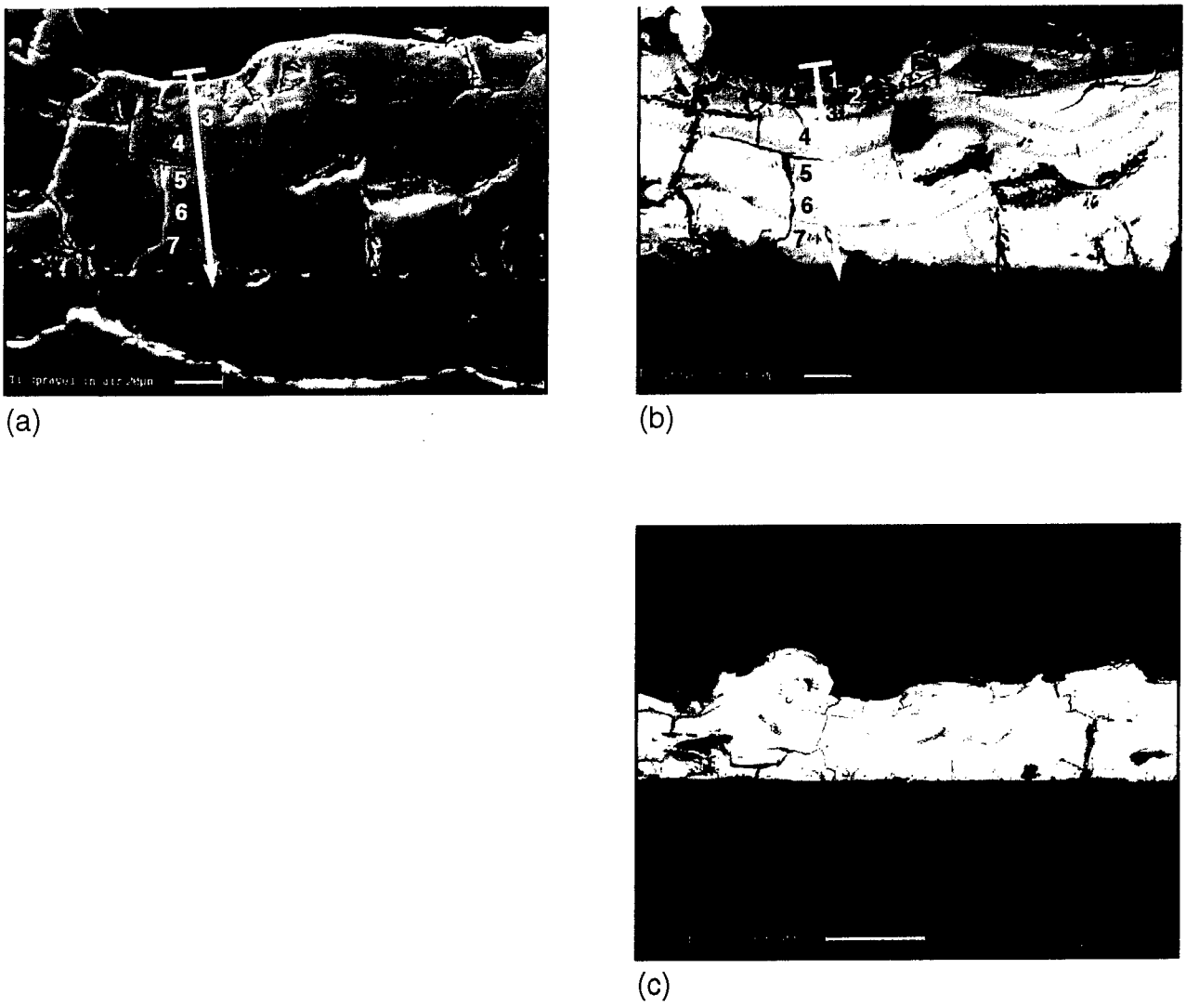

Figure 4.4: SEM photomicrographs of TiPA cross-section: (a) SE image, 350X; (b) BE image, 350X; (c) BE image, 140X. Arrow shows path of ASEM traverse and the location of seven Ti gradient bands in the coating.

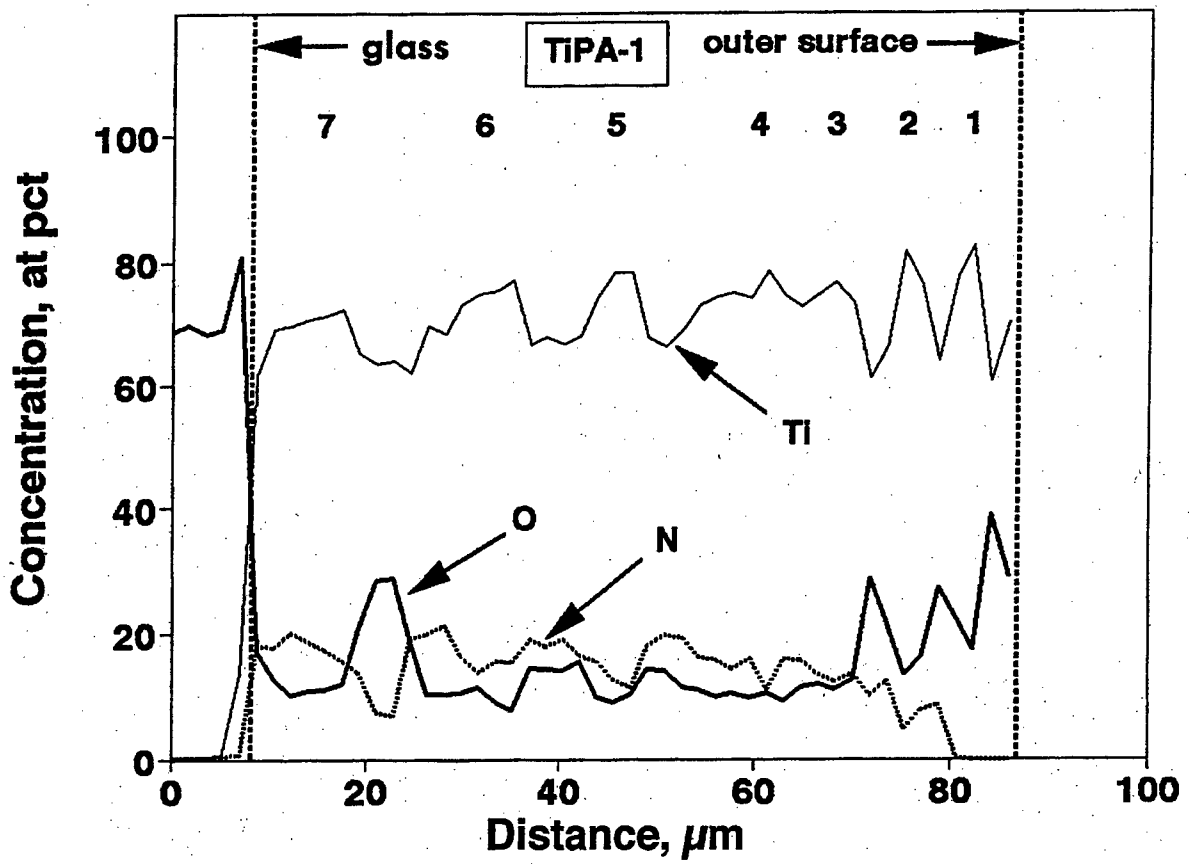

Figure 4.5: ASEM composition depth profile for TiPA cross-section shown in Figure 4.4. Glass-coating interface and outer surface of coating are shown with seven Ti gradient bands.

Typically the dark layer of each gradient band is characterized by a sharp interface with a light layer on the side towards the substrate, and by a diffuse interface with a light layer on the side away from the substrate. The sharp interface appears to mark the interior surface of the oxidized skin formed on the molten droplet, the boundary between the oxidized skin and the unreacted interior (see Figure 4.3). Upon striking the substrate, the oxidized skin splits and unfolds, probably in fragments, with the fragments entrained on the surface of the splat. The diffuse interface marks the outer surface of the oxidized skin of an earlier splat, which has reacted with the core contents of the next splat as it impacts the surface.

In other words, the denser Ti-rich core of a droplet crushes against the oxidized surface of the earlier splat, then spreads over it, leaving an α-Ti rich layer covering the oxidized surface of the earlier splat. In doing so, the Ti-rich core reacts with the oxidized layer, convective mixing may occur in the process, and produces the diffuse interface. Concentration gradients would appear to be substantially higher at the sharp interface than the diffuse interface. Furthermore, other properties of the coating dependent upon composition and structure (internal stress, electrical

resistivity, density and mechanical properties) will also vary more rapidly across the sharp interface.

Figures 4.4(a) and 4.4(b) show substantial cracking of the coating both parallel and normal (transverse) to the coating/glass interface. Cracks parallel to the coating/glass interface tend to form in the dark layer of the gradient bands where the concentration of Ti(O,N) is highest and the coating would be most brittle. The cracks tend to propagate along the sharp interface as opposed to other locations within the dark layer. This, of course, is the region with the highest concentration gradient.

The transverse cracks suggest the presence of substantial internal stresses within the coating. The transverse cracks are typically linked by parallel cracks extending along the dark layer of the gradient bands. In many cases the transverse cracks cross multiple gradient bands, indicating cracking was delayed until coating application was partially or totally completed and the coating was cooling.

Figure 4-4(c) shows no separation of the coating from the glass substrate. Instead cracks within the coating are shown to cross the coating-substrate interface and link into a network of cracks in the substrate, caused perhaps by thermal shock to the glass. For this to occur, the bond between the coating and substrate must be fairly strong to prevent parting at this interface. XRD results show that the Ti reacted with the glass substrate to form Ti_5Si_3. This compound probably accounts for the strong bond of the coating to glass.

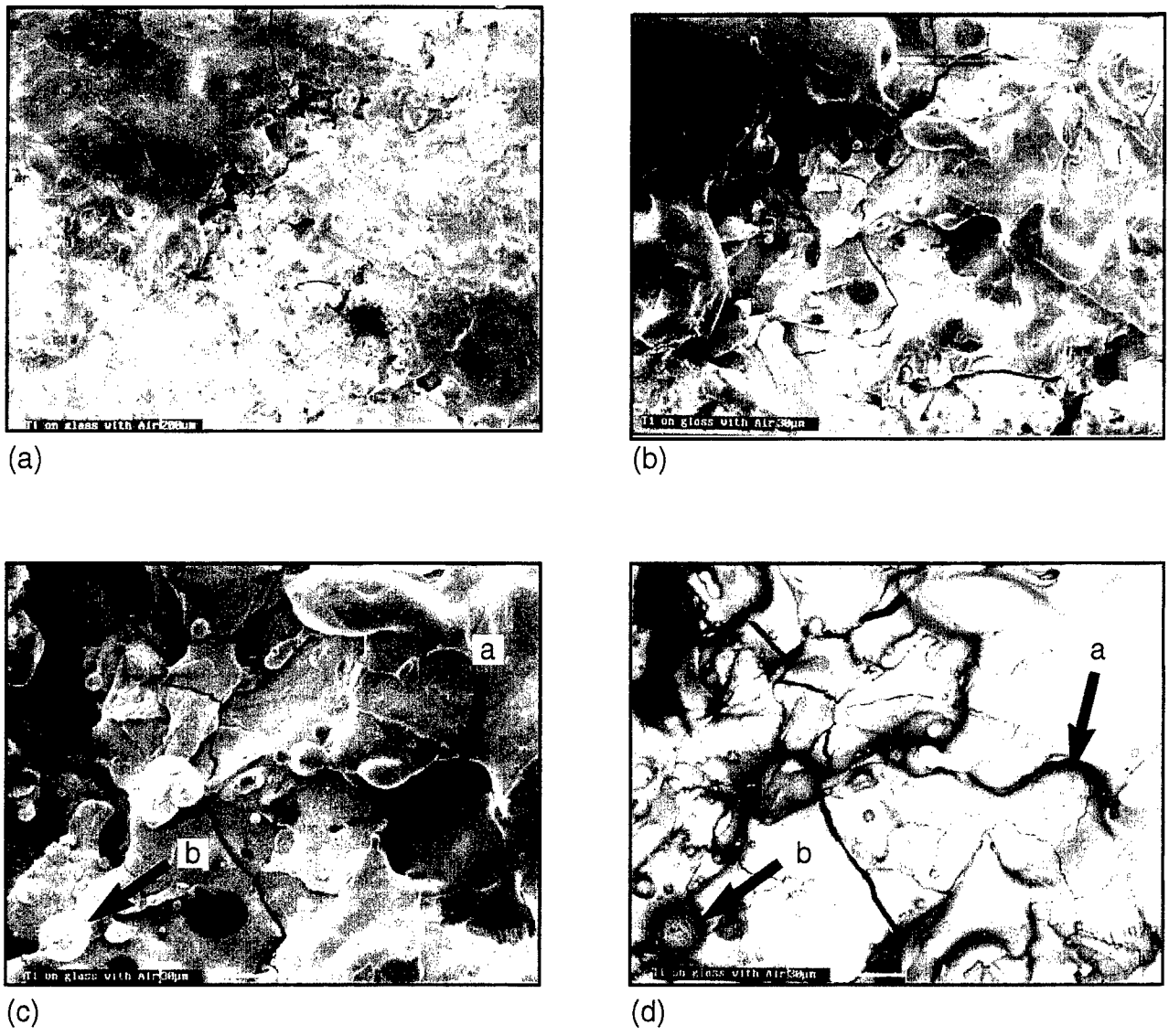

Figure 4.6: SEM photomicrographs of TiPA surface: (a) SE image, 65X; (b) SE image, 165X; (c) SE image, 330X; (d) BE image, 330X. Arrows: a) small, highly oxidized, finely cracked splat; b) small, highly oxidized droplet that froze before impacting the surface.

The surface of TiPA is shown in Figure 4.6. Figure 4.6(a) shows a rough area of splats fused together and a much smoother area which appears to have been glazed by higher heat input. Glazing could be produced by small local variations in the heat input to the coating during anode application. The effect would be two-fold: to weld adjacent splats into a more monolithic structure; and to promote further reaction of the Ti with the atmosphere.

A wide range in splat sizes is apparent in Figure 4.6, representing the droplet size distribution in the molten spray. Cracks are visible in the coating surface at higher magnification; larger cracks cross multiple splats. SE and BE images of the same area, Figures 4-6(c) and 4-6(d), show a

small splat (a) containing a high concentration of Ti(O,N) which is heavily cracked, in contrast to adjacent splats richer in α-Ti. The small droplet (b) solidified before impacting the surface. It has a small thermal mass and a large surface area-to-volume ratio (which favors reactions with O and N) and contains a high concentration of Ti(O,N). Highly oxidized droplets such as these can become incorporated in the coating structure as the anode is being applied (see later photomicrographs for examples, Figures 4.10, 12 and 14).

A cross-section of TiPN, typical of coatings applied on glass using nitrogen atomization, is shown in Figure 4.7. The BE image, Figure 4.7(b), shows banding of the coating, indicating gradients in coating composition similar to those observed in Figure 4.4(b) for coatings on glass using air atomization. The composition depth profile, Figure 4.8, shows the presence of six gradient bands which can be visually observed in the BE image, Figure 4.7(b). The depth profile shows that N levels are typically higher, around 20 at pct, and O levels are lower, 10 at pct or less, when nitrogen atomization is used.

Cracks parallel and transverse to the glass/coating interface are visible in Figure 4.7(c) and link with cracks in the glass substrate caused by thermal shock to the glass. The network of parallel and transverse cracks again suggests the presence of substantial internal stresses within the coating. There was no disbonding of the coating from the glass, indicating a good bond at this interface. Examination of a number of coatings formed on Pyrex glass using both air and nitrogen atomization indicated there was less cracking and a more uniform coating chemistry for the coatings produced using nitrogen atomization.

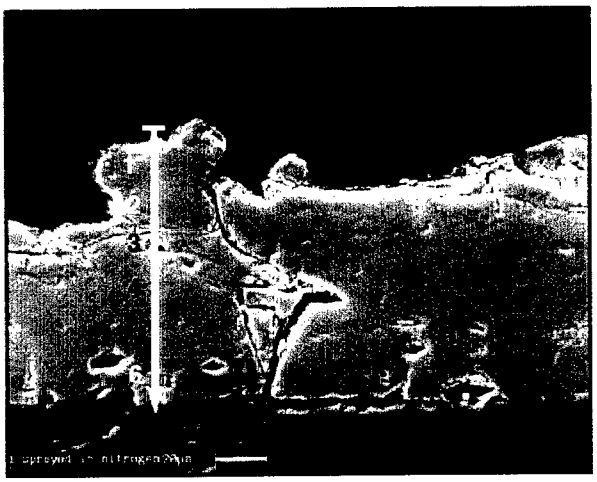

(a)

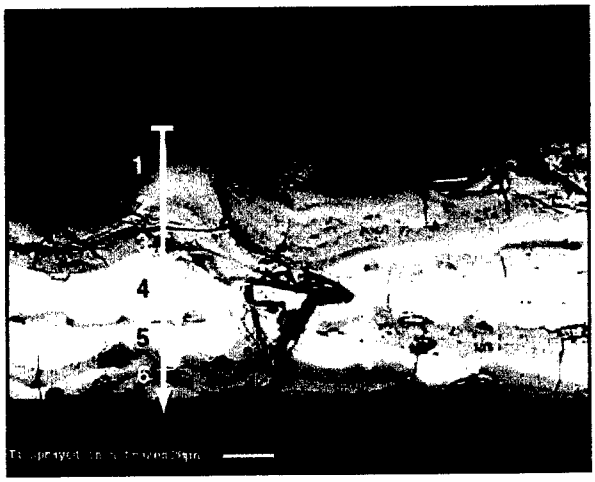

(b)

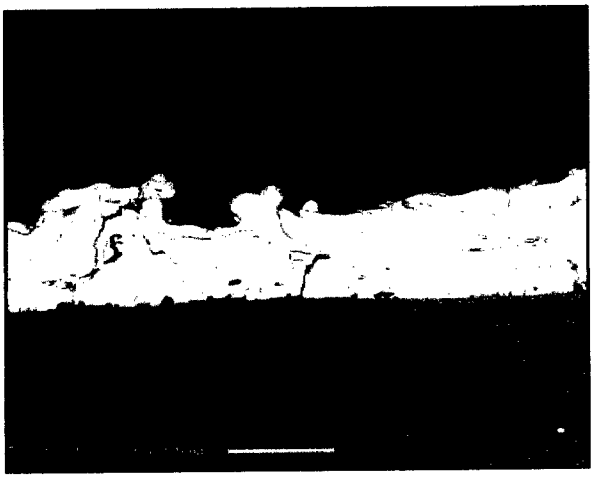

(c)

Figure 4.7: SEM photomicrographs of TiPN cross-section: (a) SE image, 350X; (b) BE image, 350X; (c) BE image, 140X. Arrow shows path of ASEM traverse and the location of six Ti gradient bands in the coating.

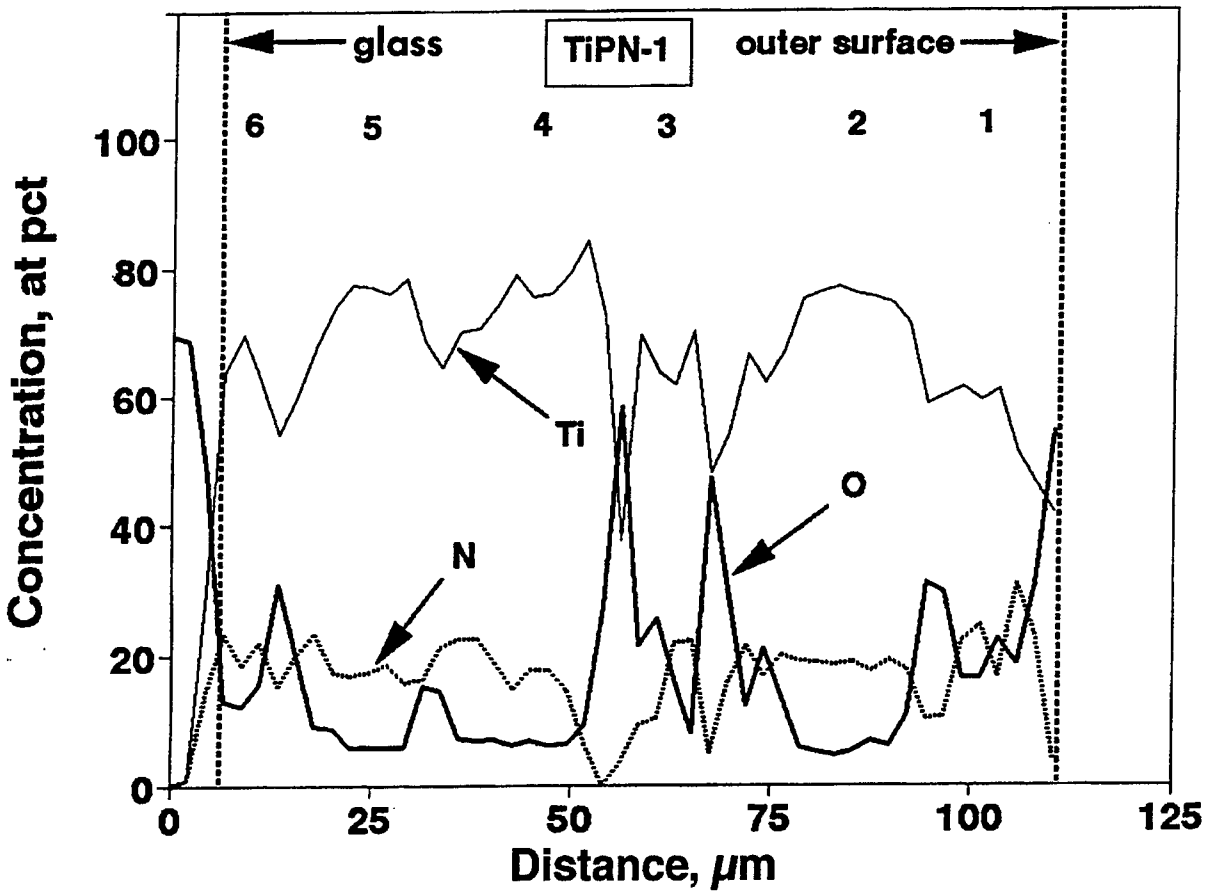

Figure 4.8: ASEM composition depth profile for TiPN cross-section shown in Figure 4.7. Glass-coating interface and outer surface of coating are shown with six Ti gradient bands.

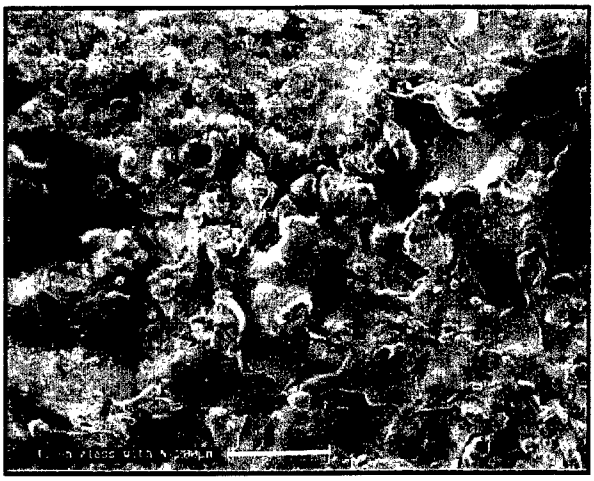

(a)

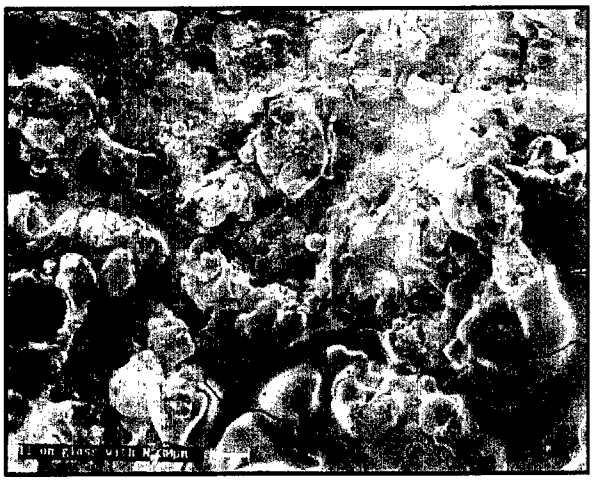

(b)

(c)

Figure 4.9: SEM photomicrographs of TiPN surface: (a) SE image, 65X; (b) SE image, 1650X; (c) SE image, 330X.

The surface of the coating on TiPN is shown in Figure 4.9. It is similar to that produced using air atomization and has areas roughened by coalesced "splats" and areas smoothed by glazing. A network of cracks segments the coating surface.

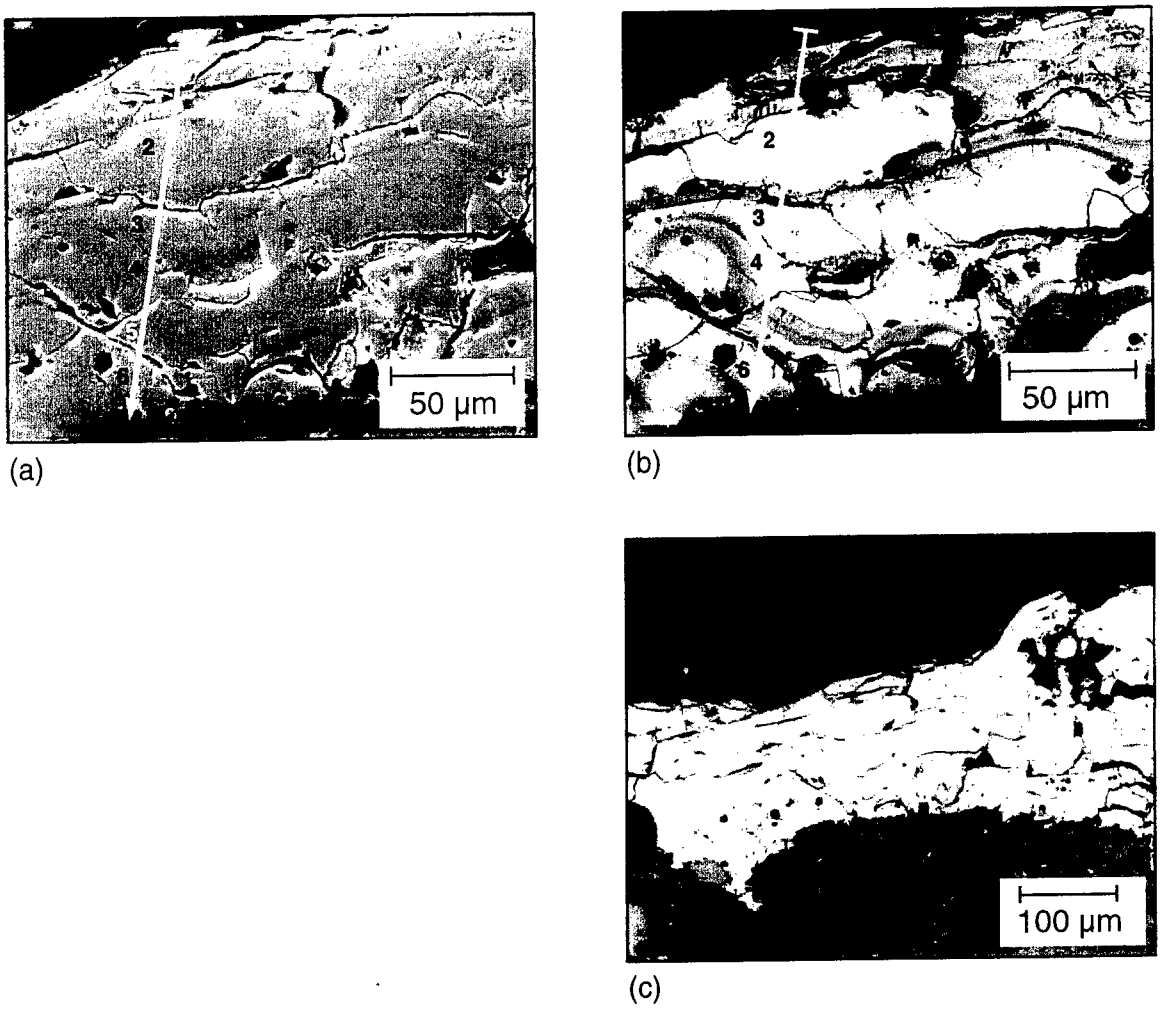

Figure 4.10: SEM photomicrographs of TiCA cross-section: (a) SE image, 320X; (b) BE image, 320X; (c) BE image, 130X. Arrow shows path of ASEM traverse and the location of six Ti gradient bands in the coating.

A cross-section of TiCA, typical of coatings applied on concrete using air atomization, is shown in Figure 4.10. Figures 4.10(a) and 4.10(b) are SE and BE images of the same area. In general, the coating appears to have formed a good mechanical bond with the irregular surface of the concrete substrate, Figure 4.10(c). While there are gaps and voids scattered along the coating-concrete interface, the coating fills all but the smallest of these recesses and closely follows the surface contours of the concrete.

There are very distinct gradient bands and substantial cracking within the coating, shown in Figure 4.10(b). The concentration depth profile, Figure 4.11, shows Ti, N and O concentration levels similar to those observed for TiPA, Figure 4.5. Six gradient bands are apparent in the depth profile and can be matched visually with gradient bands in the BE image. Parallel cracks

tend to be located in the dark layer of the gradient bands at the sharp interface. Transverse cracks link the parallel cracks. Some of the transverse cracks cross into the concrete and link with cracks in the cement paste, shown in Figure 4.10(c).

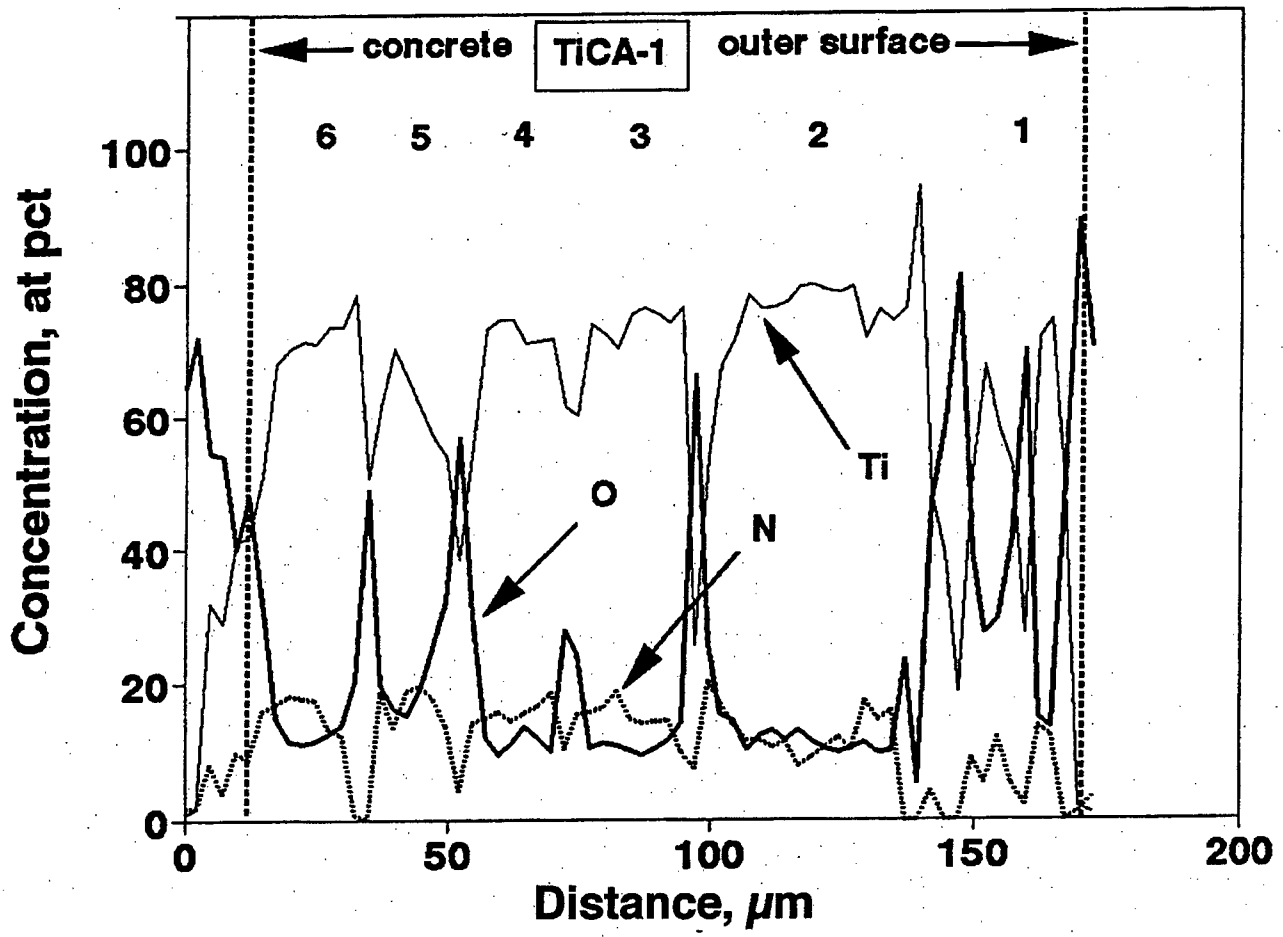

Figure 4.11: ASEM composition depth profile for TiCA cross-section shown in Figure 4-10. Concrete-coating interface and outer surface of coating are shown with six Ti gradient bands.

(a)

(b)

(c)

Figure 4.12: SEM photomicrographs of TiCN cross-section: (a) SE image, 350X; (b) BE image, 350X; (c) BE image, 140X. Arrow shows path of ASEM traverse and the location of five Ti gradient bands in the coating.

A cross-section of TiCN, typical of coatings applied on concrete using nitrogen atomization, is shown in Figure 4.12. The condition of the coating-concrete interface and the mechanical bond with the concrete appears to be similar to that formed using air atomization. Gradient bands and cracking are apparent. As with coatings formed on Pyrex glass, the composition of coatings formed on concrete using nitrogen atomization tended to be more uniform with less cracking than for coatings formed using air atomization. Like TiPN, depth profiles showed the N concentration was typically around 20 at pct while the O concentration was about 10 at pct, as shown in Figure 4.13. Five gradient bands are apparent in the depth profile and can be visually matched with similar features in the BE image, Figure 4.12(b).

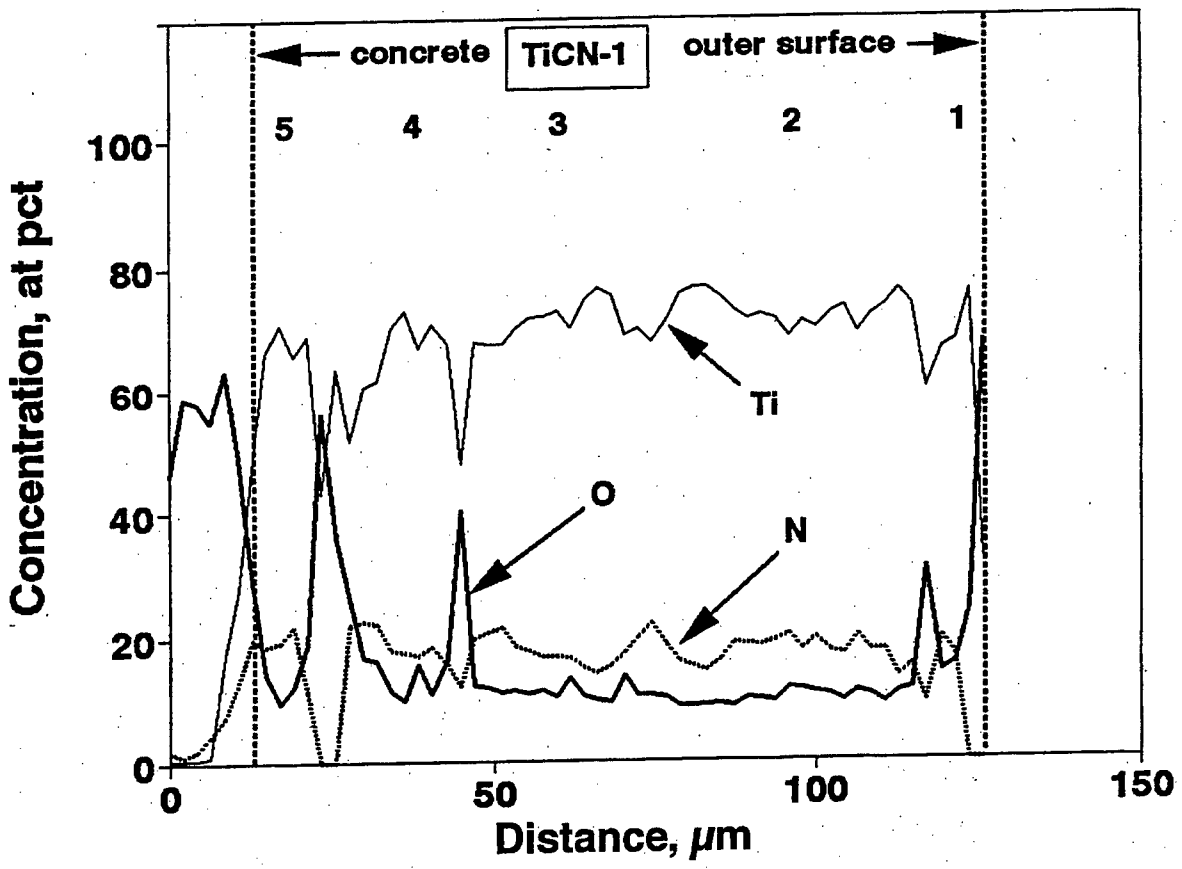

Figure 4.13: ASEM composition depth profile for TiCN cross-section shown in Figure 4.12. Concrete-coating interface and outer surface of coating are shown with five Ti gradient bands.

The composition data in the ASEM depth profiles, Figures 4.5, 4.8, 4.11, and 4.13, were averaged over the thickness of the coating from the atmosphere-coating interface to the coating-substrate interface and are shown in Table 4.10. The minimum and maximum elemental concentrations in these data were also tabulated, as shown in Table 4.11. On average, the coating composition was (in at pct): using air atomization, 18.5 oxygen, 13.8 nitrogen and 67.5 Ti; using nitrogen atomization, 13.5 oxygen, 16.8 nitrogen and 69.6 Ti. (As weight percents, these concentrations were: using air atomization, 7.9 oxygen, 5.2 nitrogen and 86.9 Ti; using nitrogen atomization, 5.7 oxygen, 6.2 nitrogen and 88.1 Ti.) Oxygen levels decreased and nitrogen levels increased using nitrogen atomization compared to air atomization. Oxygen levels were higher than nitrogen levels for air atomization, lower for nitrogen atomization. The (O+N)/Ti ratio was lower for nitrogen atomization, suggesting more of the Ti was available as metallic titanium (i.e., α-Ti) when nitrogen atomization was used.

Table 4.10: Average coating composition, from ASEM composition depth profiles.

Coating Sample	Figure No.	Coating composition, at pct			(O + N)/Ti atom ratio
		O	N	Ti	
Air atomization					
TiPA	4.5	17.7	14.6	67.5	0.48
TiCA	4.11	19.3	13.0	67.5	0.48
average		**18.5**	**13.8**	**67.5**	**0.48**
Nitrogen atomization					
TiPN	4.8	13.2	17.1	69.6	0.43
TiCN	4.13	13.9	16.5	69.5	0.43
average		**13.5**	**16.8**	**69.6**	**0.43**

Minimum and maximum element concentrations varied considerably for all three elements. O levels varied more widely than N. With one exception, maximum N levels tend to be around 20 at pct. Referring to the Ti-N phase diagram, Figure 4.2, the concentrations in Tables 4.10 and 4.11 put N largely in the region where α-Ti is the stable phase, for example line 1. N can be expected to be present largely as an interstitial in the α-Ti matrix.

Table 4.11: Minimum and maximum element concentrations in coatings, from ASEM composition depth profiles.

Coating Sample	Figure No.	Number of gradient bands	Concentration, at pct					
			O		N		Ti	
			min	max	min	max	min	max
TiPA	4.5	7	8	39	5	21	63	83
TiCA	4.11	6	5	81	0	20	19	94
TiPN	4.8	6	5	58	3	31	38	84
TiCN	4.13	5	9	56	0	23	43	76

Oxygen has a higher solubility than nitrogen in the α-Ti matrix, 34 at pct (*Bumps, et al., 1953*) versus 22 at pct (*Bars, et al., 1983; Etchessahar, et al., 1987*). Never the less, the high levels of oxygen found in the dark portions of the coatings, exceeding 34 at pct for each sample, suggest that oxygen is present both as an interstitial in α-Ti and as a titanium oxidation product. Only one nonmetallic titanium phase was found in the coating by XRD, a fcc structure like TiN or γ-TiO. As the XRD results suggest, this phase is thought to be Ti(O,N), with both O and N substituted in the fcc structure. The high O levels in the dark layer of the gradient bands suggest that this layer is richer in the titanium oxidation product and that this product is Ti(O,N). XRD found no evidence that this phase transformed to other oxidized Ti structures that might be stable at lower temperatures.

SE and BE images in Figure 4.14 show the location of incipient cracks and their relation to the gradient bands. The sharp interface of the oxidized layer is given by Arrow "a", the diffuse

interface by Arrow "b". The locus of voids and microcracks is along the sharp interface and represents a weak boundary in the coating. Arrow "c" points out a similar region where microcracks and voids follow the path of a dark layer richer in Ti(O,N) than the adjacent material.

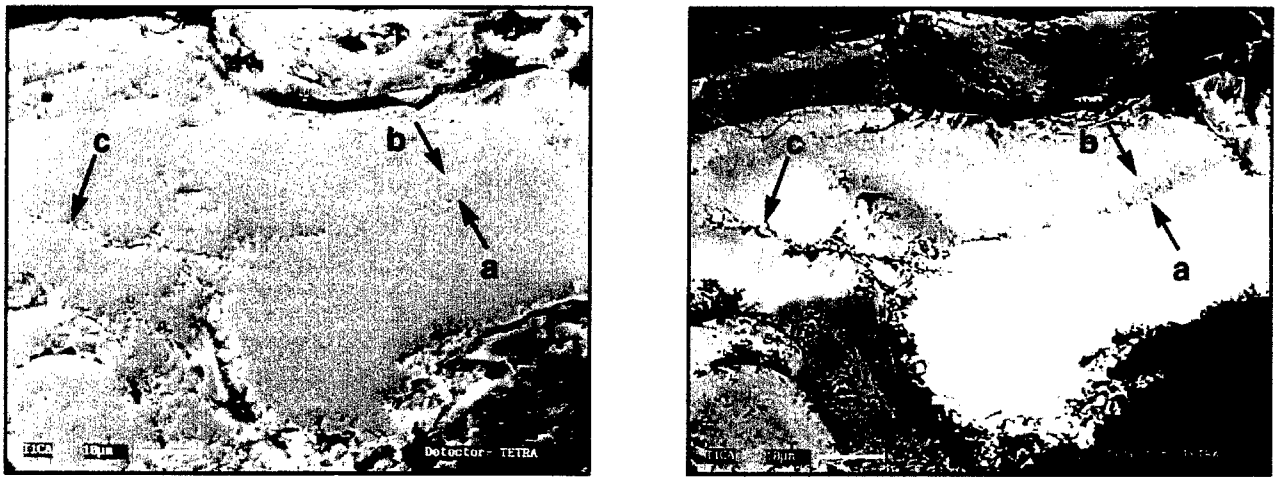

(a) (b)

Figure 4.14: Cracks in Ti gradient bands: (a) SE image, 900X; (b) BE image, 900X. Arrows: a) incipient crack along sharp gradient boundary; b) diffuse gradient boundary; c) crack along Ti(O,N)-rich boundary.

Finally, the structure of the Ti coating revealed by the SE and BE images is, in some ways, substantially different from that observed for thermal-sprayed zinc anodes *(Covino, et al., 1995; Covino, et al., 1996)* and for many other thermal-sprayed materials (*Krepski, 1993a; Leigh, et al., 1995*). Composition, structure and mechanical properties of the Ti coating are unique, representing a reactive material sprayed in an oxidizing environment. Individual splats are welded to each other forming a cohesive structure, albeit one incised by many brittle interfaces and vulnerable to damage from internal stresses. However, in terms of size of the splats, the Ti coatings are similar to these other coatings (*Krepski, 1993a*). Rough measurements from the BS images show the splats to be nominally 10 - 25 μm thick and 100 - 200 μm in width, with a considerable dispersion in splat sizes beyond these values.

4.4.5 X-ray Photoelectron Spectroscopy

Survey scans for the substrate side of flakes from sample TiPA showed predominantly Si and O with trace amounts of Ti and N. Depth profiling yielded relatively constant concentrations of Si and oxygen of 28 and 57 at pct, respectively. This agrees with the composition of SiO_2 and corresponds to the glass layer adhering to the substrate side of the flakes removed from Pyrex.

Survey scans of the *in situ* coating on samples TiPN and TiPA detected only Ti, C, O and N in significant concentrations. Carbon disappeared within the first 120 s of etching, indicating it was adventitious carbon and not present in significant amounts in the coating.

Table 4.12: XPS depth profile data for sample TiPN.

Sputter cycle	Sputter time, s	Equivalent sputter depth, μm	Concentration, at pct				(O + N)/Ti atom ratio
			C1s	O1s	N1s	$Ti2p_{3/2}$	
1	0	.0000	31.2	51.5	0.7	16.7	3.13
2	120	.0084	2.0	60.0	5.8	32.3	2.04
3	240	.0168	3.0	54.5	7.7	34.8	1.79
4	360	.0252	2.9	49.1	9.9	38.2	1.54
5	480	.0336	2.0	45.9	11.8	40.2	1.44
6	600	.0420	1.9	42.8	13.3	42.1	1.33
7	720	.0504	1.9	39.8	15.0	43.2	1.27
8	840	.0588	1.9	37.6	16.1	44.4	1.21
9	960	.0672	2.3	36.3	16.2	45.2	1.16
10	1080	.0756	3.1	34.7	16.2	46.1	1.10
11	1200	.0840	1.6	34.0	17.4	47.0	1.09
12	1320	.0924	2.5	31.9	18.5	47.1	1.07
13	1440	.1008	2.4	31.6	18.5	47.5	1.05
14	1560	.1092	1.0	30.2	19.3	49.5	1.00
15	1680	.1176	1.8	28.6	19.7	49.8	0.97
16	1800	.1260	2.0	27.9	20.1	50.0	0.96
17	1920	.1344	2.2	27.2	19.9	50.7	0.93
18	2040	.1428	1.7	27.2	20.8	50.4	0.95
19	2160	.1512	2.2	25.6	20.7	51.5	0.90
20	2280	.1596	2.0	26.1	20.4	51.5	0.90

Sample TiPN was sputter etched for 20 cycles of 120 s each for a total depth of 0.15 μm. This represents only the outermost surface of a coating roughly 100 μm thick. The composition of the surface after each cycle is given in Table 4.12. The cumulative sputter depth was estimated from the measured SiO_2 sputter rate of 0.7 A per second and assuming that the sputter rate for Ti and its compounds was not greatly different from SiO_2. The ratio (O+N)/Ti was computed as an indicator of the coating stoichiometry. The data show carbon disappearing after sputtering less than 120 s. The high O concentration at the outer surface was probably associated with the C. Oxygen concentrations decrease with depth of sputtering. In contrast, N and Ti concentrations are low at the outer surface but increase with depth of sputtering. The stoichiometric ratio, (O+N)/Ti, ranges from 2 near the outer surface (discounting contributions from carbon oxides) to less than 1 after roughly 0.11 μm has been sputter etched. These values suggest an outer surface containing a very thin layer of TiO_2 that quickly transitions into one that is composed of Ti(O,N)

and metallic Ti, i.e., α-Ti, containing interstitial O and N. This is shown by successive X-ray photoelectron spectra for Ti, N and O in Figures 4.15 through 4.17 respectively.

In Figures 4.15 through 4.17, the spectra for the first scan cycle referred to in Table 4.12 is oriented at the lowest position in the plot. Successive spectra are then stacked along the y-axis above this initial spectrum. The first spectra represents the composition of the "as-received" coating surface and the top spectra represents the composition after sputter etching for 2280 s. The binding energy of photoelectrons is given on the x-axis in electron volts. The binding energy of the photoelectrons varies with the type of environment from which the electron is emitted. The area under the peaks of these spectra is proportional to the concentration of the specific element in a particular binding state.

For example, the first spectra in Figure 4.15 contains two peaks typical of Ti. The larger is the $Ti2p_{3/2}$ peak and the smaller is the $Ti2p_{1/2}$ doublet associated with the $Ti2p_{3/2}$ peak. The binding energy of the $Ti2p_{3/2}$ peak in the first scan is at 459.3 eV, close to the binding energy of 458.8 eV characteristic of Ti in a TiO_2 matrix (*Chastain, 1992*). After sputter etching for 2 or 3 cycles, the peak at 459.3 eV disappears and a new peak emerges at 455.3 eV that increases in size with further sputtering. This peak is close to that characteristic of Ti in TiO (455.1 eV), Ti in TiN (455.8 eV) or Ti in a metallic Ti matrix (454.1 eV) (*Chastain, 1992*). The $Ti2p_{3/2}$ peak at 455.3 eV was most likely the sum of contributions from TiO, TiN and metallic Ti bonds in the sample volume analyzed. In fact, the observed peak shifts towards lower binding energies with increasing sputter etching, which signals an increasing contribution from metallic Ti. Thus, the spectra indicate: (1) TiO_2 is present only on the outermost surface of the coating; (2) a mixture of TiO, TiN and metallic Ti underlies the surface; and (3) the metallic Ti concentration increases with depth in the coating, at least for the depth of coating measured by this technique.

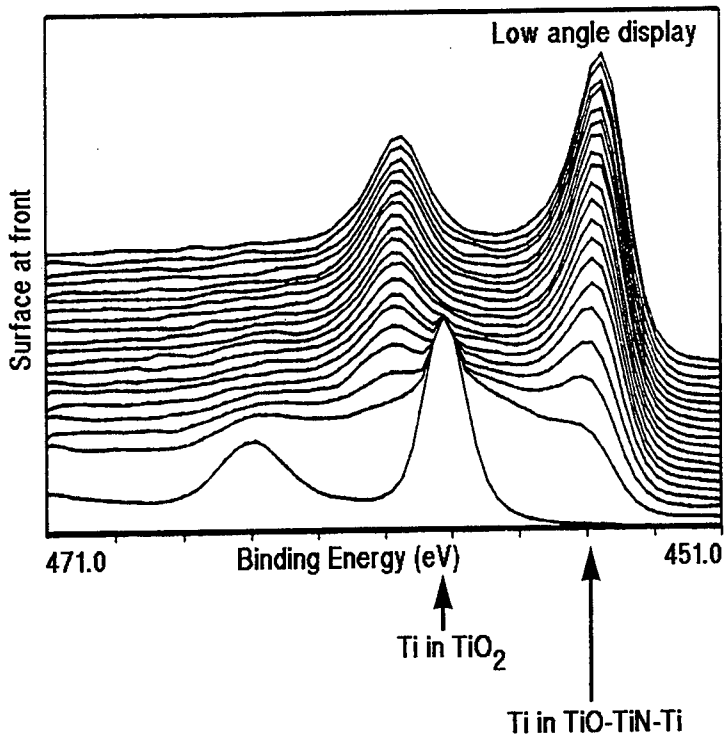

Figure 4.15: $Ti2p_{3/2}$ and $Ti2p_{1/2}$ peaks as a function of sputter etching for sample TiPN.

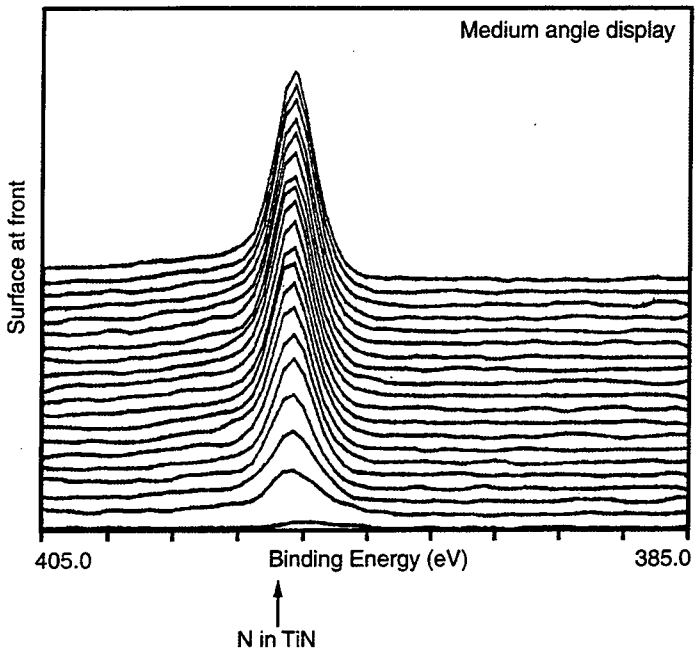

Figure 4.16: N1s peak as a function of sputter etching for sample TiPN.

Figure 4.16 shows spectra for the N1s peak of nitrogen. The peak is located at around 397.4 eV, close to the value of 396.9 eV characteristic of N in a TiN matrix (*Chastain, 1992*). There is little N at the surface, but the concentration quickly builds as more coating is removed by sputter etching.

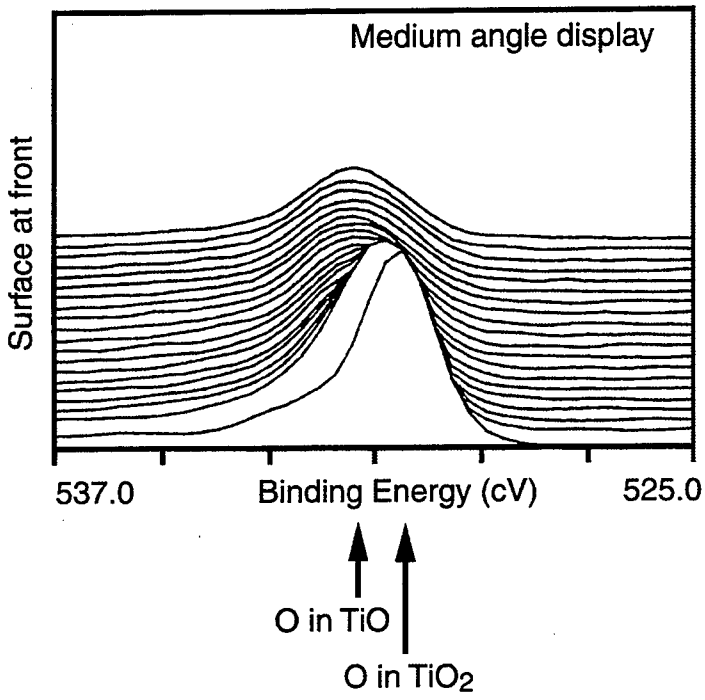

Figure 4.17: O1s peak as a function of sputter etching for sample TiPN.

Figure 4.17 shows spectra for the O1s peak of oxygen. In the first spectra, the peak is located at 530.4 eV, close to the value of 529.9 eV for O in a TiO_2 matrix (*Chastain, 1992*). With sputter etching, this peak quickly shifts to a binding energy value of 531.4 eV. While no data are available in the literature for the binding energy of O in TiO, it must be assumed, given the limited number of O compounds possible in the coating and the results for Ti, that the peak at 531.4 eV represents the binding energy characteristic of O in TiO.

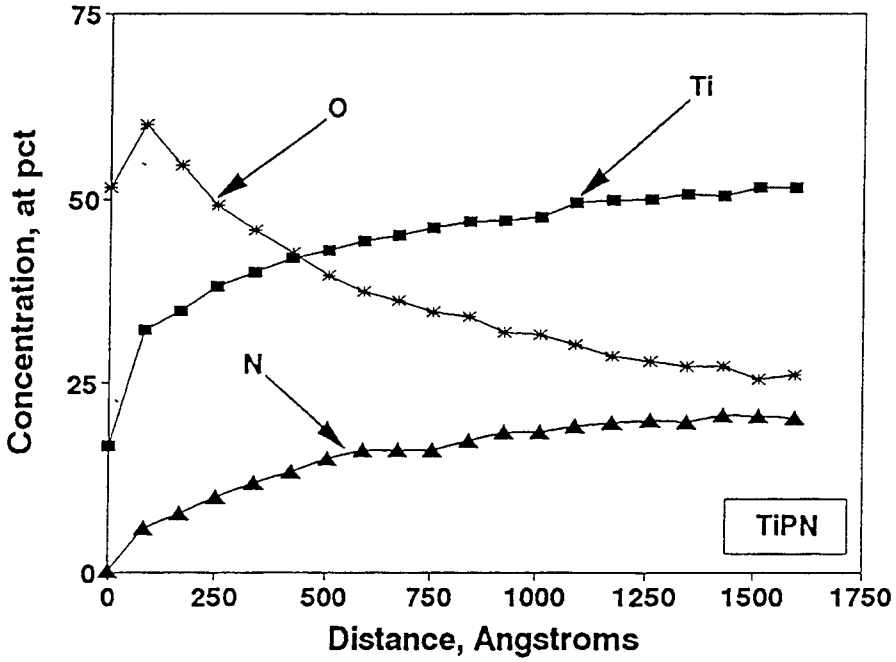

Figure 4.18: Composition depth profile for sample TiPN.

Referring again to Table 4.12, values of the stoichiometric ratio (O+N)/Ti less than 1 near the end of sputter etching indicate the possible presence of metallic Ti within less than 0.2 μm of the coating surface. This agrees with the shift in binding energy for the $Ti2p_{3/2}$ peak from 455.3 eV (for TiO/TiN) towards 454.1 eV (for metallic Ti) near the end of sputter etching. The composition of the anode near-surface region formed using nitrogen atomization is shown by the depth profile in Figure 4.18, created from the data in Table 4.12. After several sputter cycles, O decreased with increasing depth in the coating. On the other hand, N and Ti concentrations both increased with depth. The anion-to-cation ratio, (O+N)/Ti, decreased from 2 at the surface (discounting contributions from carbon), to 1 at a depth of 0.11 μm. This indicates a thin outer region of TiO_2 which transitions quickly to one composed of metallic Ti and Ti(O,N).

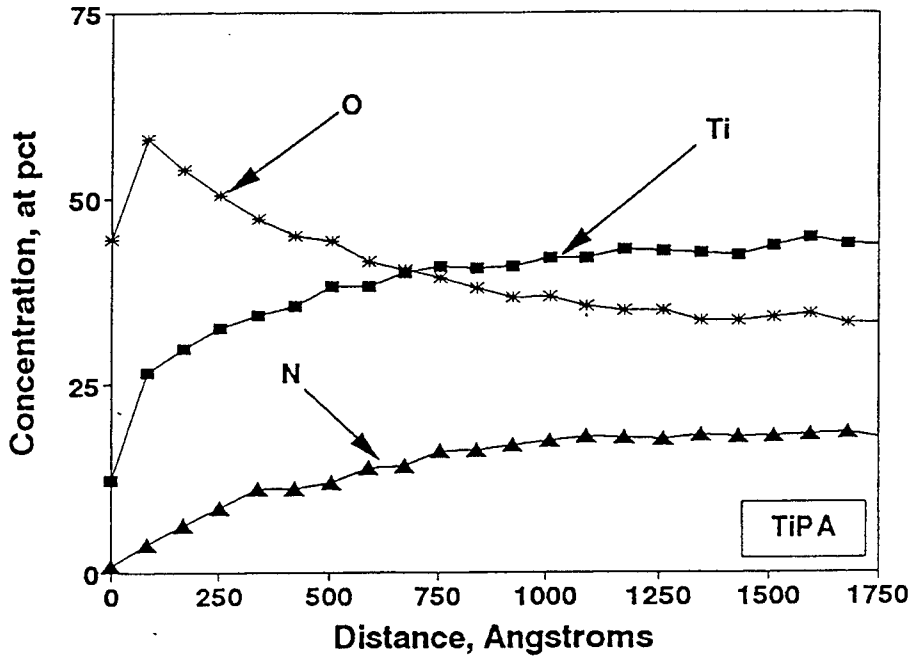

Figure 4.19: Composition depth profile for sample TiPA.

Sample TiPA formed using air atomization was sputter etched for 30 cycles of 120 s each, for a total depth of 0.24 μm. Composition depth profiles are plotted in Figure 4.19, showing data for 21 of the 30 sputter etch cycles. The composition depth profile has the same general features as for the coating formed using nitrogen atomization. The nitrogen curve was almost identical for the two cases, but the titanium curve was lower and the oxygen curve higher using air atomization. These results suggest the Ti(O,N) concentration is higher within the coating when air atomization is used, and the α-Ti fraction is lower. As a consequence, the anion-to-cation ratio declines with depth more slowly when using air atomization, and the coating surface appears to be more highly oxidized. These results offer further evidence that using nitrogen as the atomizing gas would increase the metallic Ti content of the anode.

4.4.6 Coating Microstructure

The microstructure of thermal-sprayed anodes depends upon cooling rate and chemical composition. Equilibrium solidification typically occurs at cooling rates below 10^4 K/s. Above this rate, rapid solidification processes can occur and nonequilibrium metastable microstructures can form having increased solute solubility and decreased grain size (*David and Vitek, 1989*). Cooling rates were computed for molten splats on titanium and concrete substrates using both the thick and thin weld cooling rate equations (*Weisman, 1981*). Computed cooling rates ranged from 10 to 150 K/s, well below those that would lead to rapid solidification (*Cahn, 1983;*

Collins, 1986), and well below those observed for metal thermal spray coatings on metal substrates (*Krepski, 1993b*). Thus it would appear that local equilibrium would be maintained at the melt/solid interface during the application of thermal-sprayed titanium anodes on concrete. As a consequence, the splat freezing structures would be characterized by the composition and temperature at the solidification front given by the equilibrium phase diagram (*Collins, 1986*).

Freezing structures are shown in Figure 4.20 for representative splat compositions given in Table 4.13. Figure 4.20(a) shows the location of the areas imaged and analyzed. Figures 4.20(b) and 4.20(d) show structures formed following line 1 in Figure 4.1 for the binary Ti-O system (similar for the binary Ti-N system) where Ti concentrations are high (i.e., > 80 at pct). α-Ti dendrites are the first solid phase to freeze from the molten splats. With further cooling a peritectic reaction, involving molten Ti and α-Ti, forms a second solid phase, β-Ti. Since diffusion in solid phases is slow compared to molten Ti, the peritectic reaction will not proceed to completion and segregation will occur with the β-Ti coating the α-Ti dendrites. The β-Ti contains substantially lower concentrations of interstitial O and N than the α-Ti. Thus, in BE images 4.20(b) and 4.20(d), the dark dendrites are the initially formed α-Ti. The β-Ti that formed at elevated temperatures reverts to α-Ti at lower temperatures since O and N are α-Ti stabilizers. This transformation to α-Ti is confirmed by the XRD data. Hence, the lighter interdendritic material is α-Ti resulting from this transformation and contains lower levels of interstitial O and N than the dendrites.

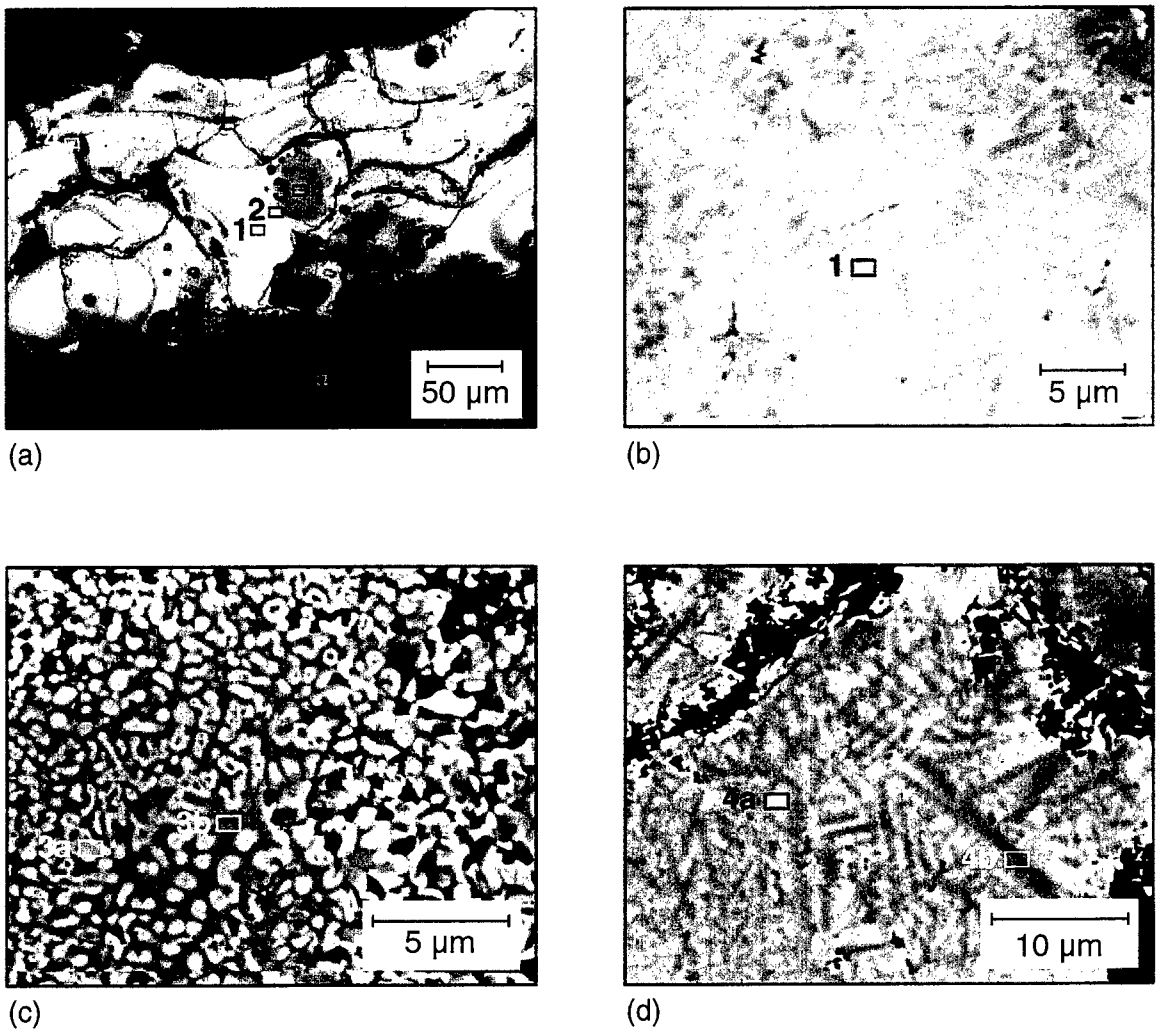

Figure 4.20: Freezing structures in TiCA formed using air atomization, BE images: (a) General view showing four analysis areas, 200X; (b) analysis area 1, 2400X; (c) analysis areas 3a and 3b, 3600X; (d) analysis areas 4a and 4b, 1800X.

The freezing process is substantially different when the melt contains low levels of Ti (i.e., < 60 at pct). Figure 4.20(c) shows a typical structure that would result following line 2 in Figure 4.1. α-Ti dendrites again are the first solid phase to freeze from the molten splats. With further cooling, the fcc Ti(O,N) structure freezes from the melt and coats the α-Ti dendrites. The α-Ti dendrites contain substantially less O and N than the Ti(O,N). Thus, in BE image 4.20(c), the light phase is the α-Ti dendrites, and the dark phase is the interdendritic Ti(O,N). Based on the XRD results, there is no evidence that the fcc Ti(O,N) transforms to other structures that are stable at lower temperatures.

Table 4.13: Composition of phases in freezing structures, coating sample TiCA.

Image area in Figure 4.20	Area description	Composition, at pct			anion/cation ratio (O + N)/Ti
		O	N	Ti	
(b)--1	white	9.0	1.5	89.4	0.12
(a)--2	light gray	12.4	18.0	69.5	0.43
(c)--3a	light phase	28.4	15.7	55.9	0.79
(c)--3b	dark phase	42.1	17.3	40.5	1.47
(d)--4a	light phase	10.9	0.0	89.1	0.12
(d)--4b	dark phase	8.7	9.0	82.3	0.22

4.4.7 Coating Resistance

Figure 4.21 compares resistivity values obtained from the literature for a range of materials with those computed for foils using the foil thickness and the resistance measured with the ODOT resistance probe. Figure 4.21 shows that the probe gives accurate measurements of the resistance of thin metallic films or foils which, when combined with thickness measurements, yield reasonable estimates of the material resistivity.

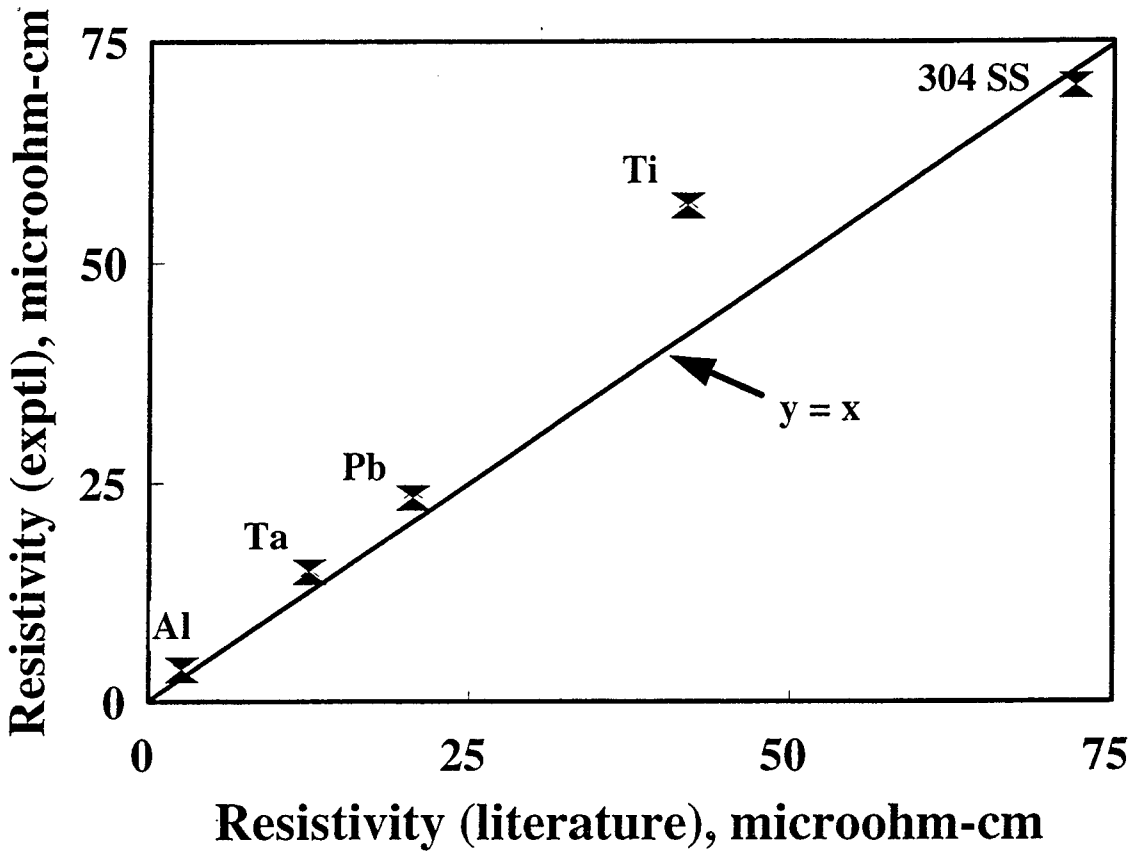

Figure 4.21: Comparison of literature resistivity values with those computed from resistance measurements made with the ODOT resistance probe on metal foils.

The resistance of the uncatalyzed, unaged anode coatings produced on glass plates are expressed in Table 4.14 as apparent resistivities using average thickness values obtained from SEM photomicrographs of the coating cross-sections. The term apparent resistivity is used because the computed resistivity value includes the effects of a number of factors affecting coating properties, including non-homogeneous chemistry and discontinuities in the coating caused by cracking and voids. The measured resistivity values are substantially higher than those given for constituents of the anode (Ti, TiO and TiN) and reported in Table 4.4. Assuming continuous filaments of the constituent materials and weighting the resistivity of the constituent materials by their average volume fraction based on the data in Table 4.8, the computed resistivity of the coatings was 58 μΩ-cm for air atomization and 52 μΩ-cm for nitrogen atomization. These values are well below the measured values and suggest that the electron path is far more convoluted and constrained than suggested by the nominal coating dimensions and coating chemistry.

Table 4.14: Anode coating resistivity.

Atomizing gas	Correction factor, C (see Fig. 2.2)	Thickness, cm	Resistance, ohms	Apparent resistivity, μΩ-cm		Tortuosity factor
				Measured	Computed	
air	1.0	0.0095	0.375	3562	58	61
nitrogen	1.0	0.0080	0.270	2160	52	42
Ratio of air and nitrogen tortuosity values = 1.4						

A tortuosity factor can be defined which empirically accounts for differences between the measured and computed resistivity arising from such factors as: (1) a highly variable coating cross-section from variations in coating thickness and transverse cracks; (2) an electron path length that is substantially increased by extensive cracking within the coating; and (3) oxidized interfaces between splats that accentuate the effects of non-homogeneous splat chemistry. The tortuosity factor is computed by taking the ratio of the measured resistivity and the computed resistivity. The tortuosity factor for air atomization was 61, and for nitrogen atomization it was 42. Visual and chemical evaluation of the anodes showed the coating formed using nitrogen atomization exhibited less cracking, had a more uniform composition, and they contained lower oxide and nitride levels than anodes formed using air atomization. The 30 pct lower value for tortuosity using nitrogen atomization should be an important consideration in using the coating for ICCP systems. It suggests that nitrogen atomization has benefits that directly affect both application specifications for the anode and service of the anode as a current carrier.

4.5 COATINGS SUMMARY

4.5.1 Coating Chemistry

The thermal-sprayed Ti anode coatings contained no metallic contaminants except those originating in the Ti feedwire. The principal constituents of the coating were Ti, O and N. The O and N result from reactions of the molten Ti droplets with the atomizing gas and air entrained in the atomizing gas. Oxygen is the more reactive of the two gases. For example, at 850° C the parabolic rate constant for the Ti-O reaction is almost two orders of magnitude higher than for the Ti-N reaction (*Hauffe, 1965; Kubaschewski and Hopkins, 1962b*). While in flight, the molten Ti droplets acquire an oxidized skin rich in O and N. Both nitrogen and oxygen react with titanium by diffusion of the gas into the titanium and internal oxidation (*Hauffe, 1965*). The oxidized skin ruptures on impact, and the Ti-rich core with the skin fragments spread across the surface to form a splat.

Coatings formed using air atomization typically contained on average (in at pct): 18.5 oxygen, 13.8 nitrogen and 67.5 Ti; those formed using nitrogen atomization were 13.5 oxygen, 16.8 nitrogen and 69.6 Ti. (As weight percents, these concentrations are: air atomization -- 7.9 oxygen, 5.2 nitrogen and 86.9 Ti; nitrogen atomization -- 5.7 oxygen, 6.2 nitrogen and 88.1 Ti.) Assuming a portion of the O and N were present as interstitials in metallic Ti, these

concentrations suggest that a substantial fraction of the Ti, perhaps 50 pct or more, was present in the anode as metallic Ti.

4.5.2 Coating Mineralogy

The coating contained two distinct phases, the hcp α-Ti and a fcc structure like TiN or α-Ti. The second phase is thought to be Ti(O,N) with O and N substituted in the fcc structure. No rutile (TiO_2) or β-Ti were detected in macro-samples of the coating. TiO_2 was observed in a very thin layer, less than 0.02 μm thick, on the outer surface of the coatings and was found nowhere else in the coatings. The metallic α-Ti contained substantial amounts of O and N as interstitial constituents. As binary systems, α-Ti can contain up to 22 at pct N and up to 34 at pct O. The exact concentrations of N and O in the α-Ti of the anode coatings is not known, nor is it known how N and O might affect the solubility of the other. However, the analytical results and the solubilities for the binary systems suggest a fairly high concentration of interstitial N and O in the coating, perhaps 20 - 30 at pct total.

4.5.3 Coating Microstructure

Computed coating cooling rates were sufficiently low, ≤ 150 K/s, that splat freezing structures could be characterized by the composition and temperature at the solidification front given by equilibrium phase diagrams. In general, the coating microstructure consisted of two freezing structures. When titanium concentrations were sufficiently high (i.e., > 80 at pct), an α-Ti dendritic structure was formed with α-Ti interdendritic phase. The composition of this structure was not homogeneous. Interdendritic β-Ti formed following a peritectic reaction with the α-Ti dendrites, and the interdendritic β-Ti then transformed to α-Ti. This resulted in dendritic and interdendritic α-Ti phases containing different levels of interstitial O and N. When titanium concentrations were substantially lower (i.e., < 60 at pct), an α-Ti dendritic structure again formed. However, in this case the interdendritic phase was Ti(O,N).

The coating had a layered or banded cross-section resulting from gradients in splat composition produced by reactions with O and N from the surrounding gaseous environment. Each gradient band consisted of a layer rich in α-Ti and a layer rich in Ti(O,N). These layers corresponded, in a rough way, with unreacted titanium from the core of the droplet that formed a splat and oxidized skin from the droplet. Typical ranges of concentration in the gradient bands were (in at pct): oxygen -- 5 - 60; nitrogen -- 0 - 22; titanium -- 40 - 90. This variability in splat composition leads to a wide range of physical, mechanical and chemical properties for the coating.

4.5.4 Coating Properties

The average size of splats was fairly typical of thermal spray coatings, 10 - 25 μm thick and 100 - 200 μm wide. Most splats appear to have impacted the surface in a molten state and microwelded to earlier splats. A small fraction appeared to have impacted in a partially molten

or solid state. These tended to be smaller droplets with less thermal mass and a larger surface area-to-volume ratio that aids cooling and reactions with atmospheric gases.

The coating formed by the splats followed the small scale contours of the concrete surface well and appeared to form a good mechanical bond. The coating was cracked, with less cracking and a more uniform chemistry when nitrogen was used for the atomizing gas rather than air. Cracks normal (or transverse) to the substrate surface and parallel to the surface were present within the coating. Parallel cracks tended to form at the interface between splats where remnants of the heavily oxidized droplet skin contacted α-Ti-rich layers. Concentration gradients are highest at this interface, resulting in a mismatch between molecular volumes and mechanical properties of coating constituents. Ti(O,N) is a particularly brittle phase and vulnerable to internal stresses and stress risers created by the nonhomogeneous microstructure of the coating. Parallel cracks tend to be located within the Ti(O,N)-rich layer of the gradient bands. Transverse cracks are typically linked by these parallel cracks. Transverse cracks typically cross multiple gradient bands, indicating cracking was delayed until coating application was partially or totally completed and the coating was cooling.

Coatings formed using nitrogen atomization had a lower resistivity than those formed using air atomization. This result appears to be related to the more uniform composition of coatings formed using nitrogen atomization, lesser cracking and a lower concentration of titanium oxide. An empirical tortuosity factor, which incorporates these effects, was 30 pct lower for coatings formed using nitrogen atomization. This finding suggests that nitrogen atomization has benefits which directly affect both specifications for the anode application and service of the anode as a current carrier.

The locally diverse composition of the coating could influence the electrochemical and physicochemical reactions that make the coating an effective insoluble anode for ICCP. These could range from the absorption and retention of catalyst to the condensation of moisture on the coating surface to sustain the anodic reaction. These questions were not examined during the coatings characterization.

5.0 ELECTROCHEMICALLY AGED ANODES

All anodes undergo electrochemical aging in cathodic protection (CP) systems. The aging of consumable thermal-sprayed anodes such as zinc involves dissolution of the anode at the zinc-concrete interface. With time and exposure to environmental factors (temperature, moisture, cyclic wetting and drying), the dissolution products interact with the concrete in complex ways that can affect the long-term performance and service life of the anode and CP system. These interactions have been characterized for zinc anodes in laboratory accelerated aging studies and in bridge CP systems (*Carello, et al., 1989; Covino, et al., 1995; Covino, et al., 1996a and 1996b; Holcomb, et al., 1996; Bullard, et al. 1997; Covino, et al., 1997a and 1997b*). They involve electrochemical reactions; diffusion and convective transport of anode dissolution products and ionic constituents of the concrete; interactions of the anode system with the environment (particularly the exchange of moisture and chloride between the environment and structure); the stability of minerals in the concrete and in the anode dissolution products; and lastly, the formation of reaction zones that affect anode dissolution kinetics.

The consequences of electrochemical aging are important to the long-term performance of the CP system and its service life. For example, research on the consumable, thermal-sprayed zinc anode on reinforced concrete has shown that aging requires consideration not only of electrochemical consumption of zinc, but also of the impacts zinc dissolution products have on the anode bond strength and the operating characteristic of the CP system (*Bullard, et al., 1997; Covino, et al., 1996b and 1997b; Holcomb, et al., 1996*). Furthermore, accelerated laboratory studies have shown that frequent wetting of the anode (as would result from precipitation, fog and dew) leads to a substantially longer service life than when the anode is "dry" for extended periods (*Bullard, et al., 1997; Covino, et al., 1996b; Holcomb, et al., 1996*).

Electrochemical age is sometimes misunderstood regarding anode service life. Often the age of an anode is specified in terms of years of service when, in fact, the cumulative charge passed by the anode is the important measure of age. All other factors being equal, an anode operating at twice the current density of another will have twice the age for the same period of time. Of course, all factors are not equal. In particular, mass transport rates and chemical reaction rates are determined by fundamentally different factors. Both have an important influence on the long-term performance and service life of these anodes. In particular, changing the anode current density may alter the relative rates of these processes in a way that significantly affects conditions at the anode-concrete interface and, subsequently, anode service life.

The results in Section 4.0 and elsewhere (*Cramer, et al., 1998; Holcomb, et al., 1997*) show the non-consumable thermal-sprayed titanium anode is composed of a hexagonal close-packed α-Ti phase containing interstitial oxygen and nitrogen and a nonmetallic Ti(O,N) phase with O and N substituted in the face-centered cubic structure. At the operating conditions of bridge CP systems, this anode is electrochemically inert and requires an electrocatalyst to support a reaction useful for CP systems (*McGill, et al., 1996; Bennett, et al., 1995a and 1995b*). The catalyzed

anode reaction is the breakdown of water. In a basic environment, such as unaged concrete, this reaction is:

$$4\,OH^- \Rightarrow O_2 + 2\,H_2O + 4\,e^- \qquad (5\text{-}1)$$

The consequence of this reaction is the loss of hydroxyl ions at the anode-concrete interface and a decrease in the interfacial pH. As this reaction progresses and the interface loses its basic character, the reaction becomes:

$$2H_2O \Rightarrow O_2 + 4\,H^+ + 4\,e^- \qquad (5\text{-}2)$$

Water is a key constituent in both of these reactions, first as a source of replenishing hydroxyl ions and secondly as the primary reactant. Consequently, delivery of moisture to the anode by humid air, dew, fog and precipitation is critical to successful operation of the titanium anode. Aging of the titanium anode requires understanding how chemical changes at the anode-concrete interface affect the anode, the stability of the cement paste near the interface, and the long-term performance and service life of the anode.

This section's purpose is to address the effects of long-term electrochemical aging on the performance of thermal-sprayed titanium anodes in impressed current cathodic protection (ICCP) systems for reinforced concrete structures. Aging will be evaluated in terms of ICCP performance, effects on anode-concrete interfacial chemistry, changes in anode properties (structure, resistivity, bond strength and coating durability), and the impact of these factors on service life.

5.1 ANODE ELECTROCHEMICAL AGING

5.1.1 Anode Application to Concrete

5.1.1.1 Laboratory Aging Experiment

Laboratory concrete slabs were prepared to physically and mechanically approximate a section of a reinforced concrete structure in a thermal-sprayed titanium anode CP system (see Section 3.4 and Figure 5.1). The concrete slabs were cast with No. 16 expanded-steel mesh covering the full dimensions of the form bottom to simulate the rebar. The size and shape of the mesh gave roughly a 1:1 surface area ratio for the steel cathode and Ti anode. Steel wire was welded to the mesh and extended above the top surface of the form to provide an electrical connection to the mesh. The cover concrete over the mesh was 32 mm (1.25") thick.

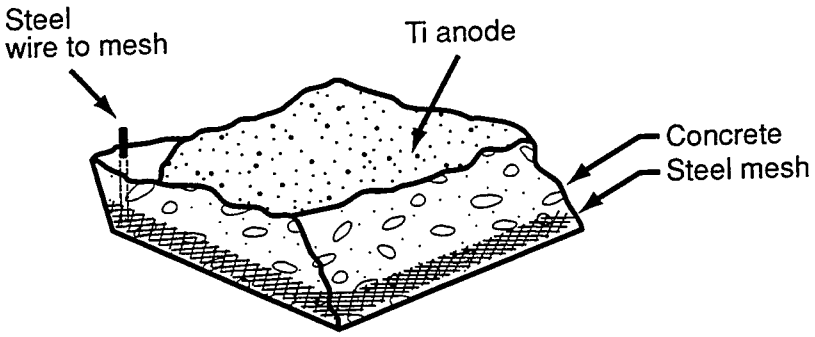

Figure 5.1: Design of the laboratory concrete slabs.

The concrete mix design, with a water-cement ratio of 0.48, approximates that used in ODOT's bridges built in the 1930s. Sodium chloride was added to the concrete mix at 3 kg NaCl/m^3 (5 lb NaCl/yd^3) to simulate that measured in coastal bridges. The coarse aggregate was 4.7 - 6.4 mm (0.20 - 0.25".) diameter and was intentionally smaller than aggregate typically used in bridge construction to obtain a more uniform current distribution in the slab between the titanium anode and the steel mesh cathode.

The slabs were cured four weeks in a moist room and then air dried for one week. Prior to applying the titanium coating, the top face of each slab was sandblasted to remove the weak, cement paste layer that formed on this surface, to expose a small amount of aggregate and to give the surface a medium sandpaper texture. The top face was then blown free of loose material and dust with compressed air. The surface, around the wire leads to the steel mesh, was masked off to a distance of 2.5 cm (1") to prevent shorting between the leads and the thermal-sprayed titanium anode.

Titanium was thermal-sprayed on the top face of the slab using a twin-wire arc-spray unit. The wire was 3.2 mm (1/8") diameter commercially pure titanium. Nitrogen was used as the atomizing gas for concrete slabs 48, 49 and 50, while compressed air was used for slabs 5 and 6. The spray parameters were: 300 A_{dc} and 37 V; atomizing gas pressure - 0.62 - 0.76 MPa (90 - 110 psi); spray distance - 0.15 - 0.22 m (6 – 9"); spray angle - normal to the concrete slab surface. A custom-designed, programmable X-Y traversing system (Section 3.1.1 and Figure 3.1) was used to control the movement of the spray head to obtain a titanium coating of uniform thickness. Multiple passes of alternating X and Y traverses of the slab surface were made to produce a titanium coating nominally 100 μm (4 mils) thick.

5.1.1.2 Field Trial

The area selected for the field trial of the thermal-sprayed titanium anode on Oregon's Depoe Bay Bridge was the underdeck and beam areas of the southern-most approach span on the 1939 widening structure (i.e., west of the original 1926 bridge and nearest to the ocean). This area is identified as ICCP Zone 14. The titanium anode area was 280 m^2 (3015 ft^2). The rest of the bridge was protected using consumable thermal-sprayed zinc anodes. The thermal-sprayed titanium anode was applied using basically the same materials, equipment and procedures as used to prepare the concrete slabs for the laboratory aging experiment. Compressed air was the atomizing gas and titanium application was done manually rather than using a robotic application system. Installation of the anode in the field trial began in 1993 and is described in Section 6.0.

5.1.2 Electrochemical Aging Conditions

5.1.2.1 Laboratory Aging Experiment

The titanium anode is catalyzed by a cobalt oxide catalyst. The catalyst is applied to the anode as an acidic solution (pH 3.47) of divalent and trivalent Co containing a total of 60 g Co/L, with the divalent Co present as Co nitrate, the trivalent Co as an amine complex, and a Co(III)/Co(II) ratio of 0.25. The catalyst is applied with the ICCP system operating, i.e. the titanium anodic to the rebar, and the ICCP operation is continued for a minimum of 72 hours after catalyst application (*McGill, et al., 1996*), In this way the Co in solution is converted to the active cobalt oxide catalyst, Co_3O_4. This oxide has a spinel structure with the divalent ion in the tetrahedral interstices and the trivalent ion in the octahedral interstices (*Cotton and Wilkinson, 1966; Kubaschewski and Hopkins, 1962a*), is a p-type semiconductor (*Kubaschewski and Hopkins, 1962a; Wells, 1962*), and is a highly active catalyst for surface reactions involving oxygen (*Balandin, et al., 1964; Wells, 1962*).

The catalyst was brush applied to the Ti anode at full strength at an application rate of 0.344 L/m^2 (0.0087 gal/ft^2) approximately two months after the slabs were thermal sprayed with titanium. (See Section 3.4.) Catalyst application was done with the Ti anode energized at a dc current density of 29 mA/m^2 (2.7 mA/ft^2) and the titanium anodic to the steel mesh. Anodic polarization of the titanium anode was continued for a period of one month. Four concrete slabs (Nos. 6, 48, 49 and 50) were catalyzed in this way. A fifth concrete slab (No. 5) was used as a control and had no catalyst applied to the titanium surface.

Electrochemical aging of the five slabs was conducted in a controlled temperature-constant humidity room to maintain a certain level of moisture in the concrete and slow the rate at which the slabs dried after wetting, as shown in Figure 5.2. The temperature was 25°C (75°F), and the relative humidity typically ranged from 75 to 90 pct. During

one extended period the room relative humidity (RH) was ramped from 30 to 100 pct to examine anode response to RH.

For purposes of electrochemical aging, the slabs were connected in series, with the titanium coating serving as the anode and the steel mesh the cathode. The slabs were polarized at a current density of 21 mA/m^2 (2 mA/ft^2) and aged for 1.8 years to a total charge of 1520 kC/m^2. At the current density typically used by ODOT for coastal CP installations, this was equivalent to about 23 years anode service. The slabs were periodically wetted during aging with deionized water to simulate the wet-dry cycles experienced by coastal bridges during exposure to rain, fog and dew.

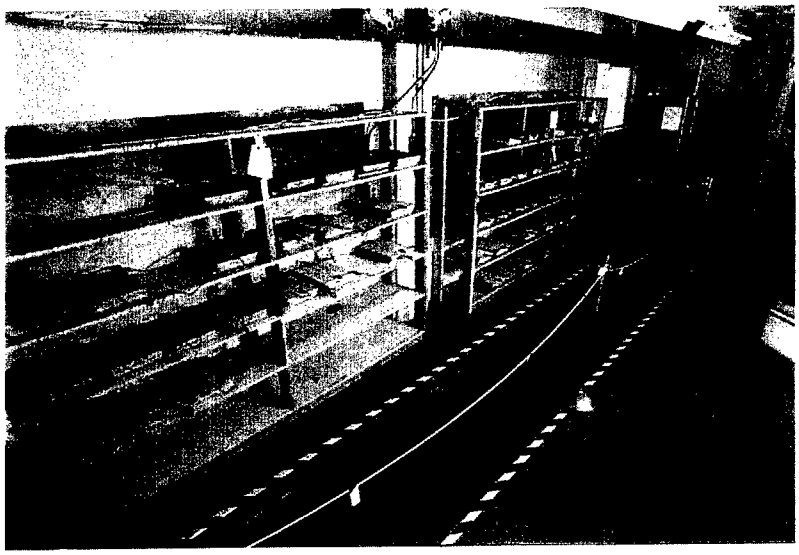

Figure 5.2: Laboratory electrochemical aging of the five thermal-sprayed titanium anodes on concrete slabs.

5.1.2.2 Field Trial

The cobalt catalyst was pressure sprayed onto the Zone 14 titanium anode of the Depoe Bay Bridge for a total application of 0.344 L/m^2 (0.0087 gal/ft^2) (see Section 6.33). Catalyst application was made as three coats, the first two at full strength and the final as a 3:1 catalyst to water dilution. A minimum of 30 minutes drying time was allowed between each coat. During application, the anode was polarized at a dc current density of 10.8 mA/m^2 (1.0 mA/ft^2), with the titanium anodic to the rebar. As an ICCP system, zone 14 was operated at a current density of 2.8 - 3.8 mA/m^2 (0.26 - 0.35 mA/ft^2) and a voltage of 1.4 - 1.7 V. Two 5.1 cm (2") diameter core samples were taken from the south-west corner of Zone 14 for purposes of characterizing the aged anode-concrete interface after approximately 1.4 years of operation. The titanium anode electrochemical age was 146 kC/m^2 at the time of coring.

5.2 CHARACTERIZATION TECHNIQUES

During electrochemical aging, both in the laboratory and in the field, the condition and performance of the anodes was monitored by a number of techniques. ICCP performance of the anode was characterized by potential-current-time measurements. The anode coating was examined for structural and chemical changes. Measurements were made of coating resistance, bond strength to the concrete, and mechanical durability. The anode-concrete interface was examined to determine: (1) the nature and extent of changes in concrete chemistry, mineralogy and structure in the immediate vicinity of the anode; and (2) the interaction of the cobalt catalyst with the anode and the concrete substrate. Samples used in characterizing aged anodes and the aged anode-concrete interface are summarized in Table 5.1 and indicated by the x's.

Table 5.1: Electrochemically-aged titanium anode samples.

TEST ANODE (aged, catalyst, atomizing gas)	Concrete slab no. or core no. (field trial)	Electro-chemical age, kC/m^2	Anode samples			Anode-concrete interface samples			
			Resist-ance	Bond strength	SEM	XRF	XRD	ASEM	pH
Laboratory Aging Experiment									
Unaged, uncatalyzed, N_2	---	0	x	x	x	x	x	x	x
Aged, uncatalyzed, air	5	1520	x	x	x			x	x
Aged, catalyzed, air	6	1520	x	x	x	x	x	x	x
Aged, catalyzed, N_2	48, 49, 50	1520	x	x	x	x	x	x	x
Depoe Bay Bridge Field Trial									
zone 14, uncatalyzed, air	---	0	x						
zone 14, air, core samples	3SW1 4SW1	146	x		x			x	x

5.2.1 ICCP PERFORMANCE

The performance of the titanium anodes, as part of an ICCP system, was determined by periodic measurement of their voltage-current-time response. For the laboratory aging experiment, this involved continuous monitoring of the voltage and current of the five slabs connected in series and daily measurement of the voltage across each slab. Laboratory humidity and temperature were also recorded with these measurements. In the field trial, the voltage and current for Zone 14 was recorded daily by ODOT as part of routine monitoring of the Depoe Bay Bridge CP systems.

5.2.2 Anode Properties

5.2.2.1 Anode Structure

The anode structure was evaluated using scanning electron microscopy (SEM). The outer surfaces of anodes and polished cross-sections of anodes attached to the concrete substrate were examined. Samples of the outer surface of the anodes were obtained by using a hammer and chisel to chip small pieces from the laboratory concrete slabs and from the Depoe Bay Bridge core samples. Samples for cross-sections were cut with a diamond saw from the laboratory slabs and the bridge cores. Prior to cross sectioning, the anode surfaces were infused with epoxy to stabilize them and permit cutting without disbondment of the anode from the concrete. Cross-sectioned samples were then mounted on-edge in epoxy and polished to a 1 μm diamond surface finish. The SEM used in the anode characterization study, Section 4.0, was used here.

5.2.2.2 Anode Resistivity

The resistance of the titanium anode was measured with the a multi-pin resistance probe (see Section 2.2.1). No surface preparation was required for these measurements. The probe measured only the resistance of the thermal-sprayed anode since the underlying concrete was orders in magnitude more resistive when dry. Resistance measurements were made on the laboratory slabs before electrochemical aging and at the conclusion of the aging experiment. Measurements on Zone 14 at the Depoe Bay Bridge were made under field conditions. The field measurements were made immediately after catalyzing the newly applied anode but prior to activating the ICCP system. Other measurements were made on the catalyzed anode after it was in service for roughly 1.1 years (i.e., 102 kC/m^2).

5.2.2.3 Anode Bond Strength

Aluminum dollies 50 mm (1.9") diameter, identical to those used with the Proceq portable bond strength tester, were epoxied to the titanium anode with a high viscosity,

high strength and short set time (300 s) epoxy. The epoxy was allowed to cure 24 hours. Bond strength was then measured on laboratory slabs using a universal testing machine (*Covino, et al., 1995, 1996b and 1997a*).

5.2.2.4 Coating Durability

Coating durability was qualitatively evaluated in the laboratory by forcefully rubbing a piece of hard rubber across the coating surface and observing whether or not the coating crumbled. Only two conditions were categorized with this test: (1) the anode was cohesive and rubbing the surface dislodged no coating material; or (2) the anode was friable and readily crumbled under the pressure of the rubber tool.

5.2.3 ANODE-CONCRETE INTERFACIAL CHEMISTRY

Titanium anode-concrete interfaces on laboratory concrete slabs and on cores from the Depoe Bay Bridge field trial were characterized by several techniques -- X-ray fluorescence (XRF), X-ray diffraction (XRD), analytical scanning electron microscopy (ASEM) and micro-pH electrodes. The purpose was to provide a more detailed understanding of changes in the chemistry at this interface with aging.

5.2.3.1 X-ray Fluorescence

Samples from the anode-concrete interface and from other parts of the laboratory concrete slabs were analyzed by energy-dispersive XRF spectroscopy. The analysis system was the same as used in anode characterization (Section 4.3.1). Samples were removed from the laboratory concrete slabs as fine powders by carefully separating the aged titanium anode from the concrete and then scraping the interface with a fine probe to remove a thin layer of the cement paste. A separate sample representing the bulk (unaltered) concrete was obtained from the laboratory slabs as a powder by scraping the cement paste at a site on a cross-section about 1.9 cm (3/4") from the anode.

5.2.3.2 X-ray Diffraction

The powder samples used in the XRF analyses were also used for XRD analyses. The analysis system was the same as used in anode characterization (Section 4.3.3).

5.2.3.3 Analytical Scanning Electron Microscopy

Polished cross-sections of the anode-concrete interface were analyzed by ASEM to determine local composition and structure of the electrochemically-aged interface. The cross-sectioned samples were carbon coated to reduce charging. Images, manual point analyses, line scans (using automatic point analyses), and x-ray maps of the aged anode-

concrete interface were obtained with the same SEM used in anode characterization (Section 4.3.4). Cross-sections from the laboratory aging experiment and the field trial were examined.

5.2.3.4 Micro-pH Measurements

The pH values at the anode-concrete interface were measured using an Accumet Model 925 pH meter with automatic temperature compensation and a Microelectrodes micro-combination pH electrode that required as little as 0.1 mL of solution for a measurement. Samples for analysis were obtained from the laboratory aging experiment and from the field trial (using the core samples). Calibration was done using a two-point method and pH 7 and 10 standard solutions. Measured pH values agreed well with standards from pH 4 to 10. Measured values above 10 were lower than those of standards. For example, using the pH 12 standard, the measured value was pH 11.5.

To measure the pH of the anode-concrete interface, a piece of titanium anode was carefully parted from the concrete substrate using a thin blade. A drop of high-purity water (Type I) was then applied to the exposed titanium anode surface and mixed, using a thin glass rod, with any cementitious material remaining attached to this surface. The pH of the resulting solution was measured after a 5 minute equilibration period. This pH value was defined as the pH on the *anode side of the interface*, to distinguish it from the pH on the *concrete side of the interface*.

The pH of the concrete at the interface was measured using powder scrapings carefully removed from the concrete interfacial surface exposed when the anode was parted from the concrete substrate. These scrapings were placed in a small polyethylene cup, and a drop of water was added to the scrapings to form a slurry. The pH of the slurry was measured after a 5-minute equilibration period. This pH value was defined as the pH on the *concrete side of the interface*. The pH for the *concrete side of the interface* was typically ½ to 1 full unit higher than that on the *anode side of the interface*. The reason for this is a gradient of pH near the interface, ranging from that at the interface to that of the unaltered concrete (around pH 12-12.5). The sample being analyzed to determine the pH on the *concrete side of the interface* contains less of the interfacial cementitious material and more unaltered concrete. When possible, powder scrapings were also removed from sample cross-sections at locations well removed from the titanium anode to give the pH for bulk concrete (i.e., concrete unaltered by reactions at the anode-concrete interface). Again, a drop of water was added to the powder to form a slurry. The pH of the slurry was measured after a 5-minute equilibration period.

5.3 CHARACTERIZATION RESULTS

5.3.1 ICCP Performance

The five titanium-coated concrete slabs were electrochemically aged for 1.8 years in the laboratory. The electrochemical age of the slabs was 1520 kC/m^2 (about 23 years service at the current density of 2.1 mA/m^2 (0.2 mA/ft^2) used by ODOT for coastal bridges). With the exception of the uncatalyzed anode, anode performance was stable over the entire period the anodes were aged. However, the mechanical durability of the anode surface deteriorated with aging.

Figure 5.3 shows the voltage of catalyzed and uncatalyzed slabs as a function of accumulated charge. The curve for the catalyzed slabs is the average of the curves for the four catalyzed samples (6, 48, 49 and 50). For a period equivalent to 700 kC/m^2 or 10 years, the catalyzed and the uncatalyzed anodes performed essentially the same. This appears to represent an induction period for the uncatalyzed anode, and the uncatalyzed slab voltage increased markedly with aging for longer aging times, depending upon humidity and wetting of the anode.

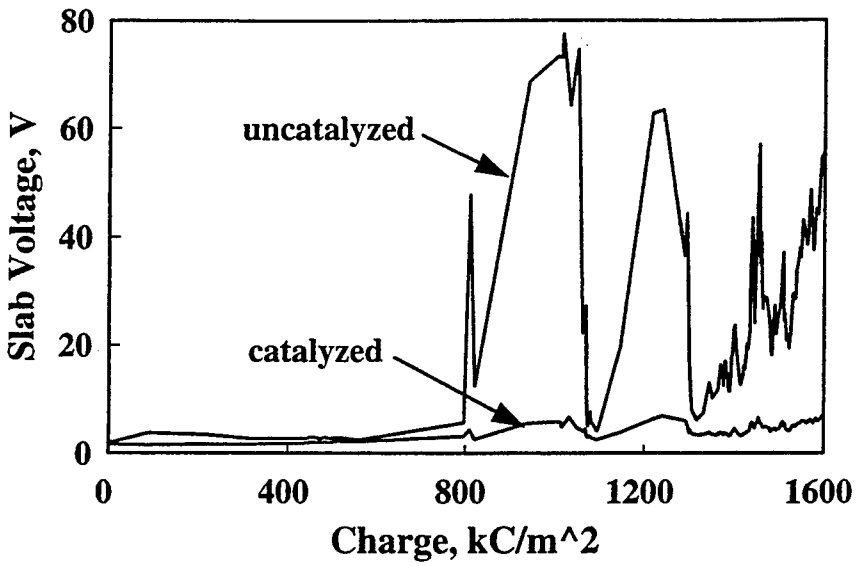

Figure 5.3: Slab voltage as a function of electrochemical aging.

The two large humps in the curve for the uncatalyzed anode beginning at 700 kC/m^2 correspond to two periods when the RH was decreased gradually to 30 pct and then raised to 100 pct. During this same period the voltage of the catalyzed anodes changed very little. Beyond 1200 kC/m^2, at a RH of 70-80 pct, the voltage of the uncatalyzed anode rose steadily. It decreased

only when the anode was periodically wetted with Type 1 water, as indicated by the jagged shape of the curve for longer aging. The voltage of the catalyzed anodes during this period was only nominally higher than when aging began.

In Figure 5.4, slab voltage is shown as a function of relative humidity for catalyzed and uncatalyzed anodes at a current density of 21 mA/m^2 (2 mA/ft^2) during the two periods when the laboratory humidity was varied from 30 to 100 pct. The voltage for the uncatalyzed anode rose sharply to unacceptably high levels with decreasing RH. In contrast, the voltage for the catalyzed anode varied from 2.5 to 7.0 volts when the humidity decreased from 100 to 30 pct RH. The decrease in voltage with increasing RH was linear and very slight, indicating the catalyzed anode performance was not strongly dependent upon RH for electrochemical aging up to 1520 kC/m^2. Furthermore, it indicates sufficient water was delivered to the catalyzed anode from the humid air to maintain the anode reaction without undue polarization of the anode. A least squares fit of the data for the catalyzed anode shows the humidity dependence of the anode operating voltage to be:

$$V = 6.98 - 0.0314\ RH \tag{5.3}$$

The uncatalyzed anode, however, showed a strong dependence on humidity, with a least squares fit of the data in Figure 5.4 giving:

$$V = 92.04 - 0.8172\ RH \tag{5.4}$$

It suggests that the uncatalyzed anode has become passive and is exhibiting limited valve metal characteristics. This agrees with the work of others (*Gusmano, et al., 1996*), where uncatalyzed titanium oxide films have been considered for use as humidity sensors because they showed increased levels of ionic conduction when water was absorbed on their surface.

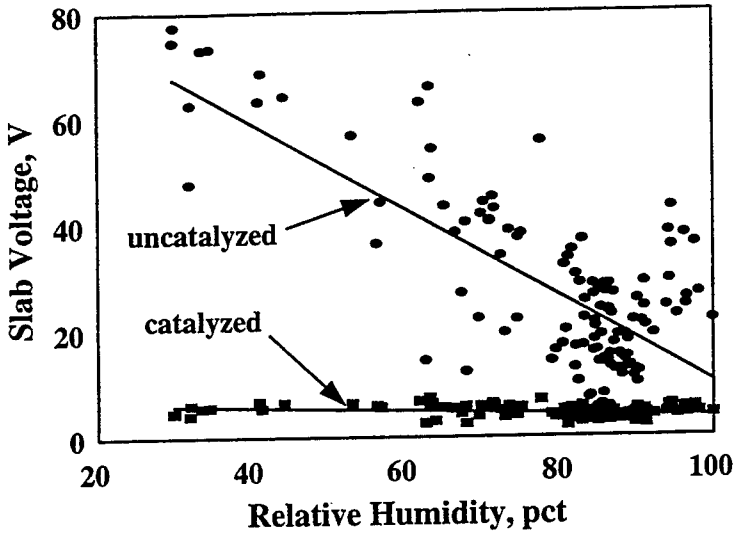

Figure 5.4: Voltage requirements of thermal-sprayed titanium anodes at current density of 2.1 mA/m^2 as a function of RH.

5.3.2 Anode Properties

5.3.2.1 Anode Structure

Electrochemical aging of the thermal-sprayed titanium anode resulted in no changes in the structure of the anode. Figure 5.5 shows the outer surface of the titanium anodes in aged/unaged and catalyzed/uncatalyzed conditions. Also shown is the thermal-sprayed Ti anode from the Depoe Bay Bridge. There was no significant difference between the structure of any of these surfaces. A similar examination of polished anode cross-sections also showed no difference in the structure of the unaged anode and the aged anode.

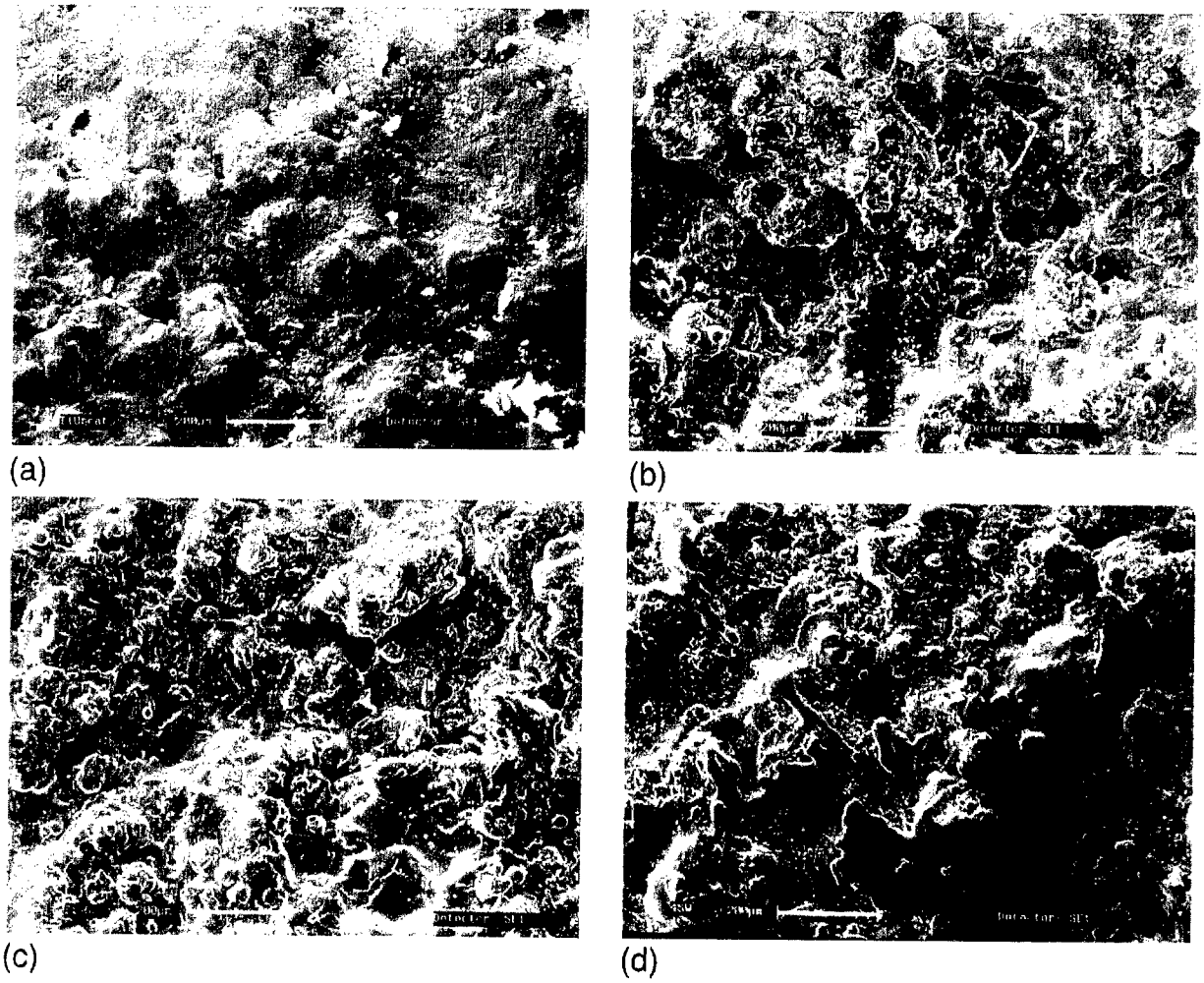

Figure 5.5: Secondary electron SEM photomicrographs of thermal-sprayed titanium anode surface before and after electrochemical aging: (a) unaged, uncatalyzed; (b) aged 1520 kC/m^2, uncatalyzed; (c) aged 1520 kC/m^2, catalyzed; (d) Depoe Bay Bridge field trial, aged 146 kC/m^2. 70X.

The average thickness of the titanium anodes was estimated from SEM photomicrographs of the polished cross-sections. These results are given in Table 5.2. They include values

for titanium thermal-spray coatings on glass and concrete plates used in anode characterization (Section 4.0). They include values for the concrete slabs used in the laboratory aging experiment and for the anode in Zone 14 of the Depoe Bay Bridge ICCP system. There was no evidence of a change in anode thickness during aging nor was coating lost in other ways, such as by spalling. The differences in average thickness simply reflect differences in initial coating thickness and are well within the range of values observed for the thermal-sprayed titanium anode.

Table 5.2: Thickness of aged anodes.

TEST ANODE (aging, catalyst, atomizing gas, substrate)	Electrochemical age, kC/m^2	Anode thickness, μm (mil)		
		Minimum	Maximum	Average
Glass plates				
Unaged, uncatalyzed, air, TiPA, see Table 3.2	0	75 (3.0)	130 (5.1)	95 (3.7)
Unaged, uncatalyzed, N_2, TiPN, see Table 3.2	0	65 (2.6)	120 (4.7)	80 (3.1)
Concrete plates				
Unaged, uncatalyzed, air, plate 1, see Table 3.4	0	128 (5.0)	329 (13.0)	149 (5.9)
Unaged, uncatalyzed, N_2, plate 41, see Table 3.4	0	77 (3.0)	169 (6.7)	113 (4.4)
Laboratory Aging Experiment				
Unaged, uncatalyzed, N_2, no slab number	0	33 (1.3)	200 (7.9)	100 (3.9)
Aged, uncatalyzed, air, slab 5, see Table 3.7	1520	33 (1.3)	166 (6.5)	100 (3.9)
Aged, catalyzed, air, slab 6, see Table 3.7	1520	50 (2.0)	210 (8.3)	90 (3.5)
Aged, catalyzed, N_2, slab 48, see Table 3.7	1520	56 (2.2)	128 (5.0)	72 (2.8)
Aged, catalyzed, N_2, slab 49 see Table 3.7	1520	28 (1.1)	104 (4.1)	60 (2.4)
Aged, catalyzed, N_2, slab 50 see Table 3.7	1520	48 (1.9)	128 (5.0)	76 (3.0)
Depoe Bay Bridge Field Trial				
zone 14, air (Cores 3SW1 and 4SW1)	146	0 (0)	166 (6.5)	83 (3.3)

5.3.2.2 Anode Resistivity

Electrochemical aging did result in changes in the apparent resistivity of the anode, Table 5.3. Resistivity values were computed (see Equation 4-1) from resistance measurements made using the ODOT resistance probe, the probe geometry (length = width) and the average anode thickness in Table 5.2. The resistivity of the unaged anode decreased after the anode had been catalyzed. This appears to be due to the conductive cobalt nitrate catalyst and adsorbed moisture associated with the catalyst within the anode coating. The resistivity of the aged, uncatalyzed anode was almost three times higher than that of the unaged, uncatalyzed anode and higher than that of the aged, catalyzed anode. The resistivity of the aged, catalyzed anode was almost four times higher than that of the unaged, catalyzed anode. Thus, in every instance, aging substantially increased the resistivity of the anode relative to the unaged anode. As there were no outward physical changes observed in the anode, the increase could be due to continued microcracking within the anode, particularly along the weak interface between splats, related to stress relaxation from mechanical property changes at the anode-concrete interface. Another factor could be progressive oxidation of anode surfaces by oxygen liberated in the anode reaction.

As noted in anode characterization, the resistivity of the unaged, uncatalyzed anode was 40 pct lower using nitrogen atomization rather than air atomization. Similarly, the resistivity of the aged, catalyzed anode produced using nitrogen atomization was 40 pct lower than that produce using air atomization. Thus, the initial benefits of nitrogen atomization were also observed after substantial aging.

The resistivity of the unaged, catalyzed Depoe Bay Bridge anode was comparable to that of the unaged, catalyzed anode from the laboratory studies (slab 6). Aging for 215 kC/m^2 increased the resistivity by a small but significant amount, i.e. 15 pct. This would suggest that resistivity measurements may be a useful way to monitor the progress of Ti anode aging.

Table 5.3: Resistivity of aged anodes.

TEST ANODE (aging, catalyst, atomizing gas, substrate)	Electro-chemical age, KC/m^2	Correction factor, C (see Fig.2.2)	Average thickness, μm	Resistance, ohms	Apparent resistivity, ρ_a, μohm-cm
Glass plate					
Unaged, uncatalyzed, air	0	1.0	95	0.375	3562
Unaged, uncatalyzed, N_2	0	1.0	80	0.27	2160
Concrete plate					
Unaged, uncatalyzed, air, plate 1	0	1.0	149	0.23	3429
Unaged, uncatalyzed, N_2, plate 41	0	1.0	113	0.365	4124
Laboratory Aging Experiment					
Unaged, uncatalyzed, air, slab 5	0	0.7	100	0.20	2857
Aged, uncatalyzed, air, slab 5	1520	0.7	100	0.58	8285
Unaged, catalyzed, air, slab 6	0	0.7	90	0.20	2571
Aged, catalyzed, air, slab 6	1520	0.7	90	0.56	7200
Unaged, catalyzed, N_2, slab 48	0	0.7	72	0.16	1646
Aged, catalyzed, N_2, slab 48	1520	0.7	72	0.44	4526
Unaged, catalyzed, N_2, slab 49	0	0.7	60	0.155	1328
Aged, catalyzed, N_2, slab 49	1520	0.7	60	0.45	3857
Unaged, catalyzed, N_2, slab 50	0	0.7	76	0.155	1683
Aged, catalyzed, N_2, slab 50	1520	0.7	76	0.42	4560
Depoe Bay Bridge Field Trial					
Zone 14, air, 7-12-95	0	0.6	83	0.228	3154
Zone 14, air, 8-27-96	102	0.6	83	0.245	3389
Zone 14, air, 3-12-98	215	0.6	83	0.264	3652

5.3.2.3 Anode Bond Strength

Anode bond strengths decreased markedly with aging, as shown in Table 5.4. The decrease was most severe for the aged, uncatalyzed anode (slab 5), decreasing from 1.17 MPa (171 psi) for the unaged, uncatalyzed anode to 0.01 MPa (0.9 psi) for the aged, uncatalyzed anode. The bond strength for the catalyzed anodes decreased to about 25 pct of the initial value, or an average of 0.29 MPa (42 psi). The bond strength of anodes formed using nitrogen atomization was marginally higher than for anodes formed using air atomization.

Table 5.4: Bond strength of anodes, laboratory aging experiment.

Slab Number	Electrochemical age, kC/m^2	Bond strength, MPa (psi)	
		Unaged	Aged
5	1520	1.18(171)*	0.01(0.9)
6	1520	1.18(171)*	0.26(37)
48	1520	1.18(171)*	0.28(41)
49	1520	1.18(171)*	0.28(41)
50	1520	1.18(171)*	0.35(51)

* = *Average for the eight slabs reported in Table 3.4.*

The decrease in bond strength was due to the formation of a thin, friable layer in the concrete adjacent to the anode during aging. This layer was stained rust red, probably due to the oxidation of Fe(II) to Fe(III) in the cement paste during aging. In the presence of the friable layer, the anode was easily abraded by drawing a blunt, hard rubber tool across the anode surface, causing the anode to crumble and flake from the concrete. The aged, catalyzed anode was more durable and less easily damaged by abrasion than the aged, uncatalyzed anode, although neither anode surface had good durability after aging the equivalent of 23 years service. On the other hand, except where the anode was abraded, the surface did not appear damaged and there was no loss of coating by spalling or other mechanisms.

5.3.3 Anode-Concrete Interfacial Chemistry

5.3.3.1 X-ray Fluorescence

The chemistry of the interface and bulk concrete of unaged and aged anodes are given in Table 5.5. Samples 2 and 5 are the scrapings of material from the interface taken immediately after Samples 1 and 4 were taken. They represent material perhaps a mm deeper into the concrete than Samples 1 and 4. The XRF results are the concentrations of the individual elements expressed as their corresponding oxide.

Table 5.5: Chemistry of anode-concrete interface in laboratory aging experiment.

Concrete sample and analysis location	Electrochemical age, kC/m^2	Element concentration (expressed as the oxide), wt pct						
		Al_2O_3	SiO_2	K_2O	CaO	TiO_2	Fe_2O_3	CoO
Unaged, uncatalyzed anode, N_2 atomizing gas (no slab number)								
Sample 1: at interface	0	10.0	71.3	1.3	14.0	2.3	1.2	NA
Sample 2: concrete just below Sample 1	0	9.9	71.6	1.1	15.1	1.2	1.4	NA
Sample 3: bulk concrete	0	9.4	71.2	1.0	16.2	0.7	1.5	NA
Aged, catalyzed anode, N_2 atomizing gas (slabs 48, 49, 50)								
Sample 4: at interface	1520	11.0	72.6	5.5	2.5	3.2	3.3	1.8
Sample 5: concrete just below Sample 4	1520	12.9	66.5	8.2	6.4	2.0	2.7	1.3
Sample 6: bulk concrete	1520	10.1	73.0	1.1	13.8	0.9	1.2	0.0

As one would expect, composition of the bulk concrete before and after aging was the same. The bulk concrete results do show the analyses are reproducible and that measured differences represent differences in the chemistry of the concrete near the anode-concrete interface. There were essentially no differences in the chemistry of the three samples taken from the unaged slab. The variation in the values for titanium do not represent a gradient of oxidized titanium in the concrete. They simply suggest some of the titanium anode was included in the sample and, as samples were taken further from the anode, there was lower likelihood they would include measurable titanium.

There were substantial gradients in composition of the concrete near the interface of the aged anode. For example, the cobalt catalyst concentration in the concrete was measurable and decreased as samples were taken further from the anode. Calcium concentrations at the interface were only 20 pct or less of that in the bulk concrete and increased with distance from the anode. This demonstrates that aging results in a depletion of calcareous minerals from the cement paste. On the other hand, constituents of insoluble minerals (i.e., aluminum and potassium in feldspars) were enriched near the interface because of the loss of soluble minerals. Iron was also enriched near the interface, in all likelihood because soluble mineral loss from the cement paste. Oxidation of Fe(II) to Fe(III) would be likely near the anode and account for the appearance of the rust red color in the cement paste adjacent to the anode-concrete interface.

5.3.3.2 X-ray Diffraction

The mineralogy of the interface and bulk concrete of unaged and aged anodes are given in Table 5.6. The samples are the same as those used in the XRF analyses, Table 5.5.

Mineral concentrations are given qualitatively in decreasing amount as primary, minor, trace and probable.

Table 5.6: Crystallographic phases at anode-concrete interface in laboratory aging experiment.

Concrete sample and sample location	Electrochemical age, kC/m^2	Mineral Phases
Unaged, uncatalyzed anode, N_2 atomizing gas (no slab number)		
Sample 1: at interface	0	Albite ($NaAlSi_3O_8$), primary Quartz (SiO_2), minor Vaterite, Calcite and Aragonite ($CaCO_3$), minor
Sample 2: concrete just below Sample 1	0	Albite, primary Quartz, minor Vaterite and Aragonite, trace
Sample 3: bulk concrete	0	Albite, primary Quartz, minor Portlandite ($Ca(OH)_2$), minor Calcite and Larnite (Ca_2SiO_4), probable
Aged, catalyzed anode, N_2 atomizing gas (slabs 48, 49, 50)		
Sample 4: at interface	1520	Albite ($NaAlSi_3O_8$), primary Quartz (SiO_2), minor
Sample 5: concrete just below Sample 4	1520	Albite, primary Quartz, minor Calcite ($CaCO_3$), trace
Sample 6: bulk concrete	1520	Albite and quartz, primary Portlandite ($Ca(OH)_2$), minor Larnite (Ca_2SiO_4), probable

The only significant difference between samples for the unaged anode was the presence of Portlandite in the bulk concrete but its absence in the region near the anode-concrete interface. This may occur as the result of heat input from the thermal-sprayed titanium and dehydration of the concrete in this region. The other significant fact is the presence of calcium carbonate minerals in all of the samples from the unaged anode, although the concentration in the bulk concrete was only probable. The loss of the calcium carbonate minerals from the region adjacent to the anode-concrete interface was the primary difference between the mineralogy of unaged and aged anodes.

5.3.3.3 Analytical Scanning Electron Microscopy

A BE SEM photomicrograph of a typical aged anode cross-section (slab 6) is shown in Figure 5.6. The titanium anode is the light band at the very top of the image. Below it lies a reaction zone characterized by the loss of cementitious material. This reaction zone grows in width as aging progresses and more hydroxyl ions are consumed by the anode reaction. The boundary between the reaction zone and underlying concrete would appear to be the reaction front for the anode reaction. Below this boundary is a layer of concrete

where the material lost from the reaction zone has been deposited in voids, pores and cracks. This layer is more dense than unaltered concrete shown at the bottom of the figure. Dense concrete layers surrounding nonconsumable anodes have been reported previously for titanium mesh anodes embedded in concrete (*Weale, 1992*).

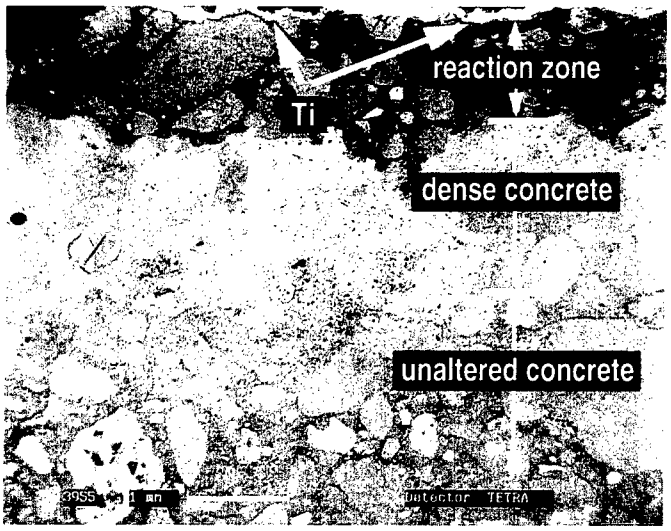

Figure 5.6: BE SEM photomicrograph of cross-sectioned, catalyzed anode (slab 6), aged 1520 kC/m^2. 13.5X.

Cracks are present in the reaction zone extending from the titanium anode to the reaction front (at the interface between reaction zone and dense concrete) but not beyond the reaction front. The evidence suggests these cracks formed during electrochemical aging since none penetrated beyond the reaction front. They were located at sites of deepest penetration of the reaction front into the concrete and appear to be conduits for moisture and hydrogen ions to the reaction front. Their presence suggests the material retained in the reaction zone is brittle and easily damaged.

Cross-sections of slab 6 (aged, catalyzed) were examined to determine the structure of concrete in the reaction zone, in the dense concrete layer below the reaction zone, and in unaltered concrete. Figure 5.7 shows the cross-section in Figure 5.6 marked with four areas corresponding to these regions. Photomicrographs of the four areas are shown in Figure 5.8. Figure 5.8(a) shows a typical microporous section of unaltered concrete, located well away from the titanium anode and the reaction zone. Figure 5.8(b) shows the concrete in a region immediately below the reaction zone that is more dense (less porous) than the unaltered concrete seen in Figure 5.8(a). The formation of a dense zone adjacent to titanium mesh anodes embedded in concrete has been observed by others (*Weale, 1992*). The reaction zone formed on aging is shown in Figures 5.8(c) and 5.8(d). It is more porous than the unaltered concrete or the dense concrete. The interface between the dense concrete and the reaction zone (Figure 5.8(c)) is the point where reaction

products from the anode attack the cement paste, broaden the reaction zone and move the zone of dense concrete deeper into the concrete slab.

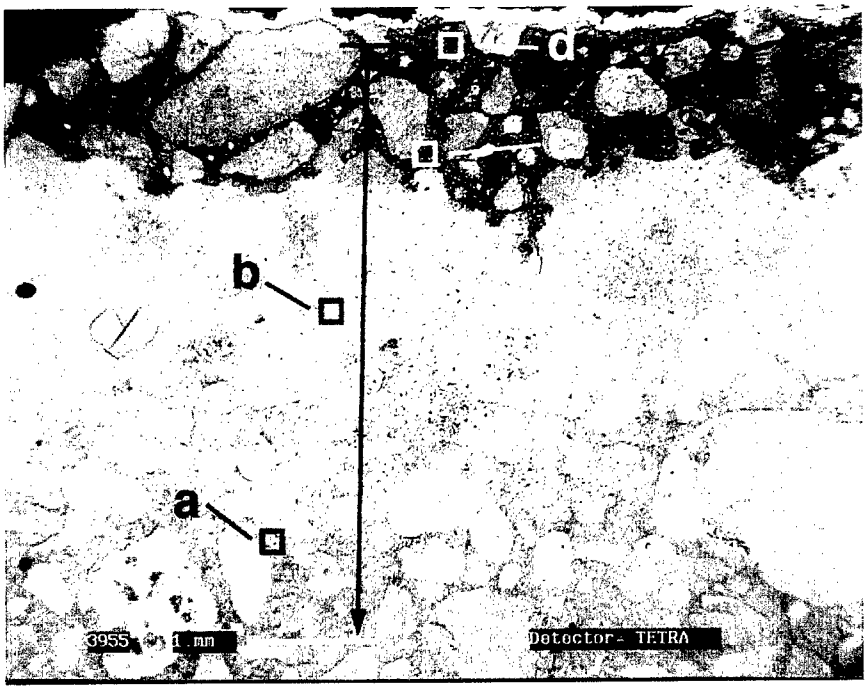

Figure 5.7: BE SEM photomicrograph of cross-sectioned, catalyzed anode (slab 6), aged 1520 kC/m^2. Four areas are shown where the SEM photomicrographs in Figure 5.8 were taken. 17X.

Acidification of the anode-concrete interface for non-consumable anodes such as the titanium anode (see Table 5.7) is well documented (*Hayfield and Warne, 1989; Nielsen-Dharmaratne and Gronvold, 1992; Pedeferri et al., 1989; NACE International, 1990*). The consequence of acidification is a deterioration of the cement paste as calcareous minerals are dissolved and displaced from the concrete matrix. This results in the reaction zone illustrated in Figure 5.6 and the structures shown in Figures 5.7 and 5.8.

The effects of acidification are strongly dependent upon current density (*Pedeferri et al., 1989*). NACE International (*NACE, 1990*) gives as a guideline a maximum current density (based on the anode area) of 108 mA/m^2 (10 mA/ft^2) to prevent significant deterioration of the concrete at the anode-concrete interface. This maximum works well for embedded anodes where a 1 to 2 mm reaction zone does not affect anode contact with the concrete or the structural integrity of the anode installation. Furthermore, the volume of cement paste in a 1 to 2 mm zone surrounding the wire in a mesh anode and available to neutralize acidic anode reaction products is 2 to 3 times that in a similar zone for a planar anode such as thermal-sprayed titanium. As a consequence, acidification has a quantitatively greater impact on the anode-concrete interface in terms of reaction zone penetration into the concrete. Furthermore, the presence of the reaction zone undermines

the mechanical integrity of the anode in a way that is of no consequence for embedded anodes. A thin, porous mortar overlay of the thermal-sprayed anode may accomplish several objectives. It would double the basic minerals available for neutralizing acidic anode reaction products. Furthermore, it would provide a means for altering the appearance of the anode surface without affecting anode operation.

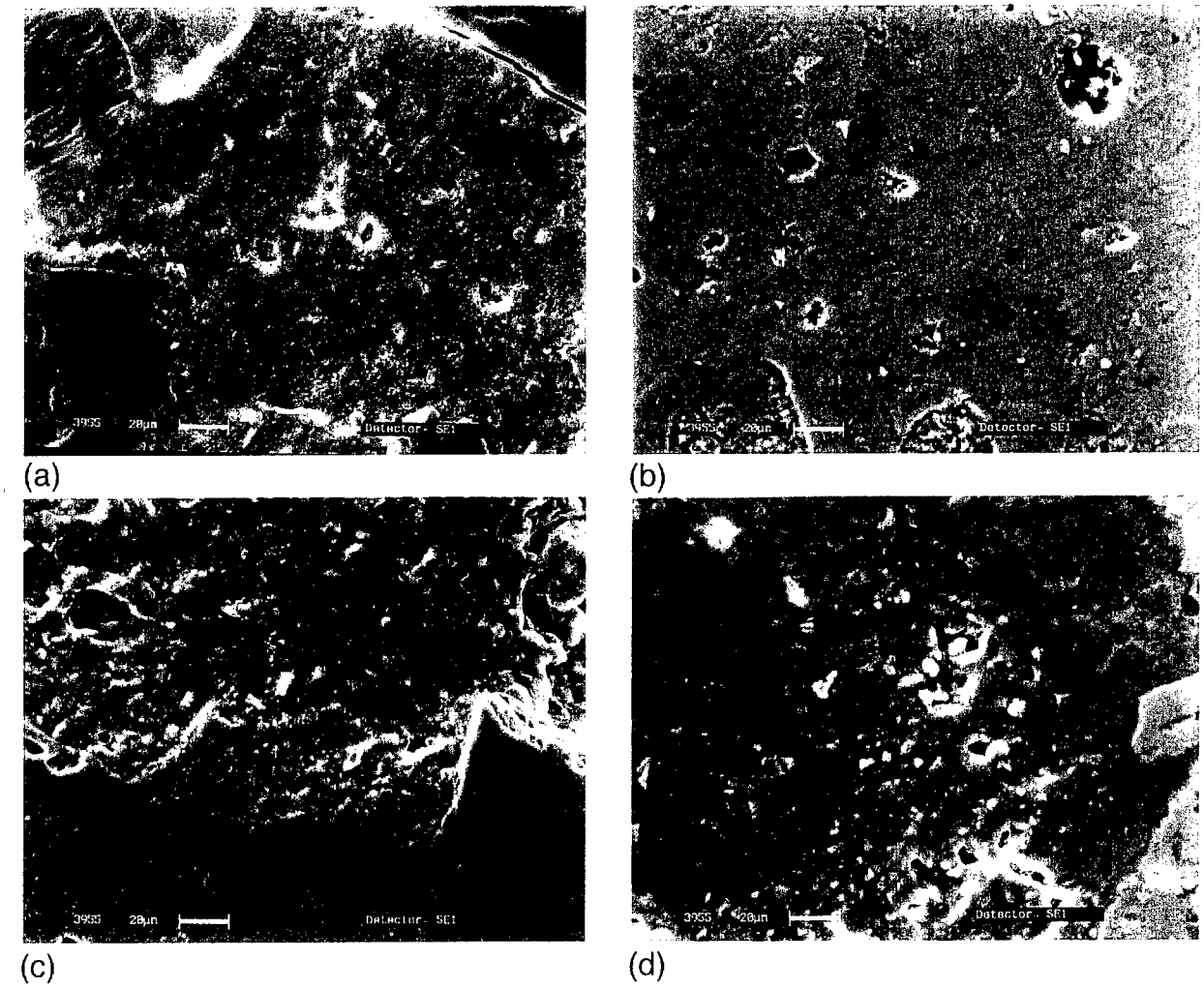

Figure 5.8: Four SE SEM photomicrographs of slab 6 areas shown in Figure 5.7: (a) unaltered concrete; (b) dense concrete; (c) concrete-reaction zone interface; (d) reaction zone. 350X.

BE SEM photomicrographs of polished cross-sections of the anode-concrete interfaces are shown in Figure 5.9. Figure 5.9(a) represents the unaged interface and Figures 5.9(b) and 5.9(c) the aged, uncatalyzed (slab 5) and aged, catalyzed (slab 6) interfaces, respectively. The reaction zone that forms on aging is clearly seen in Figures 5.9(b) and 5.9(c) as the dark region between anode and unaltered concrete. Figure 5.9(d) is a cross-section from the aged Depoe Bay Bridge anode (146 kC/m^2). There is no evidence of a

reaction zone for the Depoe Bay Bridge anode, and the interface looks similar to that of the unaged anode, Figure 5.9(a). Two factors may be involved. First, the bridge anode aging was less than 10 pct of that for the laboratory slabs and more aging may be required for a visible reaction zone to form. Secondly, the bridge anode was aged at a current density a factor of 10 lower than that used in the laboratory tests.

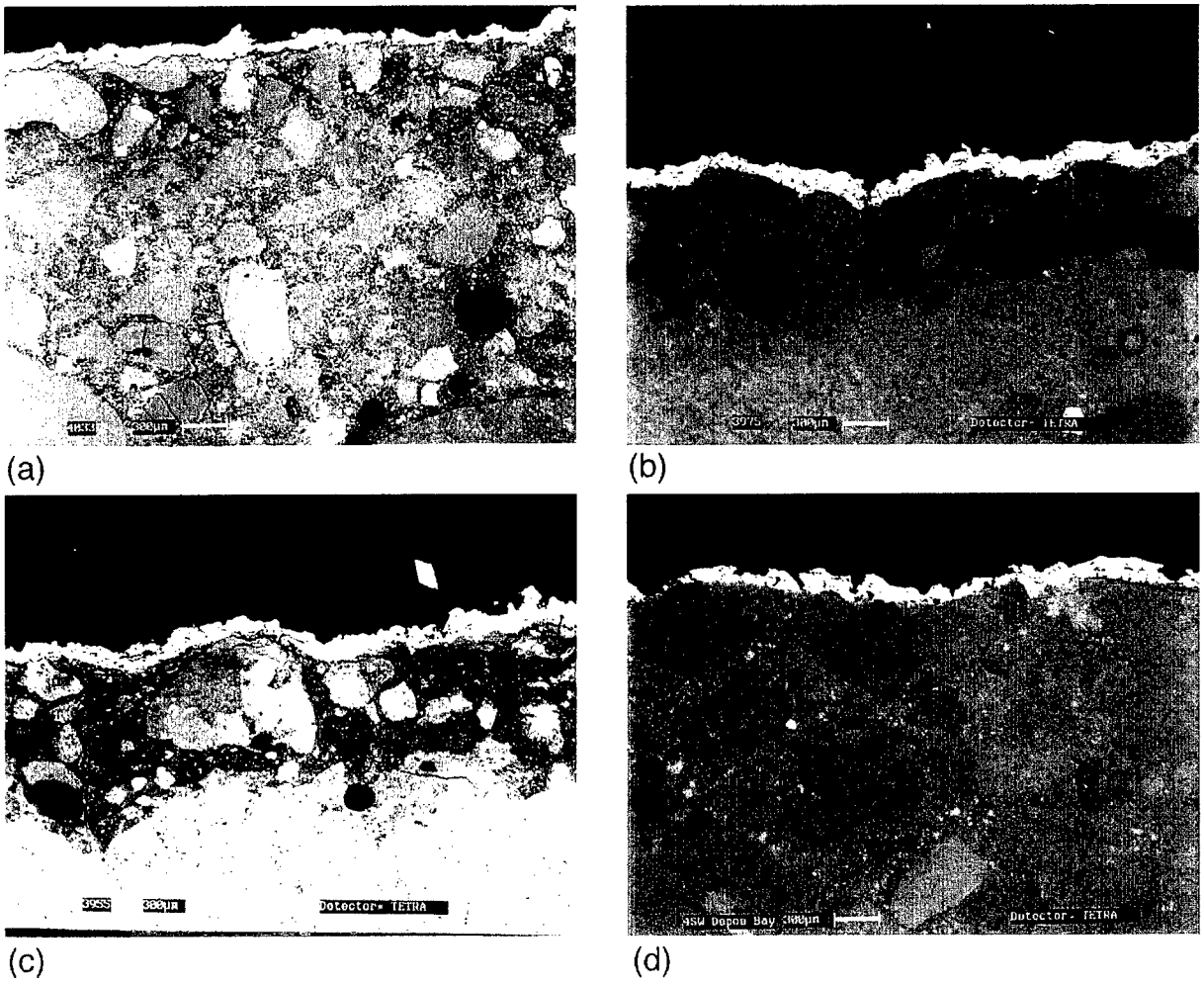

Figure 5.9: BE SEM photomicrographs of anode cross-sections: (a) unaged, uncatalyzed; (b) uncatalyzed (slab 5), aged 1520 kC/m^2; (c) catalyzed (slab 6), aged 1520 kC/m^2; (d) Depoe Bay Bridge field trial, aged 146 kC/m^2. 20X.

A BE SEM image is shown in Figure 5.10 for an aged catalyzed anode, along with element maps for Ti, Ca and Co obtained by EDS x-ray analyses of the same area. The titanium anode is the bright band across the top of Figure 5.10(a) and the corresponding bright band in the element map for Ti, Figure 5.10(b). No dissolution of titanium and migration of Ti into the concrete is evident. Figure 5.10(c) shows that the region identified is the reaction zone stripped of the Ca initially present in the cement paste. This is due to dissolution and removal of soluble calcareous minerals from the cement paste as hydroxide ions are consumed, or hydrogen ions are produced, by the anode reaction. The skeletal material that remains in the reaction zone contains the insoluble constituents of the concrete - silica and alumina minerals and the fine aggregate. The skeletal material that remains provides the mechanical support for the anode as it ages. Based on the cracks visible in Figure 5.6, this material is expected to be brittle.

Penetration of the cobalt catalyst into the reaction zone to the reaction front is evident in Figure 5.10(d). In fact, the highest concentrations of Co are located primarily at the reaction front. This suggests the site of the anode reaction moves into the concrete and becomes dispersed throughout the reaction zone as aging proceeds, with perhaps greatest activity at the reaction front. Dispersion of the catalyst into the concrete bodes well for the long term survival of the catalyst at the anode. Within the concrete, the catalyst is more protected from the leaching effects of repeated wettings of the anode. Furthermore, movement of the cobalt from the titanium-concrete interface into the reaction zone does not appear to adversely affect long anode operation (see Figures 5.3 and 5.4). In fact, movement of the cobalt into the reaction zone may be necessary to assure a long service life for the catalyzed thermal-spray titanium anode.

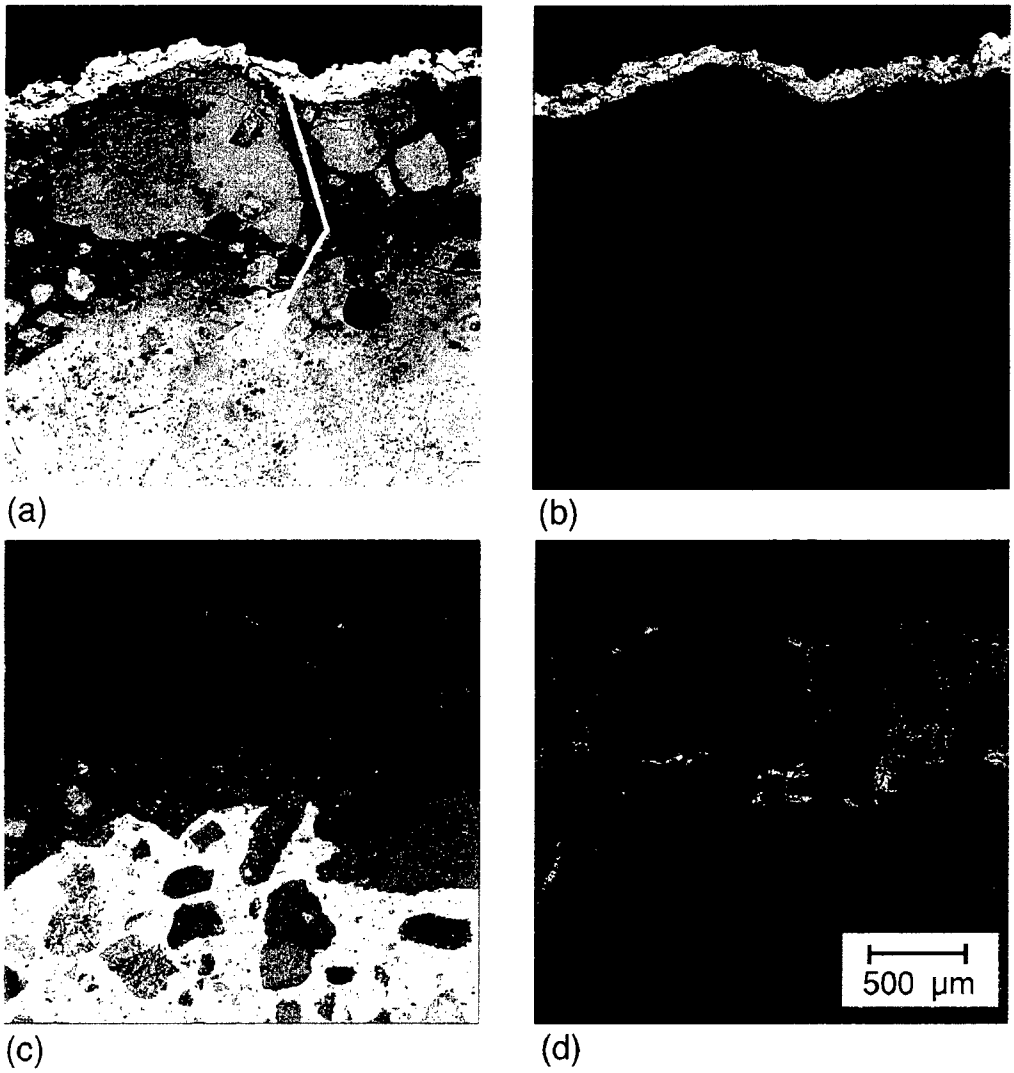

Figure 5.10: Cross-sectioned, catalyzed anode (slab 6), aged 1520 kC/m^2: (a) BE SEM image; (b) Ti K_α x-ray map; (c) Ca K_α x-ray map; (d) Co K_α x-ray map. Arrow in (a) shows path of ASEM traverse for composition depth profile. 25 X.

Figure 5.11 gives the composition depth profile for the traverse indicated by the arrow in Figure 5.10. This figure shows line scans for Ti, O, Ca, Si and Co. Other elements were included in the analysis but are not shown here. The thermal-sprayed titanium coating is the first part of the line scan, extending from 0 to approximately 0.06 mm in this figure. At the titanium-concrete interface there appears to be an overlap region where Ti, Ca and Si exist at detectable levels. Dissolution of the Ti and diffusion into the concrete is unlikely. It seems more likely that the x-ray spatial resolution is responsible for this overlap region. The reaction zone (i.e., where calcium levels are reduced to near zero levels) extends for approximately 0.6 - 0.65 mm, the reaction front. Co is present in the reaction zone, with local concentrations as high as 8 at pct. The elevated Si levels in the reaction zone are an artifact caused by the absence of the soluble Ca minerals. Beyond

the reaction zone, the Ca and Si levels are similar to those for bulk concrete, 20 and 25 at pct, respectively. These results are in agreement with those from powder samples removed from the anode-concrete interface, Table 5.5.

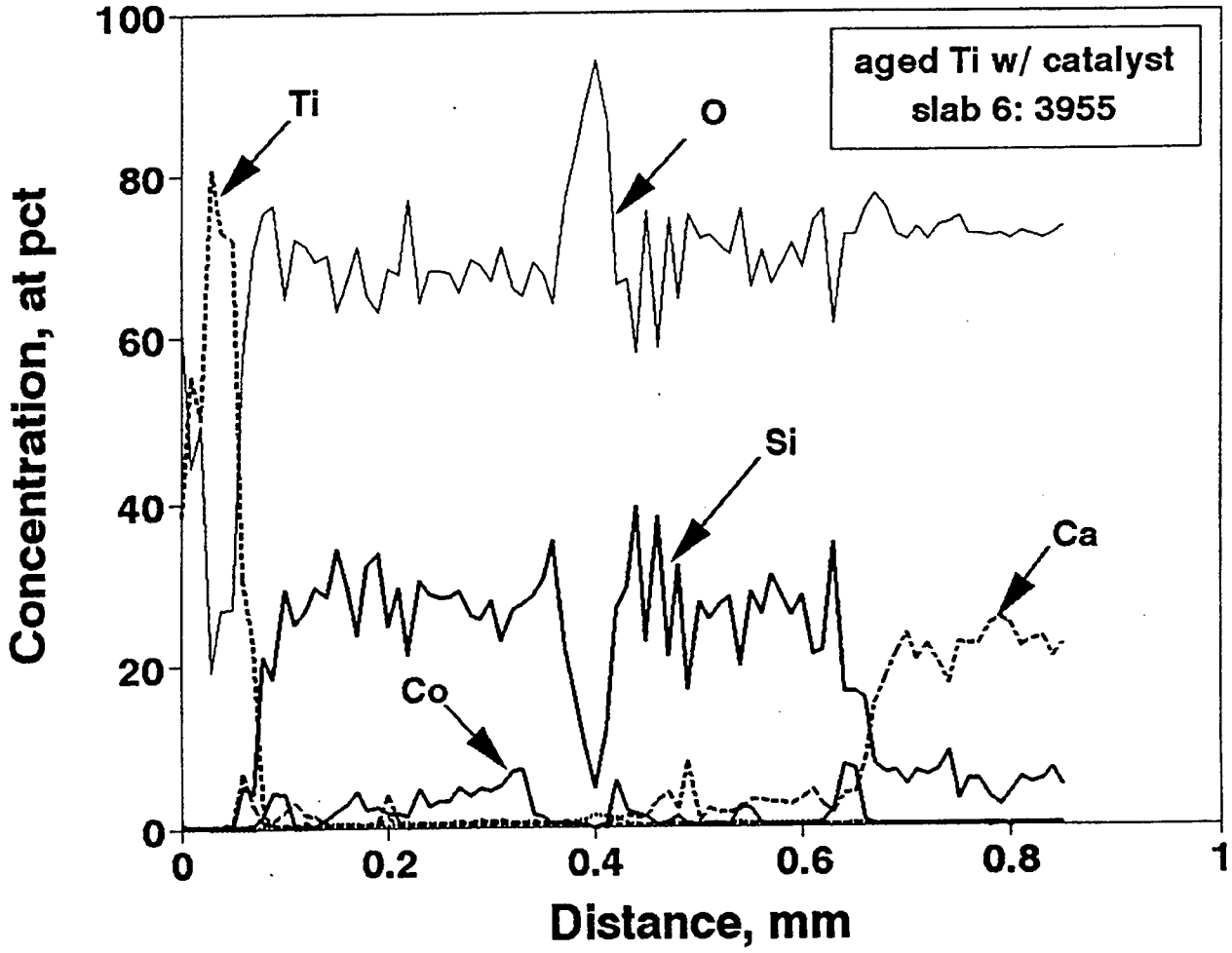

Figure 5.11: Composition depth profile for catalyzed thermal-sprayed titanium anode (slab 6) after electrochemical aging; path of traverse is shown in Figure 5.10(a).

A BE SEM image is shown in Figure 5.12 for the aged, catalyzed anode from the Depoe Bay Bridge, along with element maps for Ti, Ca and Co obtained by EDS x-ray analyses of the same area. The dark cracks in the SEM image, Figure 5.12(a), are due to drying and shrinkage during petrographic preparation. Figure 5.12(b) shows the titanium anode is insoluble and no Ti enters the cement paste. Figure 5.12(c) shows calcium was not leached from the concrete adjacent to the titanium coating. Because this cross-section was taken after only 146 kC/m^2, it is possible that leaching of the calcium was not yet visually detectable. Alternatively, there may be a critical current density for titanium anodes below which the cement paste does not deteriorate by leaching of calcium minerals (*Weale, 1992*). High concentrations of the cobalt catalyst remained at the

anode-concrete interface, Figure 5.12(c). Preexisting cracks in the concrete near the interface were filled with precipitates containing the cobalt catalyst, particularly several long cracks that extended deeply into the concrete. The cobalt catalyst appeared to have resisted leaching by precipitation for the short period of the field trial and, instead, moved into the cement paste by diffusion and convection, particularly along cracks.

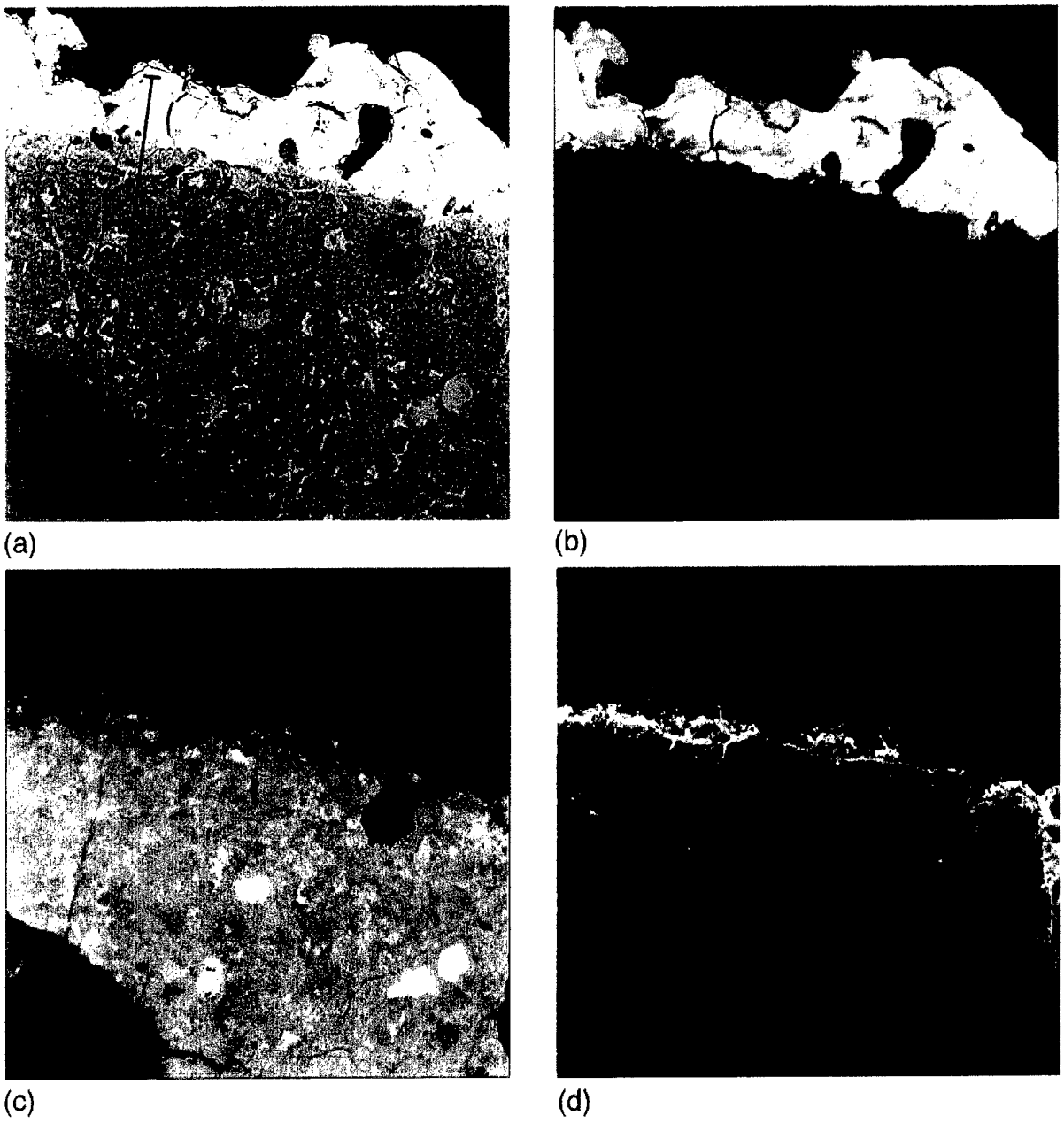

Figure 5.12: Cross-sectioned, catalyzed thermal-sprayed titanium anode from the Depoe Bay Bridge field trial after electrochemical aging 146 kC/m^2: (a) backscattered electron SEM image; (b) Ti K_α x-ray map; (c) Ca K_α x-ray map; (d) Co K_α x-ray map. Arrow in (a) shows path of ASEM traverse for composition depth profile. 150X.

A WDS composition depth profile for the traverse indicated in Figure 5.12(a) is shown in Figure 5.13. The narrow region near the titanium-concrete interface where titanium and calcium appear to coexist is similar to that observed for the laboratory slabs, Figure 5.11. It is thought to be due to the sample seen by the electron beam and not to dissolution and migration of anode material. No depletion of calcium was found in the concrete adjacent to the anode-concrete interface, but the calcium concentration near the interface is lower than that deeper in the concrete. The sharp drop in Ca and rise in Si, at about 2.8 mm, is due to the presence of a silica particle. The majority of the cobalt was located at the titanium-concrete interface at concentrations as high as 7 at pct. The Co peak at about 1.8 mm corresponds to the long lateral crack seen in Figure 5.12(d). It represents Co-containing precipitated material that has filled a preexisting crack.

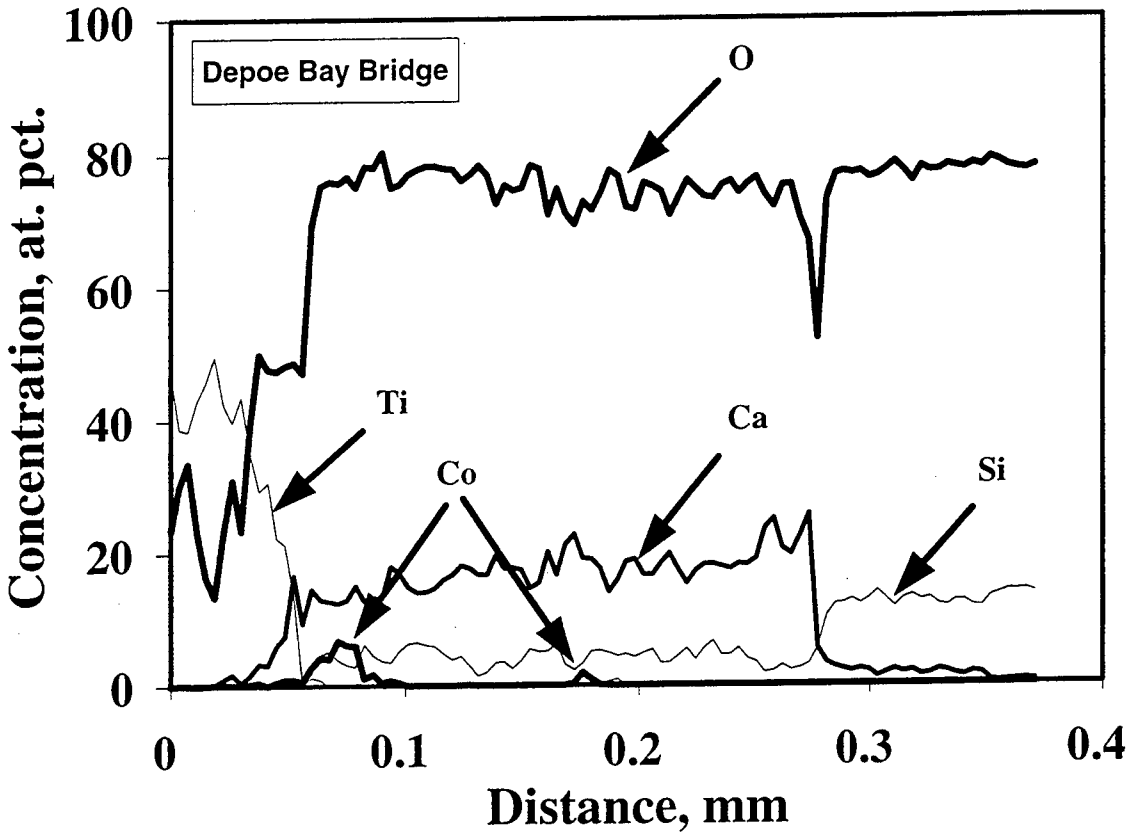

Figure 5.13: Composition depth profile for catalyzed anode from Depoe Bay Bridge after electrochemical aging 146 kC/m^2; path of traverse is shown in Figure 5.12(a).

While there was no evidence of a reaction zone at the anode-concrete interface for the Depoe Bay Bridge anode, measurements showed the coating resistivity had increased 7 pct with aging. As noted earlier, this could be interpreted as indicating etching of the cement paste had begun. A threshold level of aging related to the initial buffering capacity of the concrete may retard formation of a visible reaction zone. A second

interpretation, of more interest perhaps in terms of CP system service life, would suggest that accelerated aging exaggerated the effects of the anode reaction on the anode-concrete interfacial chemistry. In this argument, the anode reaction, diffusion of ionic species, and convective transport near the anode-concrete interface are governed by different mechanisms. The anode reaction is driven by the current density of the accelerated experiment. Diffusion rates are affected only secondarily by linkage with the anode reaction, and convective transport not at all. Thus, the complex interplay of these processes may lead to conditions that allow high pH environments to be maintained at the anode-concrete interface at the current density used by ODOT for coastal CP systems. In fact, research on titanium mesh anodes embedded in concrete suggests there is a critical current density below which damage to concrete caused by the anodic reactions is minimal (*Weale, 1992*). If the pH of the anode-concrete interface at the Depoe Bay Bridge remains high with aging, as the initial data indicate, then the service life of the non-consumable titanium anode may not be significantly affected by aging at low current densities. Aging will have to proceed further at the Depoe Bay Bridge to distinguish between the two scenarios discussed above.

5.3.3.4 Micro-pH Measurements

As shown in Table 5.7, pH measurements for the anode-concrete interface gave values as low as 5.2 for the aged, uncatalyzed slab and 6.2 for the aged, catalyzed slabs. These values are substantially lower than the value of 11 measured for the unaged anode. They are sufficiently acidic to favor the dissolution of calcium minerals in cement paste near the anode-concrete interface (*Pourbaix, 1974*). An earlier report on titanium mesh anodes showed calcium carbonate minerals were removed from the region near the anode and reprecipitated as calcite and vaterite in voids further from the anode (*Weale, 1992*). The presence of calcium carbonate minerals in the region near the unaged anode and absence of these minerals for the aged anode was shown by the XRD measurements, Table 5.6. These changes are caused by the anode reaction (Equations 5-1 and 5-2) and lead to etching of the cement paste to destabilize the interface between the anode and concrete. The structure of insoluble minerals that remains is brittle and readily damaged by abrasion. The reduced anode bond strength and durability of the anode is due to the poor mechanical properties of this structure. Coating resistivity increased due to continued microcracking of the anode coating and loss of conductive path, resulting from a combination of factors, involving coating internal stress and mechanical properties; composition and structure heterogeneity; and the brittle reaction zone formed on aging.

Table 5.7: pH of anode-concrete interface and bulk concrete.

TEST ANODE (aging, catalyst, atomizing gas, measurement location)	Electrochemical age, kC/m²	pH	
		Titanium side	Concrete side
Laboratory Aging Experiment			
Unaged, uncatalyzed, N_2: anode-concrete interface (no slab number)	0	11.1	10.4
Unaged, uncatalyzed, N_2: bulk concrete (no slab number)	0	NA	13.1
Aged, uncatalyzed, air: anode-concrete interface (slab 5)	1520	5.7-5.9	7.1-7.9
Aged, uncatalyzed, air: bulk concrete (slab 5)	1520	NA	12.0
Aged, catalyzed, air and N_2: anode-concrete interface (slabs 6, 48,49,50)	1520	6.2-7.7	6.9-7.6
Aged, catalyzed, air and N_2: bulk concrete (slabs 6, 48,49,50)	1520	NA	12.9-13.5
Depoe Bay Bridge Field Trial			
Zone 14, air: anode-concrete interface (3SW-1, 4SW-1)	146	11.4	11.4
Zone 14, air: bulk concrete (3SW-1, 4SW-1)	146	NA	12.4

5.4 ANODE ELECTROCHEMICAL AGING SUMMARY

Laboratory accelerated studies and a field trial have shown the principal effects of electrochemical aging on the performance and properties of thermal-sprayed titanium anodes. Even at the relatively high current densities of the laboratory studies -- 21.5 mA/m² (2 mA/ft²) -- the voltage demands of the catalyzed thermal-spray titanium anode CP system were relatively low (< 12V) for electrochemical aging of 1520 kC/m² (equivalent to 23 years service at the current density used by ODOT for coastal bridge CP systems) and relative humidities of 30 - 100 pct. The titanium-concrete interface deteriorated chemically and mechanically with aging due to interactions of the anode electrochemical reactions with the concrete chemistry near the interface. Such deterioration was not observed at the Depoe Bay Bridge after 146 kC/m² of electrochemical aging, although indicators (resistivity, Ca depth profile) were observed that some deterioration may occur with longer aging. While the bond strength of the titanium anode to the concrete declined with aging, little to none of the coating was lost by spalling during the aging process. The cobalt catalyst remained near the anode-concrete interface within a reaction zone and continued to support the anodic reaction even after aging for 1520 kC/m².

6.0 FIELD INSTALLATION

6.1 DESCRIPTION

The site selected for the field trial was the Depoe Bay Bridge in Depoe Bay, Oregon, as shown in Figure 6.1. The structure, spanning the channel into Depoe Bay on the Oregon Coast Highway, consists of two connected parallel structures. The original McCullough designed structure was constructed in 1926 and was widened by constructing the adjoining structure in 1939. The resulting structure has a roadway width of 15.25 m (50 ft) and a length of 96 m (314.7 ft) at centerline. Both the original and the 1939 structures consist of one reinforced concrete deck girder (RCDG) approach span on the north, a 45.75 m (150 ft) concrete arch span, and three RCDG approach spans to the south.

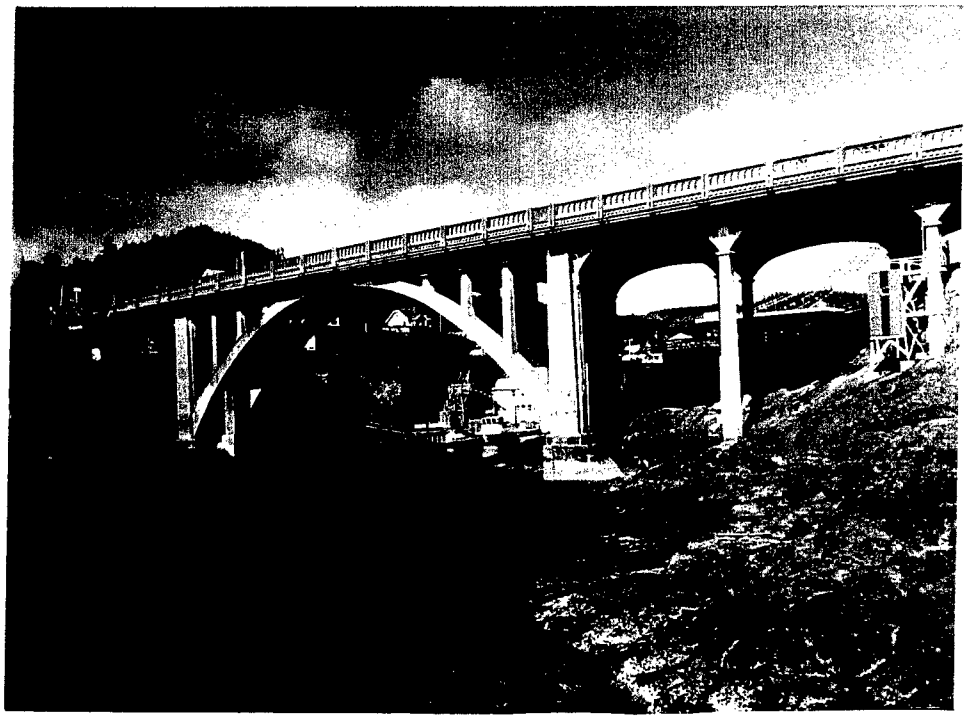

Figure 6.1: Depoe Bay Bridge

The area of the bridge selected for titanium application was the underdeck and beam areas of the southern-most approach span on the 1939 structure. The 1939 structure is west of the original structure and nearer to the ocean. This area on the structure has the advantage of having reasonable access from the ground, should future work or testing be required on this

experimental section. Since this is a historic structure, the sidewalk overhang and the western face of the architectural curtain wall, including the west face of the outer beam, were sprayed with zinc, so the appearance of the western face of the bridge is uniform. From the perspective of historic preservation, the color contrast between arc-sprayed zinc and arc-sprayed titanium would have unacceptably altered the appearance of the bridge.

6.2 SPECIFICATIONS

The complete specifications used for the field installation are included in Appendix A. Some modifications to these specifications were required and are discussed in this report. The field trial work was completed as an experimental feature of an existing contract for rehabilitation and cathodic protection of the Depoe Bay Bridge.

6.3 INSTALLATION

6.3.1 Current Contact Plates

The current contact plates provide the electrical connection between the wires from the zone power supply to the arc-sprayed titanium anode. Typically, CP systems are designed to limit the voltage drop in the anode to 300 mV or less, to achieve uniform current distribution in the zone. The spacing of the plates for this project was designed to limit the voltage drop in the anode to 300 mV or less, at a current density of 21.5 mA/m^2 (2 mA/ft^2). The contact plates furnished by Eltech Research Corporation were constructed from 1.52 mm (0.060") thick titanium. The dimensions of the plate were 76 mm x 127 mm (3" x 5") with a serrated perimeter (shown in Figure 6.2).

The plates were attached with two titanium screws to the concrete surface after installation of the titanium. The plates were attached to the surface by installing plastic anchors flush with the concrete surface, inserting epoxy into the holes for the anchors and threading a titanium screw with a washer into the anchor. Electrical connection to the plate was made by attaching a wire, with ring connector, to a titanium bolt through a tab in the center of the plate.

The serrations were intended to bite into the titanium coating to achieve good electrical contact between the plate and the titanium. The installed plates, however, did not achieve good contact along the entire perimeter of the plate. The plate was too stiff to pull down tight to the surface when the anchor screws were installed. Even where good contact was achieved along some of the plate perimeter, the resistance between the sprayed titanium and the plate was higher than desired.

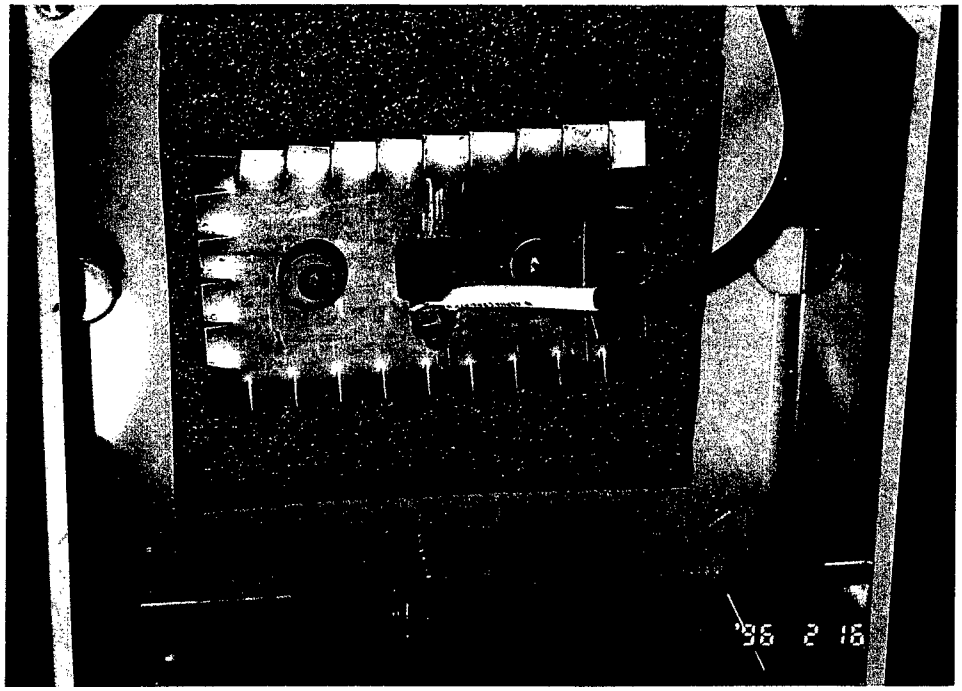

Figure 6.2: Surface Mounted Current Distribution Plate

In an attempt to decrease distribution-plate-to-sprayed-titanium resistance, the plate design was changed to an embedded-type plate similar to that used on ODOT's sprayed zinc systems. The new 63.5 mm (2.5") diameter plate was constructed from a 3.175 mm (0.125") sheet of titanium with a titanium bolt welded to the center of the plate for the wire connection. Two countersunk holes were installed in the plate to attach the plate to the concrete with a plastic anchor and titanium screw, as shown in Figure 6.3.

The plate was installed by core drilling approximately 4.8 mm (3/16") into the concrete and chipping out the center of the core with a chipping gun. Two holes were drilled in the concrete for the anchors, and the excavation was filled with DP-420 epoxy from 3M. The plate was installed flush with the surrounding concrete and was held in place by the anchor screws. After the epoxy cured, any epoxy that had run onto the surface of the concrete or the plate was ground off, leaving a clean concrete surface, narrow ring of cured epoxy and clean top surface of the titanium plate.

When the titanium was sprayed onto the plate, the titanium did not adhere to the epoxy. Since the titanium coating is thin, the titanium did not bridge the epoxy-filled gap between the titanium plate and the concrete, leaving the current distribution plate isolated from the surrounding sprayed titanium. This led to a second change in the distribution plate design.

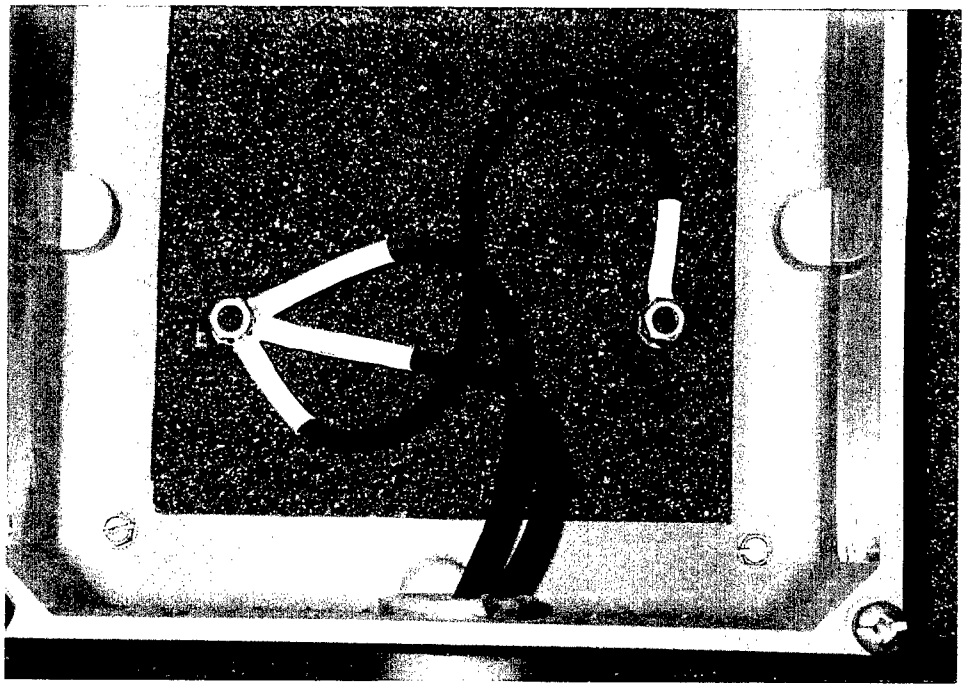

Figure 6.3: Flush-mounted current distribution plates with temporary wiring installed.

A minimum 13 mm (0.5") deep area was excavated and patched with Rederoc HBA patching material. Plastic anchors were installed to hold the plates in place, and the plates were pressed into the patch material until the plates were flush with the surrounding concrete surface, providing a smooth surface for installation of the thermal-sprayed titanium. The resulting installation provided good contact between the current distribution plate and the arc-sprayed titanium. Measurements with a Fluke 87 digital multimeter indicated a resistance of zero ohms between the titanium bolt at the center of the plate and the arc-sprayed titanium adjacent to the perimeter of the plate.

The size of the plate affects the amount of anode area that can be served by a single plate and limit the voltage drop to 300 mV. Two round plates were installed adjacent to each other, as shown in Figure 6.3, to approximate the perimeter of the 5" x 3" plates. For the installation at Depoe Bay Bridge, one current distribution plate (or set of round plates) was installed for each 46.5 m^2 (500 ft^2) of surface area. A calculation of the maximum amount of area per current distribution plate is shown in Appendix B.

6.3.2 Titanium Installation

6.3.2.1 Equipment

The equipment used for the field trial was a Thermion Bridgemaster arc-spray system. The power supply used initially was a PowCon 630SM inverter-type supply. This is the same system being used for applying zinc to the Depoe Bay Bridge using 4.76 mm (3/16") zinc wire; however, several modifications were required to spray titanium. The feed rolls, liners and contact tips were changed to accommodate the smaller 3.175 mm (0.125") diameter titanium wire. Hardened feed rolls are required to spray titanium because of the increased wear associated with the harder titanium wire.

Titanium wire is much stiffer than zinc wire, and the wire retains some curvature as it comes off the spool. Wire straighteners were installed to straighten the wire as it entered the wire feed unit. An arc-shorting system was installed (see Section 2.2.2), and a short circuit detection system was connected to the gun control circuit (see Section 2.2.3).

6.3.2.2 Titanium Wire

The wire specified for use on this project was 3.175 mm (0.125") annealed, Grade 1 or 2 titanium wire. Grade 1 and 2 titanium wires are high-purity, commercial grades of titanium that differ in oxygen and iron content (Grade 1 Fe-0.2%, O-0.18%; grade 2 Fe-0.3%, O-0.25%). The increase in oxygen and iron content increases the strength of Grade 2 but also decreases its ductility. The wire actually supplied for installing the arc-sprayed titanium on the bridge was 3.175 mm (0.125") wire meeting the AWS A5.16-90 ERTI 1 specification. This specification is for a weld-filler, metal wire that fits within the Grade 1 specification, and it has lower iron and oxygen content (Fe-0.1%; O-0.1%). The wire was annealed at 704° C (1300° F) for one hour. The Brinell hardness of annealed Grade 1 titanium is 120 HB (67.5 HRB) compared to a value of 200 HB (93 HRB) for annealed Grade 2 (*Bauccio, 1993*).

6.3.2.3 Application

Several problems were encountered during the field spraying of the titanium. The operator of the spray equipment experienced great difficulty achieving a smooth arc. The arc-shorting control system was apparently too slow to stop the wires from shorting, so the wires tended to fuse frequently causing an extensive amount of downtime for the spray equipment. When the feed wires fuse at the tip of the gun, the operator must stop, remove his air hood, clip the wires off at the tip and put back on his air hood. Since this procedure is inconvenient and time consuming, the operators had the tendency to hold the trigger down to try to melt the fused wires. The problem with this technique is, if the wires are solidly fused, the wires will heat back into the spray tip and fuse to the tip. When this happens, a very time consuming tip replacement process must take place.

When the fused wires do melt without fusing to the spray tip, they are propelled away from the gun as a large piece of molten wire. This flying piece of molten wire does not cool as quickly as the small spray particles, so the wire created a burn hazard for the operator and a fire hazard for the plywood work deck.

Smooth arc operation seemed to be at least partially related to movement of the gun head. Quick changes in the bending radius of the gun leads tended to interrupt the arc. This relationship was thought to be caused by the stiffness of the titanium wire. The wire retained some curvature even after passing through the wire straighteners. When the leads are moved, the stiffness and the curvature of the wire cause movement of wire within the spray tips and, therefore, a changing arc gap. Wear of the spray tips seemed to cause this problem to become worse since greater wire misalignment is possible with increasing internal diameter of the spray tips.

Spray tip wear was a significant problem encountered during spraying. The copper alloy used for the spray tips has a Rockwell B hardness value of 45 and an electrical conductivity of 95% IACS. As discussed in Section 4.3.2.2, the hardness for annealed Grade 1 titanium is 120 HB (67.5 HRB). Charge is transferred to the wires via sliding contact with the spray tips. The large difference between the hardness of the titanium wire and the spray tips caused rapid wear of the spray tips. The tips were wearing out at the approximate rate of two sets of tips per 11.4 kg (25 lb) spool of wire.

Because of these problems experienced, spraying on the project was suspended until possible solutions could be considered. Approximately one-quarter of the area had been sprayed in 102 hours when spraying was stopped. The production rate for this initial phase was 0.7 m^2 (7.35 ft^2) per hour.

Investigation of what could be done to make the wire less stiff revealed that, although annealed wire was specified, unannealed wire was delivered to the job. Not only is the unannealed wire more stiff, but the hardness difference between the wire and the spray tip was greater than discussed above. Fully annealed wire was ordered for spraying the remaining area. Interestingly, the annealed wire was sold for the same price as the unannealed wire. The annealed wire was expected to improve the alignment problem by reducing wear and by being less resistant to lead movement.

Also, to further combat the wear problem, the Albany Research Center, U.S. Department of Energy, constructed a set of spray tips from an age-hardened M25 beryllium copper alloy. This alloy has a Rockwell B hardness of 114, but its conductivity is only 22% IACS. Although this material is hard enough to greatly reduce the wear problem, it was not conductive enough to effectively transfer charge to the wire. When these tips were tried on the spray gun, an arc could not be established between the wires. A different beryllium copper alloy (alloy 3) with a Rockwell B hardness range of 95 - 102 and a conductivity of 48 - 60% IACS was tried with similar results.

For the second phase of spraying, a Miller model FC-6 constant potential DC welding power supply was substituted for the PowCon 630 SMP supply. This change produced

substantial improvement to the arc operation. Arc-spraying with the Miller power supply produced smooth arc operation and a stable arc voltage. To understand this difference in operation between the two supplies, the characteristics of each were investigated.

The PowCon supply is rated at 630 amps and 44 volts. These specifications are derated at 100% duty cycle to 450 amps and 38 volts. The Miller supply is rated 600 amps and 40 volts at 100% duty cycle. The PowCon supply is a switchmode supply which uses a feedback circuit to maintain constant output power. The Miller supply is a rectifier and transformer-type supply with no feedback.

The PowCon supply depends on the feedback and electronic control to maintain the desired output power. During spraying the output voltage of the supply fluctuated continuously. The operating characteristics of the titanium arc-spray process are probably much different from the operating characteristics of wire feed welding for which the power supply was designed. It is possible the operating variations for arc-spraying titanium exceed the compensating ability of the feedback circuit. An unstable control circuit could explain the observed fluctuation of the output voltage.

Since the PowCon supply was being operated toward the upper end of its output range, the difficulty sustaining an arc may also be related to protective, power-limiting circuitry in the PowCon supply and the constant power operating characteristic. When a wire begins to fuse, the PowCon supply may not be capable of supplying the instantaneous current peaks required to prevent the wires from shorting.

The Miller supply, however, is designed to maintain a constant voltage output. Since this voltage is dependent on arc gap, the Miller supply operates to maintain a constant arc gap. There is no feedback control circuit, but as conditions change at the spray tips, the amount of current increases or decreases to maintain the constant voltage. The large inductance which is typical in the output circuit for this type of supply enables the supply to provide short-term current output exceeding the rating of the power supply when it is required to maintain the desired voltage.

The change in power supplies provided a major improvement to the spray quality and improvement to the production rate. Approximately 190 hours were required to complete approximately 209 m^2 (2250 ft^2) remaining in the experimental zone. In this time, there were only 27.55 hours put on the spray machine hour meter. This computes to a machine production rate of approximately 7.6 m^2 (81.8 ft^2) per hour, but an actual production rate of only approximately 1.1 m^2 (11.8 ft^2) per hour.

The annealed wire reduced the wear rate on the spray tips; a set of spray tips lasted for approximately one set of 11.4 kg (25 lb) spools. Although the annealed wire increased spray tip life, much of the down time during the spraying was still attributed to adjustment and replacement of spray tips. Significant production rate improvement could be obtained with more wear-resistant spray tips.

An additional influence on the production rate for the titanium spraying was the heat experienced by the operator. The heat from the titanium spraying creates a difficult working environment for the operator. To combat the operator fatigue resulting from the high temperatures, the operators took more break time than is typical for zinc spraying.

The total titanium usage for the project, including waste, was 342.3 kg (753 lb). This is significantly more than was expected. The expected maximum titanium usage rate was 0.807 kg/m^2 (0.165 lb/ft^2). The actual titanium usage rate was 1.22 kg/m^2 (0.25 lb/ft^2) — a 50% increase over the maximum expected usage rate.

There are several possible explanations for this higher-than-expected usage rate. The usage rate was clearly affected by the difficulty experienced during the initial spraying. During the first phase of spraying, when a stable arc could not be established, the operator pointed the gun at the ground until the arc stabilized. Since frequent difficulty was experienced during this initial phase, there was probably a significant portion of wire used trying to adjust the equipment for consistent arc performance.

As a result of the heat and the shower of sparks associated with arc-spraying titanium, the operators had difficulty maintaining the specified spray distance. The operators had a tendency to increase the spray distance, which decreases deposit efficiency. Also, there are some areas in the zone which have a much lower coating resistance than was specified. In these areas, titanium usage would have been higher than expected.

The average coating resistance, however, was investigated and found to be 0.233 ± 0.044 ohms/square (95% confidence interval). Data from the shop spray portion of this study was used to develop a relationship between sample weight gain and coating resistance for the spray parameters used during field spraying. The equation developed was

$$R = -1.426\ln(w) + 3.2 \qquad \textbf{(6-1)}$$

where: R = coating resistance (ohms/square) and

w = weight gain of sample.

The fit of the equation to the experimental data provided an R^2 of 95.5%. The equation was used to investigate the impact of variation from the specified coating resistance on titanium usage. If an average deposit efficiency of 80% is assumed and the 95% confidence interval limits for the mean coating resistance are plugged into the regression equation, the titanium usage at the confidence interval limits can be calculated to vary from a 5.5% increase to a 2.5% decrease versus the titanium usage required to achieve the specified coating resistance. Variation in coating resistance, therefore, cannot explain a very significant portion of the increase in titanium usage experienced.

During this second phase of spraying, a set of spools of 2.4 mm (3/32") diameter wire was sprayed. This smaller size wire seemed to spray more smoothly. The wire was sprayed at 390 A and 37 V compared to 300 A and 40 V for the 3.2 mm (1/8") diameter

wire. Since current is a measure of feed rate, the smaller wire actually can be sprayed with a feed rate 30% greater than the feed rate for the 3.2 mm (1/8") diameter wire. Although the smaller wire has a cross-sectional area of only 56% of the larger wire, the net effect is just a 25% reduction in the calculated production rate. However, if the smaller wire can be sprayed with less down time, it may offer the opportunity for an increase in the total production rate.

6.3.3 Catalyst

According to the developers of the catalyst for the arc-sprayed titanium coating, Eltech Research Corporation, application of the catalyst must take place with an impressed current system operating, and the system must remain in operation for a minimum of 72 hours after catalyst application. For this installation, the power supply was set to deliver 5.4 mA/m^2 (0.5 mA/ft^2). The amount of Eltech-supplied catalyst specified to be applied to the titanium was 0.344 l/m^2 (0.0087 gal/ ft^2) minimum; however, the application rate must allow the catalyst to absorb without dripping or running from the surface.

The catalyst was delivered from Eltech premixed in a drum. The quantity of catalyst to be applied was 110 l (29 gal). The coverage of this quantity equated to 0.392 l/m^2 (0.0095 gal/ ft^2) which allowed for 10% waste during application of the catalyst.

The original plan was to apply the catalyst in two coats. The first coat would require slightly more than half of the catalyst from the drum. The remaining catalyst would then be diluted with water to equal the volume of catalyst used in the first coat. After allowing for drying time between coats (30 minutes minimum), the remaining catalyst would be applied at the same rate as the first coat.

The catalyst installation was applied by two workers each using a 7.6 l (2 gal) pressurized spray tank, as shown in Figure 6.4. After completing the first coat of the catalyst, approximately 50 l (13.3 gal) of the catalyst had been used. The second coat used approximately 31 l (8.3 gal), leaving approximately 28 l (7.4 gal) in the drum. Water was added to the drum to dilute the remaining catalyst to approximately 37.9 l (10 gal) prior to the third and final coat. The fact that the catalyst application required three coats instead of two probably resulted in more uniform coverage of the catalyst. The entire process took two workers four hours to complete, including set up and clean up. After completion of catalyst application, the power supply was operated at 10.8 mA/m^2 (1 mA/ft^2) for one week before returning to 2.1 mA/m^2 (0.2 mA/ft^2).

After the catalyst has dried, it is not possible to visually detect a difference between catalyzed and uncatalyzed titanium. If it is desired to verify complete catalyst coverage, project specifications should specify that application of the catalyst take place in the presence of the inspector.

An additional factor which should be considered when specifying catalyst application is the amount of waste resulting from using the spray process for vertical and overhead surfaces. At

the completion of the catalyst application, the plywood decking below the sprayed surface was very damp from the catalyst overspray. The application efficiency, however, was not measured.

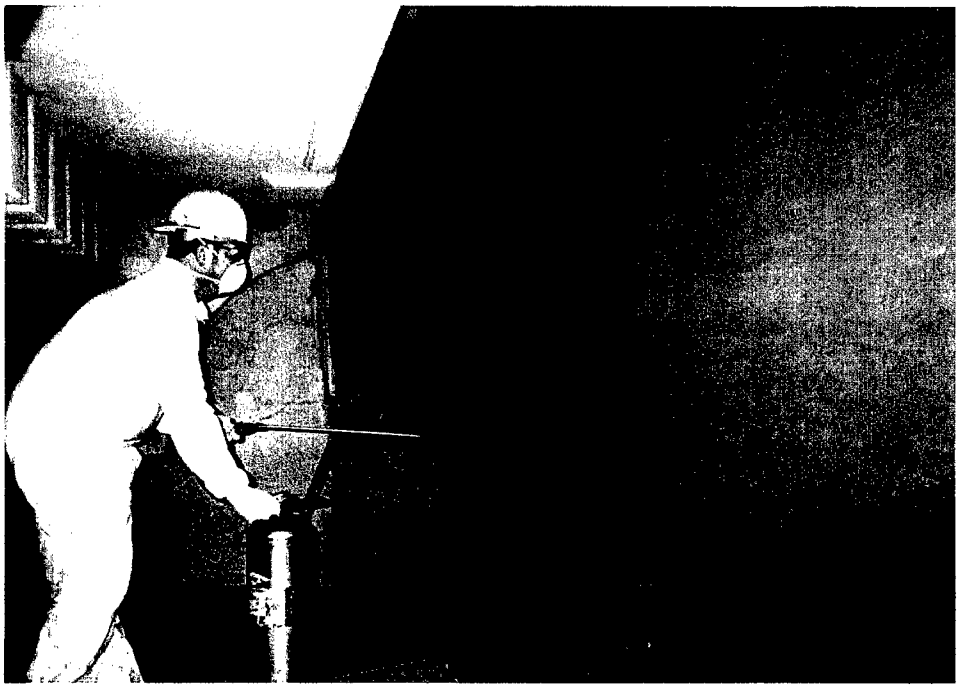

Figure 6.4: Catalyst application

6.4 FINAL TESTING

6.4.1 Visual inspection

Approximately one month after completion of the titanium and catalyst installation, a visual inspection was performed. Three rust stains were located, indicating the presence of tie wires at the surface of the concrete. These tie wires were not detected by the short circuit detection system and did not show up in the voltage drop measurements discussed below. Apparently, the wires were either not making good electrical contact with the titanium or were not connected to the rebar. Although the presence of the wires did not seem to be affecting system performance, the wires were removed to prevent future problems.

The visual inspection also revealed some small areas where the coating had disbonded. The areas were typically of irregular shape, as shown in Figure 6.5. The disbonded areas are typically 50 mm in diameter or less, although, there are some larger areas. Further investigation into the

areas that had disbonded revealed two distinct characteristics. All areas that delaminated were either areas where the coating was much thicker than specified or patches which had not received proper surface preparation prior to installation of the coating.

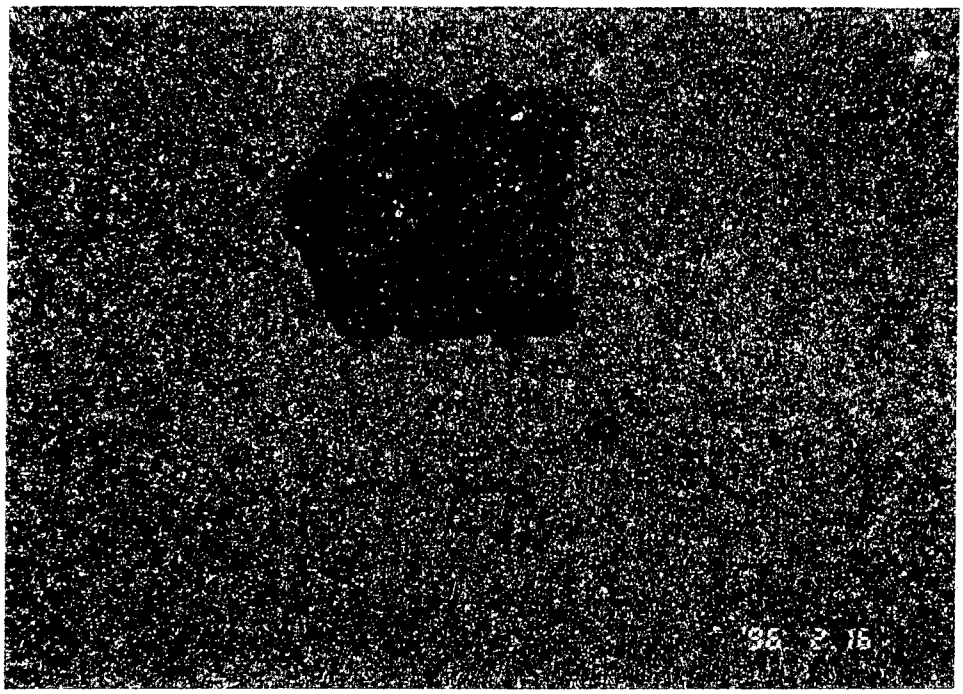

Figure 6.5: Typical disbonded area

Coating resistance measurements made near the disbonded areas revealed that in all cases, except near the unprepared patch areas, the coating resistance was 0.10 ohms/square or less. This was significantly less than the specified coating resistance of 0.25 ohms/square and indicated a coating much thicker than specified. The unprepared patch areas were surface metal patch areas that were patched after the surface preparation for the zone had been performed. The patches tended to have a smooth, weak concrete slurry on the surface of the cured patch.

The reduction in bond strength with coating thickness is well documented for many different thermal-sprayed coatings, as discussed in Section 3.2. The mechanism that causes this observed phenomenon has not, at this point, been clearly demonstrated. Gudge, et al., determined through experimental work and numerical modeling that a plasma-sprayed tungsten coating contains increasing residual stress with increasing coating thickness (*Gudge, et al, 1990*). The postulate is that residual stresses are formed during three separate phases. First, the coating is applied in layers which heat to an average temperature that is greater than the temperature of the concrete substrate. Next, the coating cools to the average temperature of the substrate, and the bonding of the coating to the substrate constrains contraction of the coating. Finally, the coating and substrate cool to ambient temperature and differences in thermal expansion coefficients between the coating and substrate create further stresses.

Decreasing bond strength with coating thickness is explained by the higher temperature differences that occur between the coating and the substrate during the process of depositing a thicker coating. This theory applies well to coatings applied in one continuous process. The bond-strength samples for this study, however, were coated in discrete one-pass layers. The samples were weighed between each pass, allowing time for cooling of each coating layer, and causing the coating to go through multiple heating and cooling cycles.

The statistical analysis of these samples showed no significant correlation between number of spray passes and bond strength, but the correlation between bond strength and coating resistance (inversely proportional to coating thickness) was clearly demonstrated.

Greving, et al., described a mechanism which may explain the results observed in this study. Their work with a 95% nickel, 5% aluminum coating on a steel substrate showed no increase in residual stresses with coating thickness. However, they did observe a substantial decrease in coating bond strength with increased coating thickness (*Greving, et al., 1994*). The theory used to explain these observations is called the free-edge effect and is drawn from experience with the disbonding within laminated composites. This theory analyzes what happens to the planar residual stresses at the edge of a coating. A coating edge occurs at a coating defect as well as at the boundary of the sample. In a steady state, the forces within a coating must be balanced, so at a coating edge, the planar tensile stresses within the coating, having no balancing planar forces outside the coating at the free edge, create a moment that tends to lift the coating at the free edge. As the coating thickness increases, this moment increases.

There are additional properties of arc-sprayed titanium that increase its susceptibility to damage from residual stresses within the coating. Titanium is an allotropic element meaning it can exist with two different lattice structures. At temperatures below 882° C ± 2° (1620° F), titanium has a hexagonal close packed lattice structure referred to as the α phase. Above this temperature, pure titanium has a body-centered cubic structure referred to as the β phase. The lattice parameters for the β phase are larger than the lattice parameters for the α phase. The melting temperature for titanium is 927° C ± (1670° F ±). During the arc-spraying process, the α phase, Grade 1 titanium wire melts and on a cooling portion converts to the β phase. As the titanium cools further, the β-Ti returns to the smaller α phase providing an additional source of residual stresses in the deposited coating.

Coupled with these sources of residual stresses, there are factors that make the coating more brittle. At elevated temperatures, oxygen and nitrogen are highly soluble in the titanium. In addition, the oxidation rate of the titanium increases with increasing temperature (*Donachie, 1988c*). The presence of these interstitial elements and of titanium compounds (particularly γ-TiO) causes the titanium to become more brittle and thus more susceptible to fracture.

The observed coating disbondment is probably the result of a combination of the material properties of arc-sprayed titanium and the residual stresses resulting from the spray process. Further work is needed to define, for specification purposes, the minimum coating resistance (i.e., maximum coating thickness) for which acceptable bond can be achieved. This maximum

value, however, is also dependent on substrate variables. For example, the weak concrete slurry surface of the unprepared patch areas allowed coating failure at normal coating thickness.

To date, the disbonded areas have not grown in size, and additional disbonded areas have not appeared. With manual application of the coating to the bridge, it may be difficult to completely avoid areas of excess thickness. However, if the size and quantity of disbonded areas remain small, these areas will not reduce the effectiveness of the cathodic protection system.

6.4.2 Anode Voltage Drop

After installation of the titanium anode and catalyst, the DC voltage drop in the anode was investigated. The system was designed to have a maximum of 300 mV of voltage drop in the anode at 21.5 mA/m^2 (2 mA/ft^2). To perform this test, the system was connected to a constant current power supply operating at 3 amps (10.7 mA/m^2 or 1 mA/ ft^2). The positive lead of a Fluke 87 digital multimeter was connected to a current distribution plate, and the negative lead was used to take voltage measurements in a grid pattern over the entire surface area of the anode, as shown in Figure 6.6.

Since the power supply was set at half the design current, the maximum expected voltage drop was 150 mV. The measurements showed reasonable agreement with the theoretical values for most of the anode area. The measurements were made with the positive lead connected to a single distribution plate, so the voltage drop measurements also included the voltage drop in the conductors between the plates and between the plate and the titanium. The voltage drop between the positive lead connection point and the other plates was in the range of 42 to 54 mV.

After compensating for the voltage drop in the wires, the maximum voltage drop in the anode appeared to be around 180 mV. The testing revealed one surface-mounted current distribution plate with poor contact to the titanium. The voltage drop between the connection point and that plate measured 195 mV. Measurements in the southeast corner of the zone, where this plate is located, were higher than expected with measurements as high as 548 mV. There were also areas in the northeast corner of the zone, which had high-voltage drop measurements around 300 mV.

Thus the anode seems to perform reasonably close to the theoretical calculations except where installation problems have occurred. The faulty surface-mounted plate will be corrected, and the reason for the high voltage drop in the northeast corner will be investigated further. When these corrections are made and the contractor completes the permanent wiring installation, this test will be repeated.

This test has proven to be useful for final inspection of the arc-sprayed titanium anode. It is difficult to visually detect all coating areas that are too thin. In one area of this zone, a 25 mm (1") wide, 45-degree beveled edge along the bottom of a beam, had been missed during catalyst spraying. This created an area of anode isolated from the current distribution plate. This area was not detected during visual inspection, but it was readily apparent through voltage drop measurements (during a preliminary voltage-drop test) that exceeded 1 volt. The test provided a

quick verification that the anode will successfully distribute current throughout the zone. The entire test for this zone took two people approximately 1.5 hours to complete.

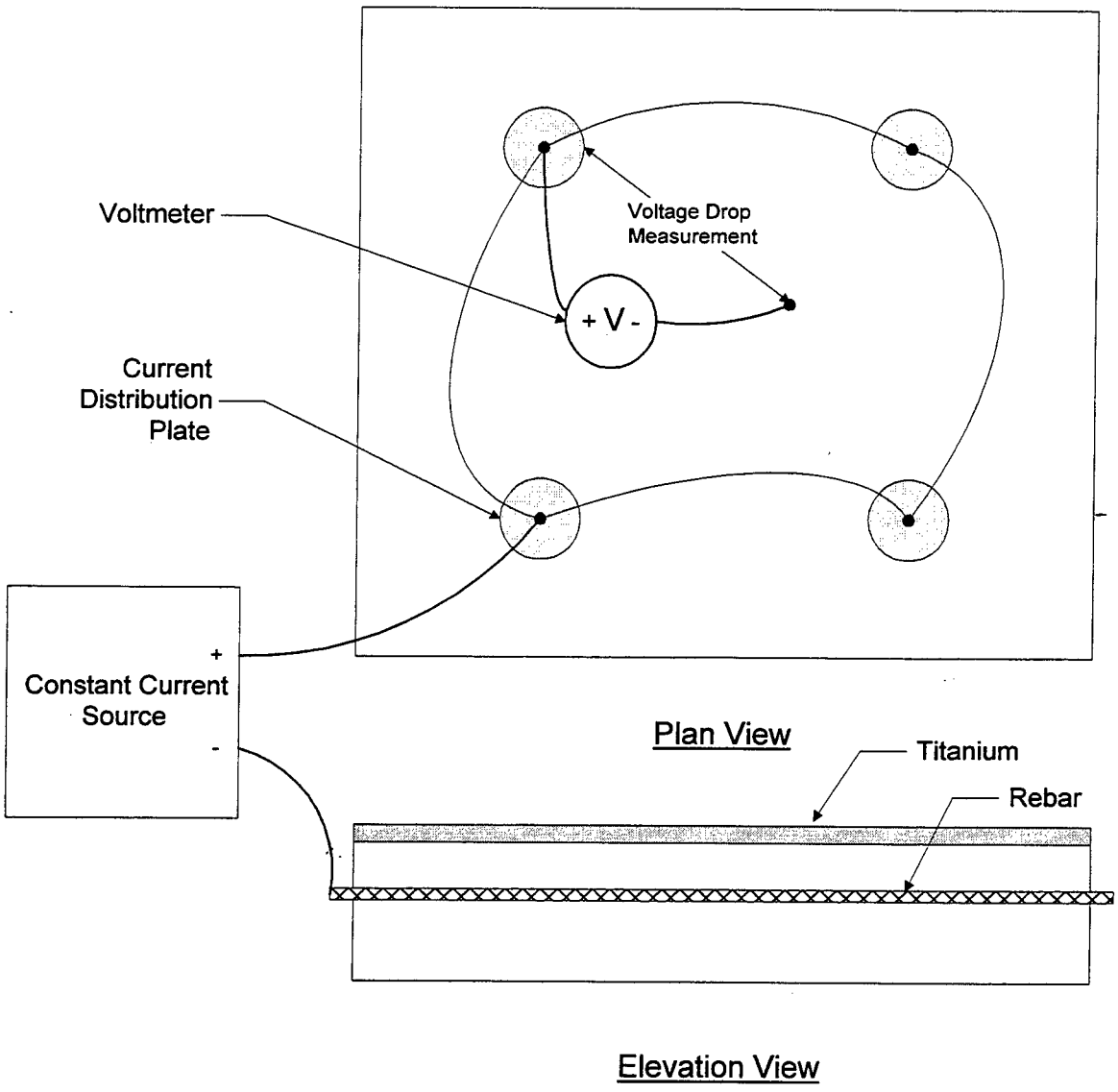

Figure 6.6: Connections for anode voltage drop testing

6.4.3 Current-Potential Relationship

About one hour after completion of catalyst application, the current supplied on the zone (an area of 280 m^2 or 3015 ft^2) by the power supply was varied, and the output voltage and the potential of the titanium anode versus a saturated calomel electrode (SCE) were recorded. The results are shown in Table 6.1. The stability of the anode potential versus the SCE verified the catalyst was working.

Table 6.1: Variation in Voltage and Potential with Changes in Applied Current

Current (amps)	Voltage (volts)	Ti Anode potential vs. SCE (volts)
0.5	0.97	0.347
1.0	1.15	0.349
1.5	1.32	0.351
2.0	1.48	0.354
2.5	1.63	0.357
3.0	1.81	0.359
3.5	1.97	0.362
4.0	2.16	0.367
4.5	2.33	0.371
5.0	2.50	0.375
5.5	2.66	0.380
6.0	2.85	0.383

6.5 COST ANALYSIS

The costs for the project are summarized in Table 6.2. The bid price for installation of zinc on Depoe Bay Bridge was \$88.80/m^2 (\$8.25/ft^2), so the cost for installing the titanium exceeded the bid cost of zinc by just 18%. Considering the difficulties experienced in this first titanium project, this result is encouraging.

Additional equipment development to reduce wear of the spray tips could substantially reduce the amount of labor shown in Table 6.2. The fact that titanium usage was 50% over the maximum expected usage indicates an improvement in the amount of titanium used can also be achieved.

Table 6.2: Cost Summary

Item	Quantity	Unit Price	Total	$/m^2	$/ft^2
Titanium Wire	342.3 kg	$41.8/kg	$ 14,308	$ 51.13	$ 4.75
Catalyst	110 liter	$16.45/liter	$ 1,810	$ 6.46	$ 0.60
Labor	292 hrs	$42.90/hr	$ 12,527	$ 44.67	$ 4.15
Freight/Misc.	—	—	$ 723	$ 2.58	$ 0.24
Total Cost			$ 29,368	$ 104.84	$ 9.74

Even at the costs incurred on this project, the titanium appears to be a good solution from the life cycle cost perspective. Assuming the titanium system can achieve a 40-year life, the cost to complete the 280 m^2 (3015 ft^2) of bridge area for this project was $29,366. Assuming the zinc system will last 20 years, with 4% inflation and a 7% discount rate, the 40-year life cycle cost for applying zinc to this same bridge area would be $38,958. If only application costs are compared, the titanium system appears to offer a $10,000 savings over zinc. At 20 years, the zinc system would also incur costs for surface preparation, mobilization, constructing access to the bridge and re-installing electrical wiring. These additional zinc system costs increase the life cycle cost advantage provided by the titanium system.

7.0 CONCLUSIONS AND RECOMMENDATIONS

Although some difficulties were experienced during the field installation, the arc-sprayed titanium coating shows promise as a cathodic protection anode. Further work is warranted, however, prior to full-scale application of this anode material. The following conclusions and recommendations are presented to summarize the results of this project:

7.1 CONCLUSIONS

7.1.1 Shop Testing

- Measurement of the coating resistance of a thermal-sprayed titanium coating provides a non-destructive technique for determining the suitability of the coating for distributing current. At a coating resistance value of 0.5 ohms/square, a 100 mm (4") diameter current distribution plate is required for each 46.5 m^2 (500 ft^2) of anode area. When measuring coating resistance on a large sheet of anode material, additional current paths at the edge of the resistance measuring probe cause the measured resistance value to be less than the actual value. The amount of reduction in the resistance value was determined empirically to be 50% (e.g., if an actual resistance value of 0.5 ohms/square is desired, the measured resistance on a large sheet of anode should be 0.25 ohms/square).

- The apparent deposit efficiency for arc-sprayed titanium is low initially, but it increases rapidly to between 80% and 90% by the third and fourth spray passes for the spray parameters investigated in this study. Several problems were identified with deposit efficiency measurements of arc-sprayed titanium, so deposit efficiency does not appear to be a good single measure for optimizing spray parameters, primarily due to the effect of the spray parameters on the conductivity of the coating.

- The best measure for evaluating the effectiveness of the coating for distributing current is the product of coating resistance and sample weight gain, which produces a quantity correlated to coating resistivity. A multiple regression equation was constructed to determine the spray parameters that would yield the best combination of low resistance and low titanium usage. The equation revealed that, for the data collected in this study, gun travel speed and the pressure of the propellant are insignificant variables. Decreasing spray distance increases the effectiveness of the coating for distributing cathodic protection current. Increasing the current at which the titanium is sprayed increases the effectiveness of the coating, although this effect is more pronounced at higher spray distance. Using nitrogen as the propellant produces a more effective coating by reducing coating resistivity. Spray parameters used for field application were 150 mm (6") spray distance and 300 A. Compressed air was used as

the atomizing gas instead of nitrogen, because the cost savings from reduced titanium usage would have been offset by the cost of providing nitrogen for this project. However, possible coating long term performance benefits resulting from nitrogen usage need further study.

- This study provided an initial examination of the bond strength of the titanium coating. Bond strength appears to be good for the variety of conditions tested. However, a relationship between coating resistance and bond strength was noted. As the coating resistance decreases the bond strength decreases. This effect is probably related to residual stresses in the coating.

- Arc-sprayed titanium does not bridge cracks or gaps well. The maximum crack width bridged during this study was 0.127 mm (0.005"). This did not appear to present problems during the field spraying trial. Resistance measurements across cracks showed satisfactory coating resistance values.

- Catalyzed operational samples were operated satisfactorily at accelerated constant current levels for over 300 days at a stable voltage. This indicated suitable operation of the catalyst, including a sample that was catalyzed to simulate an overhead surface. Unexpectedly, the uncatalyzed sample did not experience large increases to the operating voltage. The uncatalyzed sample, however, appeared much more sensitive to changes in humidity.

7.1.2 Characterization

- An arc-sprayed titanium coating is non-homogeneous due to reactions with atmospheric gases (O_2 and N_2). It contains, on average, about 88 weight percent titanium using air or nitrogen atomization. The principal constituents of the coating are α-Ti containing interstitial nitrogen, interstitial oxygen and γ-TiO with the possibility of some TiN. Alternating layers of α-Ti rich and γ-TiO rich material comprise the coating.

- Nitrogen atomization produces a coating with less cracking and more uniform chemistry than air atomization. This results in substantially lower coating resistivity than produced by air atomization. Coating cracking substantially increases the tortuosity of the electrical conduction path over the nominal dimensions on the coating.

- The presence of γ-TiO in the coating causes some undesirable coating properties. It is an unstable structure that produces internal stresses within the coating, creates stress risers for crack nucleation and brittle zones for crack propagation.

7.1.3 Electrochemically Aged Anodes

- In accelerated aging studies, the catalyzed, thermal-sprayed titanium anode operates successfully for periods equivalent to 23 years service (1520 kC/m^2) at the current density (2.15 mA/m^2 (0.2 mA/ft^2)) used by ODOT for coastal bridge CP systems. There was no

electrochemical evidence at the conclusion of the experiment that the anode would not have performed satisfactorily for much longer periods of time.

- The cobalt nitrate catalyst remains at or near the titanium-concrete interface and continues to support the anode reaction without the need for replenishment for the equivalent of 23 years of aging at typical ODOT current densities for coastal bridge CP systems.

- The structure of the titanium anode does not change visibly under microscopic examination nor is further oxidation of the anode evident as the result of electrochemical aging. However, coating apparent resistivity increases with aging.

- Anode bond strength decreases with aging, but the decrease is substantially less for the catalyzed anode. No coating losses due to spalling occur for the equivalent of 23 years of aging at typical ODOT current densities for coastal bridge CP systems.

- Voltage requirements for the catalyzed anode are less than 7.0 volts, with an average of 4.1 ± 1.4 volts, at an anode current density of 21 mA/m^2 (2.0 mA/ft^2), for relative humidities from 30 to 100 pct, and aging up to 1520 kC/m^2. Catalyzed anode voltage response to humidity was linear and relatively insensitive to RH, resulting in an anode that responds well to a wide range in concrete moisture conditions, with little change in operating conditions.

- The initial benefits of using nitrogen atomization to spray the anode coating continue with electrochemical aging and give long-term, lower resistivity and higher bond strength than when air atomization is used.

- Calcareous minerals are depleted from the concrete near the titanium-concrete interface due to acidification from anodic reaction products formed during electrochemical aging. This leaves a reaction zone with a brittle silica and alumina mineral skeletal structure to support the anode and accounts for the reduced bond strength and durability of the coating with time. However, this same brittle reaction zone may contribute to the ease of anode removal when anode replacement is considered in the future.

- The titanium anode in the Depoe Bay Bridge field trial did not show evidence of a reaction zone but resistivity measurements and Ca depth profiles suggest some deterioration may be expected with further aging. If deterioration of the concrete near the anode-concrete interface does not occur, then long-term field trial results may suggest a threshold level of current density exists below which aging of the anode has minimal effects on non-consumable anode performance or service life.

7.1.4 Field Testing

- Current distribution plates embedded flush in a concrete patch material provide the best means for providing a low resistance attachment of a power supply to the anode.

- A constant power, switchmode welding power supply does not provide stable arc operation for arc-spraying titanium. The older technology constant voltage transformer and rectifier type welding power supply is more suitable for arc-spraying titanium.

- Annealed wire should be used for improved ductility and reduction in equipment wear. One spool set of 2.4 mm (3/32") wire was tried during the field trial while the remainder of the project was sprayed using 3.2 mm (1/8") wire. The smaller diameter wire seemed to spray more smoothly, with less equipment down time, and at a higher feed rate than the 3.2 mm (1/8") wire. The approximately 25% reduction in application rate attributed to the smaller diameter of wire would probably be more than offset by a reduction in down time.

- Anode voltage drop measurements provide an excellent final inspection tool for identifying performance problems in the coating.

- Although difficulty was experienced during the field-spraying portion of this study, the costs for performing this work exceeded the bid costs for installing zinc by just 18%. Considering life cycle costs, the titanium system offers a cost advantage over the zinc system, even at the costs experienced on this project. Provided that the performance of the catalyzed titanium system is proven, this system is promising, and there is also much room for improvement in installation costs.

7.2 RECOMMENDATIONS

7.2.1 Coatings Characterization

The non-homogeneous distribution of Ti(O,N) in the coating is potentially the most damaging characteristic of the coating. It produces internal stresses within the coating, and creates stress risers for crack nucleation and brittle zones for crack propagation. It is a metastable structure that may affect the long-term properties and function of the coating in an ICCP system. Thus, the main concern would be to promote conditions that reduce the concentration of Ti(O,N) within the coating. Interestingly, the internal oxidation rate of Ti by oxygen is higher in air than pure oxygen because interstitial nitrogen expands the crystal lattice and facilitates the diffusion of oxygen (*Hauffe, 1965*). Interstitial oxygen and nitrogen would appear to be of much less concern except perhaps for how they affect internal stresses within the coating. In view of the improved coatings properties when using nitrogen atomization, compared to air atomization, the following recommendations are made to further improve coatings properties:

1. Nitrogen is an effective atomizing gas with significant benefits in the coating properties. Improve the shrouding of the thermal spray gun to exclude convective currents of air entering the jet of molten Ti droplets between the gun and the target surface. This might include a mechanical barrier to exclude convective currents or a secondary stream of nitrogen to minimize air intrusion into the jet. These changes should reduce the amount of titanium oxide in the coating and increase α-Ti.

2. Consider argon for the atomizing gas. Titanium is inert in argon. However, shrouding of the gun and spray would be just as critical as when using nitrogen as the atomizing gas. While argon is typically three times as expensive as nitrogen, the improved properties of the coating over the coating service life may warrant the additional expense. Carbon dioxide is not an acceptable atomizing gas because it decomposes at the temperature of the arc, and titanium oxides would form.

3. Metals with higher valence ions such as tungsten or tantalum could be incorporated in the Ti at low concentrations. Their presence in the oxidized skin of the droplets could, because of the semiconducting properties of titanium oxides, increase the conductivity of the oxide and reduce the oxidation rate of titanium (*Hauffe, 1965; Kubaschewski and Hopkins, 1962b*).

7.2.2 Electrochemically Aged Anodes

An anode surface treatment may be possible that retards continued etching of the concrete at the anode-concrete interface, should that prove to be a problem associated with long term operation of the anode at ODOT current densities for coastal CP systems. Such a treatment would provide material with buffering capability to counter the consumption of hydroxy ions by the anode reaction. It could also infuse the reaction zone with material to strengthen the structure of this zone and improve its durability. Such a treatment could be provided by a thin, porous mortar overlay of the titanium anode. The overlay would not be detrimental to anode operation since it would not interfere with electrical connections to the anode, the delivery of moisture to the anode, nor future applications of catalyst.

Studies of the real time (non-accelerated) aging of the titanium anode at the Depoe Bay Bridge in Depoe Bay, Oregon should be continued to determine why little or no evidence of a reaction zone was observed in short-term field aging of the anode. An effort should be made to determine if there is a critical current density for concrete deterioration and to determine the life of the cobalt catalyst.

7.2.3 Overall Recommendations

- Techniques to reduce the γ-TiO content of the coating should be investigated since this would improve the durability and conductivity of the coating. Several suggested areas for investigation are: improved shrouding of the spray jet; the use of an alternate atomizing gas; and the use of titanium alloyed with tungsten, niobium or tantalum to produce a coating with greater resistance to oxidation.

- The highly varied chemistry of the coating suggests future work on how the electrochemistry at the coating surface is effected and how internal stresses leading to coating cracking can be reduced.

- The short circuit detection system developed for use during the field trial provided results that were difficult to interpret. More work is needed to develop a system that can more reliably detect short circuits between the titanium anode and the rebar.

- Since low coating resistance appears to be linked to low bond strength and coating bond failure, further work is needed to determine the minimum allowable coating resistance for specification purposes. Perhaps more importantly, a better understanding of the bond failure mechanism may suggest techniques to eliminate or reduce residual stresses in the completed coating.

- Even with annealed wire, contact tip wear is a problem. Further work is needed to develop tips that are wear resistant and conductive enough to effectively transfer charge to the wire.

- Although 3.2 mm (1/8") diameter wire was used for the majority of work on this project, the better spray characteristics of 2.4 mm (3/32") diameter wire suggests that future work should, at least initially, focus on the use of the smaller wire.

8.0 REFERENCES

Adams, C. M., Jr. and C. E. Jackson, Heat Flow in Welding, in *Welding Handbook.* 7th Ed. Vol. 1. American Welding Society. 84-88. 1981.

Balandin, A. A., A. Bielanski, G. K. Boreskov, et al., *Catalysis and Chemical Kinetics.* Academic Press, N. Y. 60-73. 1964.

Bars, J. P., D. David, E. Etchessahar and J. Debuigne, Titanium α-Nitrogen Solid Solution Formed by High Temperature Nitriding: Diffusion of Nitrogen, Hardness and Crystallographic Parameters, *Metallurgical Transactions A.* Vol. 14A:1537-1543. August 1983.

Bauccio, Michael, editor. *ASM Metals Reference Book, Third Edition*, ASM International, 1993.

Bennett, J.E., T.J. Schue, and G. McGill, A Thermal Sprayed Titanium Anode for Cathodic Protection of Reinforced Concrete Structures, CORROSION/95, Paper No. 95504. NACE International, Houston, TX. 1995a.

Bennett, J. E., T. J. Schue and G. McGill, Protecting Reinforced Concrete Using Thermal-Sprayed Titanium Anodes, *Materials Performance.* Vol. 34 (11):23-26. November 1995b.

Berndt, C.C., S. Reddy, and M.L. Allen, Optimization of Thermal Spray Parameters for Cathodic Protection of Reinforcement in Concrete. CORROSION/95, Paper No. 95012. NACE International, Houston, TX.1995.

Blocher Jr., J. M., Nitrides, in *High-Temperature Materials and Technology*, I. E. Campbell and E. M. Sherwood, Eds. Wiley and Sons, New York NY. 391, 1967.

Boyer, Rodney, Gerhard Welsch, and E.W. Collings, editors, *Materials Properties Handbook: Titanium Alloys*, ASM International, 1994.

Brousseau, R., S. Dallaire, M. Arnott, B Baldock, and J.G. Allard, "ILZRO *Project No. ZE-399: Adhesion of Thermally Sprayed Zinc on Reinforced* Concrete," National Research Council of Canada, July 1994.

Bullard, S.J., B.S. Covino, Jr, G.R. Holcomb, S.D. Cramer, and G.E. McGill, Bond Strength of Thermal-Sprayed Zinc on Concrete During Early Electrochemical Aging, CORROSION/97, Paper No. 97232. NACE International, Houston, TX. 17 pp., 1997.

Bumps, E. S., H. D. Kessler and M. Hansen, *Trans. ASM.* Vol. 45:1008-1028. 1953.

Cahn, R. W., Alloys Rapidly Quenched from the Melt, Chapter 28 in *Physical Metallurgy*, R. W. Cahn and P. Haasen, eds. Third Edition. Elsevier Science, New York, NY. 1780-1852. 1983.

Campbell, I. E. and Sherwood, E. M., Eds., Ceramic Oxides, in *High-Temperature Materials and Technology.* Wiley and Sons, New York NY. 271. 1967.

Carello, R. A., D. M. Parks, and J. A. Apostolos, *Development, Testing and Field Application of Metallized Cathodic Protection Coatings on Reinforced Concrete Substructures*, California Department of Transportation, FHWA-CA-TL-89-04. 100 pp. May 1989.

Chastain, J., Ed., *Handbook of X-ray Photoelectron Spectroscopy.* Perkin-Elmer Corp., Physical Electronics Division, Eden Prairie MN. 261. 1992.

Collins, L. E., *Canadian Met. Quart.* Vol. 25(1):59-72. 1986.

Cotton, F. A., and G. Wilkinson, *Advanced Inorganic Chemistry.* Interscience, N. Y. 51. 1996.

Covino Jr., B. S., S. J. Bullard, G. R. Holcomb, S. D. Cramer, G. E. McGill and C. B. Cryer, Factors Affecting the Bonding of Arc-Sprayed Zinc to Concrete, in *Balancing Economics and Compliance for Maintaining Protective Coatings.* SSPC 95-09, Steel Structures Painting Council, Pittsburgh PA. 115 –128. November 1995.

Covino Jr., B. S., S. Bullard, G. R. Holcomb, S. D. Cramer, G. E. McGill and C. B. Cryer, Bond Strength of Electrochemically-Aged Arc-Sprayed Zinc Coatings on Concrete, CORROSION/96, Paper No. 96308. NACE International, Houston TX. 17 pp. 1996a.

Covino, B. S., Jr., S. D. Cramer, S. J. Bullard, G. R. Holcomb, G. E. McGill, and C. B. Cryer, Factors Affecting Thermal-Sprayed Zinc Anodes on Concrete, Paper No. 173, *Proceedings 13th International Corrosion Congress.* Australasian Corrosion. Assoc., Clayton, Vic., AU. 7 pp. 1996b.

Covino, B. S., Jr., S. J. Bullard, G. R. Holcomb, S. D. Cramer, G. E. McGill and C. B. Cryer, *Corrosion*, Vol. 53(5): 399-411. 1997a.

Covino, B.S., S.J. Bullard, S.D. Cramer, G.R. Holcomb, G.E. McGill, C.B. Cryer, A. Stoneman, R.R. Carter, Interfacial Chemistry of Zinc Anodes for Reinforced Concrete Structures. CORROSION/97, Paper No. 97233. NACE International, Houston TX. 20 pp. 1997b.

Covino, B. S., Jr., S. D. Cramer, G. R. Holcomb, S. J. Bullard, W. K. Collins and G. E. McGill, Characterization of Electrochemically-Aged Thermal-Spray Titanium Anodes on Concrete, in *Thermal Spray: A United Forum for Scientific and Technological Advances*. ASM International, Materials Park OH. 151-160. 1997c.

Cramer, S. D., B. S. Covino, Jr., S. J. Bullard, G. R. Holcomb, W. K. Collins, R. D. Govier, R. D. Wilson, and G. E. McGill, Arc-Sprayed Titanium Anode for Cathodic Protection of Reinforcing Steel in Coastal Concrete Bridges, in The Role of Characterization in Understanding Environmental Degradation of Materials, *Proceedings of the 30th Annual Technical Meeting of the IMS*, D. E. Alman, J. A. Hawk, and J. W. Simmons, Eds., Microstructural Science, International Metalographic Society, Materials Park OH. Vol. 25: 89-101. 1998.

David, S. A. and J. M. Vitek, *Intern. Mater. Rev.,* Vol. 34(5):213. 1989.

Donachie Jr., M. J., *Titanium: A Technical Guide*, ASM International, Materials Park OH. 282. 1988a.

Donachie Jr., M. J., *Titanium: A Technical Guide*, ASM International, Materials Park OH. 159. 1988b.

Donachie Jr., M. J., *Titanium: A Technical Guide*, ASM International, Materials Park OH. 69-70. 1988c.

Engineering Property Data on Selected Ceramics - Nitrides, MCIC-HB-07-Vol.I, Metals and Ceramics Information Center, Battelle, Columbus OH. 5.3.4-1 through 5.3.4-9. March 1976.

Engineering Property Data on Selected Ceramics - Single Oxides. MCIC-HB-07-Vol.III, Metals and Ceramics Information Center, Battelle, Columbus OH. 5.4.8-1 through 5.4.8-9. July 1981.

Etchessahar, E., J. P. Bars and J. Debuigne, J. *Less-Common Metals.* Vol. 134:123-139. 1987.

Gernitsky, W. A., Test Certificate 941474 (P.O. 8177), Titanium Wire Corporation, Frackville PA. January 12, 1995.

Greving, D.J., J.R. Shadley, and E.F. Rybicki. Effects of Coating Thickness and Residual Stresses on the Bond Strength of ASTM C633-79 Thermal Spray Coating Test Specimens. *Journal of Thermal Spray Technology*, 371-378, December 1994.

Gruber, H. and E. Krautz, Electrical Conductivity, Thermopower, Hall Coefficient and Magnetoresistance of Titanium Oxides with Different Oxygen Content, Z. *Metallkunde,* Vol. 77(4):203-206. April 1986.

Gudge, M., D.S. Rickerby, R. Kingswell, and K.T. Scott, Residual Stress in Plasma Metallic and Ceramic Coatings, in Thermal Spray Research and Applications, *Proceedings of the Third National Thermal Spray Conference,* Long Beach CA. 331-337. 1990.

Gusmano, G, A. Bianco, G. Montesperelli, and E. Traversa, *Electrochimica Acta*, Vol. 41(7/8): 1359-1368. 1996.

Hauffe, K., *Oxidation of Metals.* Plenum Press, New York NY. 209-228. 1965.

Hayfield, P. C. S., and M. S. Warne, Titanium Based Mesh Anode in the Cathodic Protection of Reinforcing Bars in Concrete. *Construction and Building Materials*, Vol. 3(3):152-158. September 1989.

Holcomb, G. R., S. J. Bullard, B. S. Covino, Jr., S. D. Cramer, C. B. Cryer, and G. E. McGill, Electrochemical Aging of Thermal-Sprayed Zinc Anodes in Concrete, in Thermal Spray: Practical Solutions for Engineering Problems, C. C. Berndt, Ed., *Proceedings 9th National Thermal Spray Conference,* ASM International, Materials Park OH. 185-192. 1996.

Holcomb, G. R., S. D. Cramer, S. J. Bullard, B. S. Covino, Jr., W. K. Collins, R. D. Govier, and G. E. McGill, Characterization of Thermal-Sprayed Titanium Anodes for Cathodic Protection, in *Thermal Spray: A United Forum for Scientific and Technological Advances*. ASM International, Materials Park OH. 141-150. 1997.

Holcomb, G. R. and C. B. Cryer, Cost of Impressed Current Cathodic Protection for Coastal Bridges, Materials Performance. Vol. 37 (7):22-26. 1998.

Krepski, R. P., *Thermal Spray Coating Applications in the Chemical Process Industries.* Materials Technology Institute Pub. 42, NACE International, Houston TX. 252 pp., 1993a.

Krepski, R. P., *Thermal Spray Coating Applications in the Chemical Process Industries*, Materials Technology Institute Pub. 42, NACE International, Houston TX. 16. 1993b.

Kubaschewski, O. and B. E. Hopkins, *Oxidation of Metals and Alloys*, Butterworths, London. 5-14 and 24. 1962a.

Kubaschewski, O. and B. E. Hopkins, *Oxidation of Metals and Alloys*, Butterworths, London. 213-215. 1962b.

Lackey, W. J., D. P. Stinton, G. A. Cerny, A. C. Schaffhauser and L. L. Fehrenbacher, "Ceramic Coatings for Advanced Heat Engines -- A Review and Projection," *Adv. Ceram. Mat.* Vol. 2(1):24-30. 1987.

Leigh, S. H., S. Sampath, H. Herman, C. C. Berndt, G. Montavon and C. Coddet. Quantitative Analysis of Thermal Spray Deposits Using Stereology, Proc. 8th National Thermal Spray Conference, ASM International. 273-278. September 1995.

McGill, G. E., S. D. Cramer, S. J. Bullard, B. S. Covino, Jr., and G. R. Holcomb. *Field Application of an Arc-Sprayed Titanium Anode for Cathodic Protection of Reinforcing Steel in Concrete*, Interim Report No. 5265, Oregon Department of Transportation, Salem OR. 124 pp. 1996.

McGovern, Martin S., CP OK with ODOT. *Concrete Repair Digest*, 291-295, October/November 1994.

Munster, A. and K. Sagel, Some Electrical Properties of Titanium Nitride and Titanium Carbide, *Z. Physik.* Vol. 144:139-51. 1956. (Also: Goldsmith, A., T. E. Waterman, H. J. Hirschhorn, *Handbook of Thermophysical Properties of Solid Materials*, Vol. IV. MacMillan, New York NY. 303. 1961.

NACE. *Cathodic Protection of Reinforcing Steel in Atmospherically Exposed concrete Structures.* RP0290-90, NACE International, Houston TX. 1990.

Nielsen-Dharmaratne, K., and F. O. Gronvold. Internal Anodes in Concrete Structures. *Materials Performance*, Vol. 31(6):29-32. June 1992.

Nitrogen-Titanium, Alloy Phase Diagrams, *ASM Handbook,* Vol. 3. ASM International, Materials Park OH. 2-299. 1992.

Oxygen-Titanium, Alloy Phase Diagrams, *ASM Handbook,* Vol. 3. ASM International, Materials Park OH. 2-324. 1992.

Pedeferri, P., G. L. Mussinelli, M. Tettamanti, and C. J. Mudd. Cathodic Protection of Steel in Concrete with Expanded Titanium Anode Net System. In *Proceedings U. K. Corrosion 89* (Blackpool, November 8-10, 1989), Corrosion Engineering Association (and Institution of Corrosion Science and Technology), Birmingham U. K., Vol. 3: 182-198. 1989.

Pourbaix, M., *Atlas of Electrochemical Equilibria*, NACE International. 147-150. 1974.

Stratfull, R.F. *Experimental Cathodic Protection of a Bridge Deck.* Transportation Research Record No. 500, 1-15, Federal Highway Administration Report No. FHWA-RD-74-31, January 1974.

Swiat, Wayne J. and Joseph W. Rog. *Further Improvements in Cathodic Protection,* Report FHWA-RD-87-062, 7-8. June 1987.

Uhlig, Herbert H. and R. Winston Revie. *Corrosion and Corrosion Control.* 3rd edition, John Wiley and Sons, 28, 375-382, 1985.

Weale, C.J., *Cathodic Protection of Reinforced Concrete: Anodic Processes in Cements and Related Electrolytes*, Thesis No. DX185652, The British Library, West Yorkshire, United Kingdom LS23 7BQ. 415 pp.. 1992.

Weast, R. C., Ed., Electrical Resistivity and Temperature Coefficients of Elements, *Handbook of Chemistry and Physics.* 60th Edition. CRC Press, Boca Raton FL. F-172. 1980a.

Weast, R. C., Ed., Thermal Properties of Pure Metals, *Handbook of Chemistry and Physics.* 60th Edition. CRC Press, Boca Raton FL. D-189. 1980b.

Weast, R. C., Ed., Thermal Conductivity of the Elements, *Handbook of Chemistry and Physics.* 60th Edition. CRC Press, Boca Raton FL. E-12 through E-17. 1980c.

Weast, R. C., Ed., Refractory Materials, *Handbook of Chemistry and Physics.* 60th Edition. CRC Press, Boca Raton FL. D-51 through D-60. 1980d.

Weast, R. C., Ed., Crystal Ionic Radii of the Elements, *Handbook of Chemistry and Physics.* 60th Edition. CRC Press, Boca Raton FL. F-214. 1980e.

Wells, A. F., *Structural Inorganic Chemistry.* Oxford University Press, Glasgow. 166. 1962.

APPENDICES

APPENDIX A

SPECIFICATIONS FOR FIELD APPLICATION OF ARC-SPRAYED TITANIUM

SECTION - 01251 INSTALL CURRENT DISTRIBUTION PLATES

01251.00 Scope - The Contractor shall install the current distribution plates at the locations indicated on the plans and approved by the Engineer. Current distribution plates provide the connection between the conductors from the DC power distribution system positive wires and the arc-sprayed titanium anode in zone 14.

Additional current distribution plates shall be installed where necessary to bridge cracks in the bridge. Connection to the plates is included in Section 01265, Install DC Power Distribution System.

01251.02 Timing - Current distribution plates shall be installed after installation of the titanium anode (Section 01261).

01251.11 Materials Requirements - The titanium current distribution plates and mounting screws and washers will be furnished by the State. The Contractor shall furnish the plastic anchor, the bolt and nuts required for attaching the ring connector and the epoxy required for mounting the plates. The epoxy shall be Concresive 1419 as manufactured by Adhesive Engineering Co., DP-420 as manufactured by 3M, or an Engineer-approved equal.

01251.31 Installation Requirements - The current distribution plate shall be installed and located as shown on the plans. At least one current distribution plate per each 600 square feet of anode area is required. Install each plate centered in the 600 square foot area it supplies. Where the coating is unable to bridge a crack, one distribution plate shall be installed centered over the crack to provide a conductive path across the crack. The top of the plastic anchor shall be installed flush with or slightly below the concrete surface. Control the amount of epoxy used to prevent flow of the epoxy between the titanium and the plate.

01251.71 Acceptance Criteria - The work performed under this section will be accepted if it is in accordance with all requirements of the plans, specifications, the Engineer-approved working drawings, material submittals, and work procedures.

01251.80 Measurement - Installation of the current distribution plates will be measured for payment on a unit basis per each by actual count of items in place, completed, and accepted.

01251.90 Payment - The current distribution plates will be paid for at a unit price per each for the bid item "Install Current Distribution Plates". Payment as above specified will be full and complete compensation for furnishing all labor, tools, equipment, and materials and doing all work called for by the plans and specifications.

SECTION - 01261 INSTALL TITANIUM ANODE

01261.00 Scope - The titanium anode consists of thermally sprayed titanium wire applied to the concrete surface for distribution of DC electrical charge over the concrete surface in zone 14. The Contractor shall furnish labor, materials and equipment for installation of the anode and masking to separate the zones.

01261.02 Timing - The titanium shall be applied within 24 hours after completion of the work required under Section 01255, Prepare Secondary Anode Surfaces.

Surfaces shall be scrubbed with a bristle brush and then thoroughly vacuumed or blown clean within 15 minutes before titanium spraying of the area is started. Any oil, grease, soil, water, or other foreign matter which deposits on the surface after the surface preparation has been completed shall be removed as described in 01255.31 before the titanium is applied.

The Contractor shall perform no work on this item until written approval is received from the Engineer, all supervisors and technicians have been certified for this work, and certifications have been approved by the Engineer.

01261.05 Installation Conditions - Coating application shall only be performed when the concrete surface is clean and dry and the relative humidity is less than 60% adjacent to and/or surrounding the entire current work surface.

01261.11 Equipment and Material Requirements -

(a) Masking - The masking material shall be non-conductive and shall be four inches wide between zones. Masking shall be installed to provide two inches between the titanium and any exposed metal object. Duct tape to which sprayed titanium does not adhere and which is heat resistant is an acceptable material. Multiple layers of tape may be required for adequate masking performance. The masking shall not disbond the titanium coating on adjacent surfaces when it is removed.

(b) Titanium Application Equipment - Application equipment shall be electric-arc type. The spray equipment manufacturer shall be:

Thermion, Inc.
P O Box 2136
Silverdale, WA 98383 - 2136
(206) 698 - 1539

or equivalent.

The Contractor is responsible for making the necessary modifications to the arc-spray system required to spray the titanium wire.

Spraying equipment from other manufacturers must be qualified as an equivalent by a demonstration test (planned, prepared, and conducted by the Contractor), and approved by the Engineer. This test must demonstrate equivalency under the full range of conditions which are likely to be encountered during this project. Evaluation of the demonstration will be based on 01261.71 below.

The Contractor shall be responsible for surface preparation, environmental control, conducting the test, and cleanup of the test area. This test shall be accomplished at the Contractor's expense.

The Contractor shall submit the manufacturer's equipment specifications, recommended operational procedures, and the Contractor's test plan including test facilities and procedures, for the Engineer's approval.

(c) Titanium - The coating material shall be 0.125 inch, annealed, grade 1 or 2, titanium wire. The Contractor shall submit the chemical analysis of the wire to certify the purity of titanium wire to be used on this project. The Contractor shall obtain and submit a certification to the Engineer for each lot of titanium used.

(d) Catalyst - A catalyst must be applied to the titanium anode after the titanium is applied to the concrete surface. The catalyst is available from Eltech Research Corporation, 625 East Street, Fairport Harbor, OH.

(e) Short Circuit Detection Equipment - This equipment shall consist of a constant current source that applies a constant current between the titanium and the steel, and a voltage detection system that monitors the voltage between the steel rebar and the titanium coating and causes shutdown of spraying equipment when a short circuit occurs. The detection system shall consist of a Newport digital voltmeter, number Q2005AVR2-SPC, or approved equivalent, installed in a NEMA 4 enclosure for use at the work area. The State will furnish the constant current supply. The Contractor is responsible for providing the voltage detection equipment and labor required for operation of the short circuit monitoring system.

01261.12 Technician Certification Requirement - Technician certification will take place prior to commencement of titanium spraying on the bridge. To be certified, the technician must have verifiable previous experience applying arc-sprayed zinc to a minimum of 5000 square feet of concrete surface area. The certification test shall begin by having each candidate perform titanium spraying, as specified, on prepared concrete specimens.

Concrete test specimens or approved test locations on the bridge shall be fully cured and abrasive-blasted as required under Section 01255, Prepare Secondary Anode Surfaces. The concrete test areas shall be 2 ft. x 2 ft. minimum.

One test specimen shall be provided by the Contractor for the testing of each candidate. The specimen shall be sprayed in one multi-pass operation.

The following inspection and testing will be performed on the specimens by the Engineer, who will make the final decision on certification.

(a) Visual Examination - Test specimens will be visually inspected using a lens with a magnification of 10x. To be acceptable, the coating shall have uniform appearance and follow the form of the concrete surface. The coating shall not contain any lumps, blisters, coarse texture, or loosely adhering particles, nor shall it contain any cracks, pinholes, or chips which expose the concrete substrate.

(b) Adhesion Test - Three aluminum or steel test discs will be cemented to the test area. After curing, the test discs shall be pulled from the test area with a calibrated Proceq, Model DYNA Z 5, or equal. To be acceptable, the minimum adhesion strength shall be 150 psi or greater.

(c) Resistance Test - To be acceptable the resistance of the coating shall be less than 0.25 ohms per square.

Technicians whose specimens satisfy these three requirements shall be certified as qualified Titanium Thermal Spray Technicians for this project.

An operator failing the initial certification tests may be permitted to perform one complete retest. If the operator fails the retest, he shall not be certified until completion of additional training and certification testing.

Re-testing and re-certification will be required whenever a technician's work falls below the acceptable criteria given in 01261.71.

Records of technician certification shall be maintained by the Contractor for a period of 6 months after completion of the contract work. Copies of the records shall be made available to the Engineer upon request.

01261.31 Anode Installation Requirements - During application the thermal spray nozzle shall be maintained at a travel speed and a distance from the work surface such that titanium deposit efficiency and bond strength are maximized. Travel speed should be 18 to 24 inches per second. The distance from the arc to the surface should be 4 to 7 inches.

Begin the titanium anode installation by spraying the area in which the current distribution plate will be installed. Install the current distribution plate and connect the short circuit detection system before spraying additional area. The titanium shall be installed in a continuous coating to facilitate short circuit detection. The coating shall be applied in multiple passes and shall overlap on each pass in a crosshatch pattern to ensure complete coverage. Uniform gun movement shall be used to ensure uniform thickness. Sufficient material shall be sprayed to achieve a maximum coating resistance of 0.25 ohms/square over the entire surface.

Compressed air used for spraying shall be clean, oil-free and dry, per ASTM D 4285. Air line filters and moisture separators shall be installed upstream from the spraying equipment. These shall be inspected daily for cleanliness and correct operation. Any indication of malfunctioning equipment, indicated by oil or water in the filter or traps, shall be corrected immediately.

Bend tests shall be performed by the Contractor to verify the proper operation of the equipment prior to starting work on each shift. The bend test shall consist of spraying two 2"x 4"x 0.05" carbon steel coupons with a 6 - 8 mil coating. The bend coupons shall be bent 180 degrees around a ½ inch diameter rod. The coating shall be on the tensile side of the bend test specimen. The bend test passes if there is no or only minor cracking of the coating as visually observed. The bend test fails if the titanium cracks and can be picked off with a knife blade. The titanium shall be applied to the bend coupons in the same manner and with the equipment adjusted for spraying the concrete.

01261.32 Short Circuit Detection - The short circuit detection system uses a constant current source to create a voltage between the rebar and the titanium. The detection scheme consists of monitoring this voltage and opening an alarm contact which controls the arc-spray equipment if the voltage drops below a preset level. A sharp drop in voltage is a definite indication of a short circuit. A short circuit or near short circuit will reduce the measured voltage to less than 100 millivolts.

Operation of the monitor requires one conductor from the positive input terminal of the detection equipment to be attached to the current distribution plate nearest the area in which work is being performed. A second conductor is required to connect the negative input terminal of the detection equipment to the rebar in the zone.

The Contractor may change the DC voltage at which the alarm is actuated with written approval from the Engineer.

The Contractor shall be responsible for furnishing all materials, equipment (except constant current supply) and labor to set up and operate the short circuit detection system.

The short circuit monitoring system shall be used during any work which may cause a short circuit between the titanium anode and the rebar. The system shall be used for titanium installation and for any conduit installation over titanium-coated surfaces. During the conduit installation the alarm contact shall operate a visual or audio alarm to indicate when a short is detected. When this alarm is actuated, all monitored installation work shall stop until the short circuit has been eliminated. The Contractor shall perform a functional test of the short circuit monitoring system prior to beginning the monitored work.

Elimination of detected short circuits shall be performed and paid for according to Section 01215, Locate and Remove Surface Metal.

01261.33 Catalyst Installation Requirements - The catalyst may be sprayed, brushed, or roller-coated onto the surface of titanium after the titanium is applied to the concrete surfaces. Before applying the catalyst, connect a constant current supply between the titanium and the rebar with the positive terminal of the supply connected to the titanium. Use jumpers to connect all of the distribution plates to the current supply. Set the current source to supply one milliamp per square foot of anode surface area.

Apply the catalyst at the minimum rate of 30 milliliters per square foot (0.32 quarts/sq. ft. or 323 milliliters/sq. meter). Multiple coats may be required to prevent the catalyst from dripping or running. Allow the current supply to run continuously for a period of 72 hours after completion of catalyst installation.

01261.41 Environmental Control Requirements - No discharge of noxious or hazardous waste material will be allowed onto the ground or into the air or water outside the platform/enclosure. Discharge of particulate from the enclosure shall not exceed 2 grains/1,000 cubic feet of air, (4.6 milligrams/cubic meter), in addition to complying with all applicable Oregon Department of Environmental Quality requirements. Waste containment and disposal requirements is covered under Section 01210, Prepare Waste Handling Plan.

01261.71 Acceptance Criteria - Do not perform catalysis before inspection and testing of the arc-sprayed titanium anode is complete. The work performed under this section will be accepted if it is in accordance with all requirements of the plans and specifications and the Engineer-approved working drawings, materials submittals and work procedures, and the titanium anode passes the inspections and tests described below. Anode surfaces shall be visually inspected using a lens with a magnification of 10x. To be acceptable the coating shall have uniform appearance and follow the form of the concrete surface. The coating shall not contain any lumps, blisters, coarse texture, or loosely adhering particles, nor shall it contain any cracks, pinholes, or chips which expose the concrete substrate. Unacceptable areas shall be repaired or replaced by the Contractor at no additional cost to the State. Anode repair shall be by a procedure proposed by the Contractor and approved by the Engineer. Repair work shall not be started until the Contractor receives the written approval of the Engineer.

Adhesion strength will be measured by the Engineer with a Proceq, Model DYNA Z 5, or equal. A minimum of five adhesion tests will be performed in zone 14. The target adhesion strength of the titanium coating shall be greater than 150 psi. Areas with adhesion strengths below 50 psi shall have the titanium removed and shall be recoated with titanium in accordance with these specifications.

Coating resistance will be measured by the Engineer at a minimum of 20 locations per 1000 square feet. All measurements shall be less than 0.25 ohms. Where the measurements indicate that the anode has excessive resistance, additional titanium shall be applied by thermal spraying after the surface is completely dry and any visible contamination has been removed.

Adhesion test areas (each approximately 2 inches in diameter) shall be recoated with titanium after scraping any loose or delaminated titanium caused by the adhesion test. Use care to avoid excessive coating thickness (greater than 10 mils) on the adjacent titanium surface.

01261.80 Measurement - There will be no separate measurement for individual items of work done under this Section. The estimated area to which the titanium shall be installed is 3,015 square feet.

01261.90 Payment - Payment for installing the titanium anode will be made at the lump sum amount for the item "Install Titanium Anode". Payment of the lump sum amount will be complete compensation for all labor, materials, equipment and incidentals required to perform the work specified in this section.

APPENDIX B

Calculation of Area Per Current Distribution Plate

CALCULATION OF MAXIMUM AREA PER CURRENT DISTRIBUTION PLATE

ASSUMPTIONS:

Current is distributed uniformly across surface area
R' = coating resistance per square = 0.50 ohms/square
Maximum current delivery = 0.002 A/ft^2
Cylindrical coating geometry as shown in figure B.1
Maximum desired coating voltage drop = 300 mV

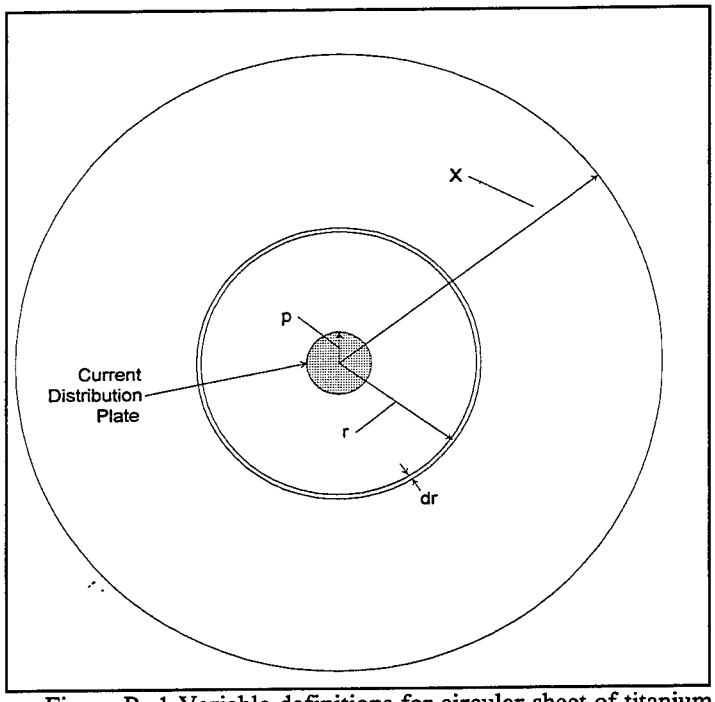

Figure B. 1 Variable definitions for circular sheet of titanium

SOLUTION:

The resistance of a thin ring of coating is defined by the following equation:

$$dR = \frac{\rho \cdot L}{A} = \frac{\rho \cdot dr}{t \cdot 2\pi \cdot r} = R' \frac{dr}{2\pi \cdot r} \qquad \text{(B-1)}$$

where:
ρ = resistivity of coating
L = length of coating section
A = cross-sectional area of coating
t = coating thickness
r = radius of coating ring
R' = coating resistance in ohms/square
dR = differential resistance in ohms

For uniform current distribution of 0.002 amps/ft^2, the current flowing through any cross-section of the coating, dr, is given by:

$$I = 0.002\pi\left(X^2 - r^2\right) \qquad \text{(B-2)}$$

Therefore, the voltage drop in the coating is given by the following integral:

$$V = \int I \cdot dR = \int_p^X 0.002\pi\left(X^2 - r^2\right) \cdot 0.5 \frac{dr}{2\pi \cdot r} = 5 \times 10^{-4} \int \left(\frac{X^2}{r} - r\right) dr \qquad \text{(B-3)}$$

Given that a maximum of 300 mV voltage drop is desired, the equation can be integrated and solved for X to determine the maximum area per distribution plate for a given plate radius:

$$\begin{aligned} 0.300 &= 5 \times 10^{-4} \left(X^2 \ln(r) - \frac{r^2}{2} \right]_p^X \\ &= 5 \times 10^{-4} \left[X^2 \left(\ln(X) - \ln(p)\right) - \frac{1}{2}\left(X^2 + p^2\right) \right] \end{aligned} \qquad \text{(B-3)}$$

Roots to this equation for various values for p were solved for using numerical techniques in Mathcad 4.0. A graph showing the values for p versus the maximum allowable anode area is shown below:

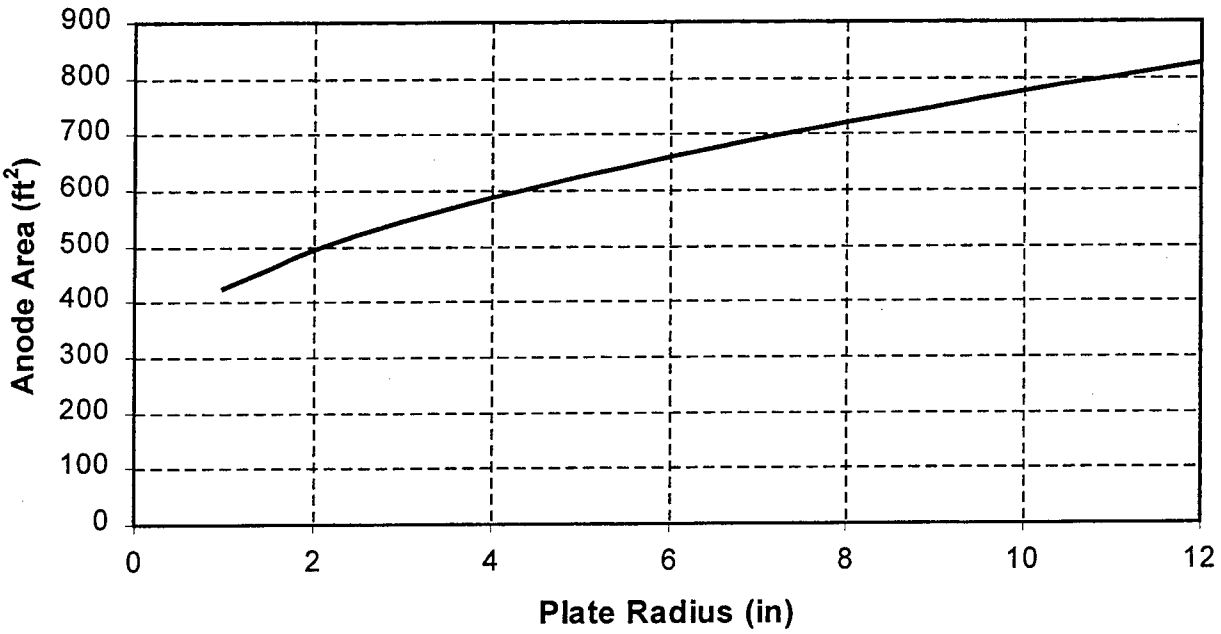

Figure B.2: Allowable titanium surface area vs. plate size – inches.

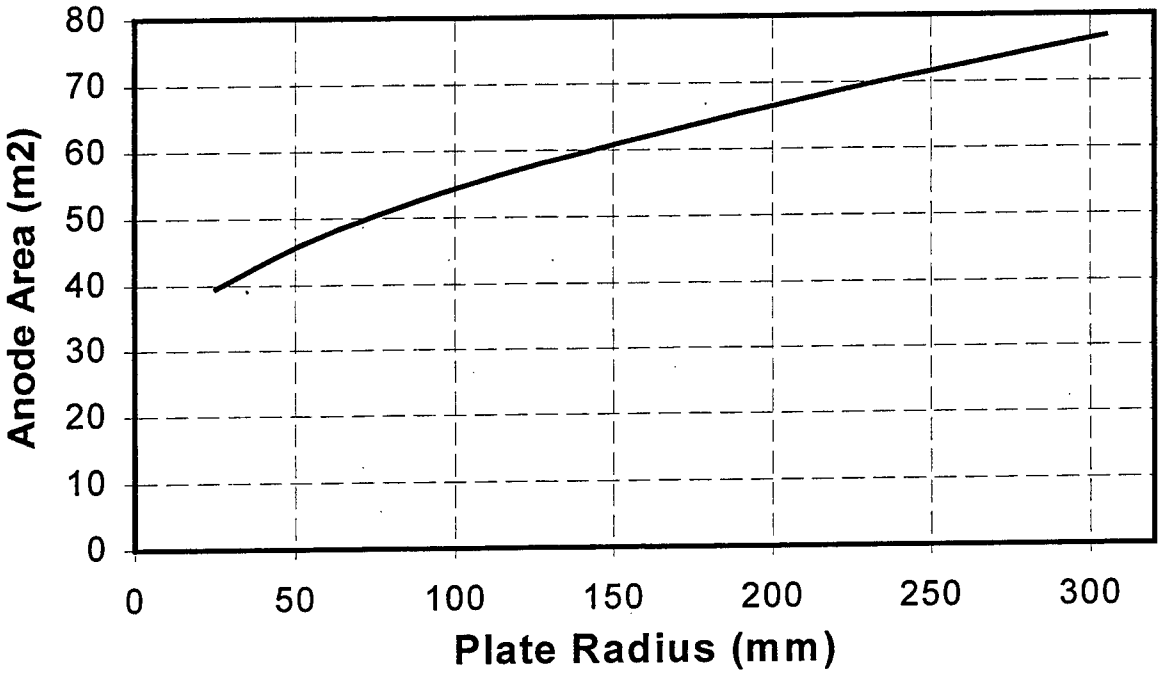

Figure B.3: Allowable titanium surface area vs. plate size – metric.